

Distribution Agreement

In presenting this thesis as a partial fulfillment of the requirements for a degree from Emory University, I hereby grant to Emory University and its agents the non-exclusive license to archive, make accessible, and display my thesis in whole or in part in all forms of media, now or hereafter now, including display on the World Wide Web. I understand that I may select some access restrictions as part of the online submission of this thesis. I retain all ownership rights to the copyright of the thesis. I also retain the right to use in future works (such as articles or books) all or part of this thesis.

Tiffany G. Hung

November 11, 2021

A Tale of Two Chemistries: Dynamics of Delay-Coupled Belousov-Zhabotinsky Oscillators; TrkB
Activators: A Review; Synthesis of TrkB Agonists

by

Tiffany G. Hung

Simbarashe Nkomo and Frank E. McDonald

Advisers

Chemistry

Simbarashe Nkomo and Frank E. McDonald

Advisers

Devon Goss

Committee Member

David Lynn

Committee Member

2021

A Tale of Two Chemistries: Dynamics of Delay-Coupled Belousov-Zhabotinsky Oscillators; TrkB
Activators: A Review; Synthesis of TrkB Agonists

By

Tiffany G. Hung

Simbarashe Nkomo and Frank E. McDonald

Advisers

An abstract of
a thesis submitted to the Faculty of Emory College of Arts and Sciences
of Emory University in partial fulfillment
of the requirements of the degree of
Bachelor of Science with Honors

Chemistry

2021

Abstract

A Tale of Two Chemistries: Dynamics of Delay-Coupled Belousov-Zhabotinsky Oscillators; TrkB Activators: A Review; Synthesis of TrkB Agonists

By Tiffany G. Hung

Part I: Synchronization of oscillatory elements drives many essential biological, chemical, and physical processes. Recent studies have reported complex partial synchronization patterns known as chimera states, which consist of coexisting coherent and incoherent dynamics. By studying small oscillator network systems, researchers hope to gain further insight into the exact principles and mechanisms behind the origin of complex dynamics. This study investigates experimentally the effect of time-delay and network structure on the dynamics of a three ferriin-catalyzed Belousov-Zhabotinsky (BZ) oscillator network and theoretically the effect of time-delay, initial conditions, and heterogeneity in a two-oscillator, ruthenium-catalyzed network on the emergence of complex synchronization patterns. Both experiments and simulations show that small BZ chemical oscillator systems support full and out-of-phase synchronization and period-cycling patterns. However, more complex behaviors, including complex coherent patterns and chaotic chimeras, are unique to the two heterogeneous oscillator system in simulations. Overall, our demonstration of the simplest BZ network that supports chimera states using a realistic model of an experimental system provides a foundation for seeking experimental evidence in simple chemical networks.

Part II: Neurotrophin-receptor interactions are critical for regulating signaling pathways responsible for neuronal growth and maintenance. Altered neurotrophin expression and receptor signaling is correlated with pathological conditions, including Huntington Disease and Alzheimer's Disease. However, therapeutic application of neurotrophins is restricted by its short *in vivo* half-life and limited pharmacological selectivity. In this review, we first discuss structural aspects of binding interactions with neurotrophins and Trk receptors. Then, we introduce synthetic small, non-peptide Trk receptor agonists that activate Trk signaling with high potency to demonstrate the potential for these agonists to serve as novel therapeutic options to target underlying disease mechanisms.

Part III: Traumatic blast-related injury, sports injury, or other blunt force trauma to the eye can damage the retina. Current treatments for injuries and diseases to ocular structures and visual systems remain inadequate. The ideal therapy can be quickly administered following injury to an eye in an emergency environment. *N*-[2-(5-hydroxy-1H-indol-3-yl)ethyl]-2-oxopiperidine-3-carboxamide (HIOC, *n*=1) is an *N*-acyl serotonin derivative that protects against blast-induced retinal degeneration and vision loss when administered shortly after blast exposure. I have synthesized the HIOC derivative with a 7-membered lactam and made progress towards synthesizing the HIOC analog with a 5-membered lactam. This work is part of the McDonald Lab's goal of developing HIOC analogs with superior blood brain/retina barrier penetrance, better selectivity for tropomyosin receptor kinase B (TrkB) activation, and higher potency.

A Tale of Two Chemistries: Dynamics of Delay-Coupled Belousov-Zhabotinsky Oscillators; TrkB
Activators: A Review; Synthesis of TrkB Agonists

By

Tiffany G. Hung

Simbarashe Nkomo and Frank E. McDonald

Advisers

A thesis submitted to the Faculty of Emory College of Arts and Sciences
of Emory University in partial fulfillment
of the requirements of the degree of
Bachelor of Science with Honors

Chemistry

2021

Acknowledgements

I would first like to thank Dr. Simbarashe Nkomo for teaching my first and last chemistry courses at Oxford College. Thank you for trusting me to advance your research and set up your lab at Oxford. Your generosity of your time, humor, knowledge, and patience has meant a lot to me as I acclimated to the experimental and simulation components of the research. You have truly shown me that anything is possible with hard work and perseverance and broadened my horizons to all the possibilities of chemistry research.

Next, I would like to acknowledge Dr. Frank McDonald. Thank you for being a strong advocate for me during my time at Emory College and giving me the opportunity to work in your lab for the last 1.5 years. Your mentorship, kindness, and patience have allowed me to gain synthetic chemistry laboratory skills, independence, and a true appreciation and love for the field of synthetic organic chemistry, inspiring me to pursue doctoral study in organic chemistry.

Conducting research in the Nkomo and McDonald labs has been two of the most rewarding parts of my Emory experience. Thank you both for the time and energy you have devoted to making me a better chemist and researcher.

I would also like to thank my undergraduate student mentor, Taylor Dover; graduate student research mentor, Emily Williamson; and postdoctoral research mentor, Dr. Christopher L. Walker. Taylor and Chris offered sage advice on parts II and III; Chris helped me analyze spectra and brainstorm novel approaches when experiments failed; and Emily never hesitated to teach me synthetic and characterization techniques. All of you have contributed to my growth as a young chemist and prepared me for graduate studies, to which I express my heartfelt and sincerest appreciation.

Thank you to the entire McDonald lab, past and present, for your support and being a great group of co-workers. It has been an absolute pleasure and honor to work with you all.

I would also like to acknowledge Dr. Devon Goss and Dr. David Lynn for serving on my committee. Dr. Goss inspired me to pursue a sociology minor and explore other subareas of sociology. Dr. Lynn taught me how to explore the systems-level properties of complex networks.

Lastly, thank you to my parents, Diane Wang and Nelson Hung, who have supported me throughout my entire life in times of stress, anxiety, and uncertainty and inspired me to pursue my educational and career goals. Your encouragement, advice, and emotional support were pivotal throughout my time at Emory, including the completion of this thesis.

Table of Contents

Chapter I: Complex Dynamics in Small Networks of Delay-Coupled Belousov-Zhabotinsky Oscillators

1. Introduction.....	1
2. Three Oscillator System.....	3
2.1 Experimental Approach.....	3
2.1.1 Preparing Oscillators and BZ Solution.....	3
2.1.2 Arrange Oscillators into Desired Network Structure in BZ Solution.....	3
2.1.3 Image Capture and Analysis.....	4
2.2 Experimental Results.....	4
3. Two Oscillator System.....	6
3.1 Model Setup.....	6
3.2 Simulation Results.....	7
3.2.1 Homogeneous Oscillators.....	7
3.2.2 Heterogeneous Oscillators.....	9
4. Conclusion.....	12
5. References.....	13

Chapter II: Structural Aspects of Binding Interactions with Tropomyosin Receptor Kinase B (TrkB)

1. Introduction.....	15
2. Neurotrophin and Trk Receptor Structures.....	17
3. Neurotrophin-Receptor Activation Models.....	19
4. TrkB Antagonists.....	22

4.1 ANA-12 (<i>N</i> -[2-[(2-oxoazepan-3-yl)carbamoyl]phenyl]-1-benzothiophene-2-carboxamide).....	22
4.1.1 ANA-12 and Neuronal Survival.....	24
4.1.2 ANA-12, HIOC, and Ocular Blast-Induced Vision Loss.....	24
5. TrkB Agonists.....	25
5.1 <i>N</i> -Acyl Serotonin Amides.....	25
5.1.1 <i>N</i> -Acetylserotonin (<i>N</i> -(2-(5-hydroxy-1 <i>H</i> -indol-3-yl)ethyl)acetamide, NAS).....	25
5.1.1a Kinetic Characteristics of NAS.....	25
5.1.1b Synthesis of NAS.....	26
5.1.1c NAS and Traumatic Brain Injury (TBI)	26
5.1.2 HIOC (<i>N</i> -[2-(5-hydroxy-1 <i>H</i> -indol-3-yl)ethyl]-2-oxopiperidine-3-carboxamide).....	27
5.1.2a Synthesis of HIOC.....	27
5.1.2b Kinetic Characteristics of HIOC.....	28
5.1.2c HIOC and Retinal Damage.....	28
5.1.2d HIOC and Subarachnoid Hemorrhage (SAH).....	29
5.2 7,8-DHF (7,8-Dihydroxyflavone).....	29
5.2.1a 7,8-DHF and Obesity.....	30
5.2.1b 7,8-DHF and Huntington's Disease.....	30
5.2.1c Chemical Modifications to 7,8-DHF.....	31
5.3 LM22A-4 ((<i>N,N',N'</i> -tris [2-hydroxyethyl])-1,3,5-benzene tricarboxamide)	32
5.3.1 LM22A-4 and Spinal Cord Injury.....	33
5.3.2 LM22A-4 and Hypoxic-Ischemic Stroke.....	34
5.4 Deoxygedunin and Deprenyl.....	34

5.4.1a Deoxygedunin and Parkinson's Disease.....	35
5.4.1b Deprenyl and Parkinson's Disease.....	35
6. Non-TrkB Specific Agonists.....	36
6.1 LM22B-10 (2-[[4-[[4-[Bis-(2-hydroxy-ethyl)-amino]-phenyl-(4-chloro-phenyl)-methyl]-phenyl]-(2-hydroxy-ethyl)-amino]-ethanol]): TrkB, TrkC agonist.....	36
6.1.1 LM22B-10 and Neuronal Survival and Process Outgrowth.....	37
6.2 Amitriptyline: TrkA, TrkB agonist.....	37
6.2.1 Amitriptyline and Huntington's Disease.....	37
6.2.2 Amitriptyline and Neurotrophic Activity.....	38
6.3 DAQ-B1/DMAQ-B1 (Demethylasterriquinone B1): TrkA, TrkB, TrkC agonist.....	38
6.3.1 DMAQ-B1 and Trk Neurotrophin Receptors.....	39
7. Conclusion.....	40
8. References.....	40

Chapter III: Assessing Lactam Ring Size in N-Acyl Serotonin Derivatives for Treating Trauma-Induced Vision Loss

1. Introduction.....	48
2. Experimental Approach.....	49
2.1 General Experimental Procedures.....	49
2.2 Synthesis of <i>N</i> -(2-(5-hydroxy-1H-indol-3-yl)ethyl)-2-oxopiperidine-3-carboxamide (HIOC).....	49
2.2.1 Synthesis of 2-oxopiperidine-3-carboxylic acid.....	49
2.2.2 Synthesis of <i>N</i> -(2-(5-hydroxy-1H-indol-3-yl)ethyl)-2-oxopiperidine-3-carboxamide (HIOC).....	50
2.3 Approach 1: Synthesis of 5-membered lactam through diethyl 2-azidoethylmalonate (7) and ethyl 2-oxo-3-pyrrolidinecarboxylate (8)	51

2.3.1 Synthesis of diethyl 2-oxidoethylmalonate (7).....	51
2.3.2 Synthesis of ethyl 2-oxo-3-pyrrolidinecarboxylate (8).....	51
Approach 1: Hydrogenation.....	51
Approach 2: Reduction of azide to amide by SnCl ₂ in MeOH.....	52
2.4 Approach 2: Synthesis of 5-membered lactam through <i>tert</i> -butyl 2-oxopyrrolidine-1-carboxylate (10), 1-(<i>tert</i> -butyl)-3-ethyl 2-oxopyrrolidine-1,3 dicarboxylate (11), and 1-(<i>tert</i> -butoxycarbonyl)-2-oxopyrrolidine-3-carboxylic acid (12).....	52
2.4.1 Synthesis of <i>tert</i> -butyl 2-oxopyrrolidine-1-carboxylate (10).....	52
2.4.2 Synthesis of 1-(<i>tert</i> -butyl)-3-ethyl 2-oxopyrrolidine-1,3 dicarboxylate (11).....	53
2.5 Approach 1: Synthesis of 7-membered lactam through a one-step approach.....	53
2.6 Approach 2: Synthesis of 7-membered lactam through <i>tert</i> -butyl 2-oxoazepane-1-carboxylate (14), 1-(<i>tert</i> -butyl)-3-ethyl 2-oxoazepane-1,3,dicarboxylate (15), and 1-(<i>tert</i> -butoxycarbonyl)-2-oxoazepane-3-carboxylic acid (16).....	54
2.6.1 Synthesis of <i>tert</i> -butyl 2-oxoazepane-1-carboxylate (14).....	54
2.6.2 Synthesis of 1-(<i>tert</i> -butyl)-3-ethyl 2-oxoazepane-1,3,dicarboxylate (15)...	54
2.6.3 Synthesis of 1-(<i>tert</i> -butoxycarbonyl)-2-oxoazepane-3-carboxylic acid (16).....	55
2.7 Synthesis of <i>N</i> -(2-(5-hydroxy-1 <i>H</i> -indol-3-yl)ethyl)-2-oxoazepane-3-carboxamide (22).....	55
2.7.1 Synthesis of <i>tert</i> -butyl 3-((2-(5-hydroxy-1 <i>H</i> -indol-3-yl)ethyl)carbonyl)-2-oxoazepane-1-carboxylate (21).....	55
2.7.2 Synthesis of <i>N</i> -(2-(5-hydroxy-1 <i>H</i> -indol-3-yl)ethyl)-2-oxoazepane-3-carboxamide (22).....	56
3. Results and Discussion.....	56
4. Conclusion.....	57
5. References.....	58

Figures and Tables

Chapter I: Complex Dynamics in Small Networks of Delay-Coupled Belousov-Zhabotinsky Oscillators

Figure 1.....	4
Figure 2.....	4
Figure 3.....	5
Figure 4.....	5
Figure 5.....	7
Figure 6.....	8
Figure 7.....	9
Figure 8.....	9
Figure 9.....	11

Chapter II: Structural Aspects of Binding Interactions with Tropomyosin Receptor Kinase B (TrkB)

Table 1.....	16
Figure 1.....	17
Figure 2.....	21
Figure 3.....	22
Figure 4.....	23
Scheme 1.....	24
Scheme 2.....	25
Scheme 3.....	26

Scheme 4.....	27
Scheme 5.....	28
Scheme 6.....	30
Figure 5.....	31
Scheme 7.....	31
Scheme 8.....	32
Figure 6.....	32
Scheme 9.....	33
Scheme 10.....	34
Scheme 11.....	35
Scheme 12.....	37
Scheme 13.....	39

Chapter III: Assessing Lactam Ring Size in N-Acyl Serotonin Derivatives for Treating Trauma-Induced Vision Loss

Figure 1.....	48
Scheme 1.....	49
Scheme 2.....	49
Scheme 3.....	50
Scheme 4.....	51
Scheme 5.....	51
Table 1.....	52
Scheme 6.....	52
Scheme 7.....	53

Scheme 8.....	54
Scheme 9.....	55

List of Abbreviations

Chapter I: Complex Dynamics in Small Networks of Delay-Coupled Belousov-Zhabotinsky Oscillators

BZ= Belousov-Zhabotinsky

FKN= Field, Körös, and Noyes

IPD= initial phase difference

LE= Lengyel-Epstein

ZBKE= Zhabotinsky- Buchholtz-Kiyatkin-Epstein

σ = coupling strength

τ = time-delay

Chapter II: Structural Aspects of Binding Interactions with Tropomyosin Receptor Kinase B (TrkB)

3-NP= 3-nitropropionic acid

7,8-DHF= 7,8-dihydroxyflavone

aa= amino acid

Akt/PI3K-Akt= phosphoinositide 3-kinase

AMPK= AMP-activated protein kinase

ANA-12= (*N*-[2-[(2-oxoazepan-3-yl)carbamoyl]phenyl]-1-benzothiophene-2-carboxamide)

ARE= antioxidant response element

Bax= BCl-2-associated X

Bcl-2= B-cell lymphoma 2

BDNF= brain-derived neurotrophic factor

C1/CC1= cysteine cluster 1

C2/CC2= cysteine cluster 2

CDI= carbonyldiimidazole

CREB= cyclic AMP response element-binding protein

D1= domain 1

D2= domain 2

D3= domain 3

D1D2D3= domains 1-3

DAQ-B1/DMAQ-B1= Demethylasterriquinone B1

DCM= dichloromethane

DDQ= 2,3-dichloro-5,6-dicyano-1,4-benzoquinone

DRQ= dorsal root ganglion

ERG= electroretinogram

ERK= MAPK= mitogen-activated protein kinase

Erk1/2= extracellular signal-regulated kinase ½

FRET= Fluorescence Resonance Energy Transfer

HIOC= (*N*-[2-(5-hydroxy-1H-indol-3-yl)ethyl]-2-oxopiperidine-3-carboxamide)

HO-1= heme oxygenase-1

IC₅₀= half maximal inhibitory concentration

Ig1= domain 4, immunoglobulin domain 1

Ig2= domain 5, immunoglobulin domain 2

IKD= intracellular kinase domain

JM= extracellular juxtamembrane region

K_d= equilibrium constant for dissociation

LM22A-4= (*N,N',N'*-tris [2-hydroxyethyl])-1,3,5-benzene tricarboxamide)

LM22B-10= (2-[[4-[[4-[Bis-(2-hydroxy-ethyl)-amino]-phenyl-(4-chloro-phenyl)-methyl]-phenyl]-
(2-hydroxy-ethyl)-amino]-ethanol))

LRM= leucine-rich motif domain

mHTT= mutant huntingtin protein

NGF= Nerve growth factor

NAS= *N*-acetylserotonin

Nrf2= NF-E2-related factor-2

NT-3= neurotrophin 3

NT-4= neurotrophin 4

p75^{NTR}= p75 neurotrophin receptor

PC12= pheochromocytoma cells

PDGF= platelet-derived growth factor receptor

PLC γ = phospholipase C gamma

p-TrkB= phosphorylated TrkB

R7= 4-oxo-2-phenyl-4*H*-chromene-7,8-diyl bis(dimethylcarbamate

R13= 4-oxo-2-phenyl-4*H*-chromene-7,8-diyl bis(methylcarbamate

RAS/Raf/MAPK cascade= mitogen-activated protein kinase pathway

RTK= receptor tyrosine kinase

SAH= subarachnoid hemorrhage

SCI= spinal cord injury

SN= substantia nigra

TBI= traumatic brain injury

TMD= transmembrane domain

Trk= tyrosine kinase receptor family or tropomyosin receptor kinase family

TrkA= tropomyosin-related kinase receptor type A

TrkA-d5= domain 5 of the extracellular domain in TrkA

TrkB= tropomyosin-related kinase receptor type B

TrkB-d5= domain 5 of the extracellular domain in TrkB

TrkC= tropomyosin-related kinase receptor type C

UCP1= uncoupling protein 1

Chapter III: Assessing Lactam Ring Size in N-Acyl Serotonin Derivatives for Treating Trauma-Induced Vision Loss

¹³C NMR= carbon-13 nuclear magnetic resonance spectroscopy

CDI= carbonyldiimidazole

DCM= dichloromethane

DMF= dimethylformamide

DMSO= dimethyl sulfoxide

¹H NMR= proton nuclear magnetic resonance spectroscopy

HIOC= (*N*-[2-(5-hydroxy-1H-indol-3-yl)ethyl]-2-oxopiperidine-3-carboxamide)

LiHMDS= lithium bis(trimethylsilyl)amide

NAS= *N*-acetylserotonin

TBI= traumatic brain injury

THF= tetrahydrofuran

TLC= thin layer chromatography

TMSOK= potassium trimethylsilylanolate

TrkB= tropomyosin-related kinase receptor type B

*Chapter I: Complex Dynamics in Small Networks of Delay-Coupled Belousov-Zhabotinsky
Oscillators*

1. Introduction

In 1665, Dutch scientist Christiaan Huygens reported his observation of synchronization phenomenon in a system of two identical pendulum clocks. Synchronization is the time-correlated behavior exhibited by interacting oscillators.¹ In our daily lives, synchronization plays an important role as our circadian rhythm is synchronized to the 24 hours day-night cycle, and synchronized neurons in the olfactory bulbs help us detect and distinguish odors.²

Oscillators are systems exhibiting periodic behavior over time and exist in biological, physical, and chemical systems.³ Here, chemical oscillators, reacting chemical species in which concentrations of one or more reaction components exhibit periodic changes over time, are studied.⁴ Interesting group dynamics result when multiple oscillators are brought together or coupled and allowed to interact with each other. Studies have shown that group dynamics depend on network structure, which is how the oscillators are connected to each other, and the strength of their interactions (coupling strength).³

The breakdown of synchrony can result in complex patterns, including the loss of rhythmic behavior or the onset of critical physiological states in biological systems. In studies of neural networks, loss of or partial synchronization has been linked to various disorders, such as Parkinson's, essential tremor, and epilepsy.⁵ Researchers are currently exploring how synchronization emerges and how it is lost to search for possibilities to experimentally control synchronization behavior.⁶

Simple systems of two identical and symmetrically coupled oscillators were for a long time believed to only support dynamic behaviors, such as chaotic states,⁷ full synchronous behavior, out-of-phase synchronization,⁸ and frequency cycling.⁹ Most of these states involve both oscillators exhibiting similar behaviors. However, a relatively new type of complex synchronization dynamics known as a chimera state, which consists of coexisting subgroups exhibiting different dynamics¹⁰, has attracted significant research attention. Since their discovery in theoretical studies in 2002¹¹ and in experimental demonstration in 2012,^{12,13} chimeras have been reported in various systems including Boolean networks,¹⁴ quantum oscillators¹⁵ and time-continuous chaotic models.¹⁶

Researchers are interested in chimera states for a variety of reasons. Dolphins and some birds have unihemispheric sleep in which one hemisphere of the brain sleeps at a time, serving as a defense mechanism.¹⁷ In humans, complex interactions and the interplay of synchronization in various regions of the brain leads to a continuum between healthy and disease states and variability in task performance.¹⁸ Chimera states may play a role in understanding complex behavior, such as Parkinson's disease¹⁹ and social systems.²⁰ However, the principles and mechanisms behind the emergence of chimera behavior remain unknown.

The existence of chimera states in idealized networks of large populations of locally²¹ or globally coupled oscillators²² was the focus of early investigations. Local coupling is when an oscillator

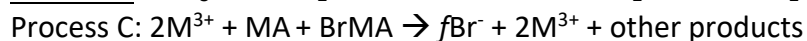
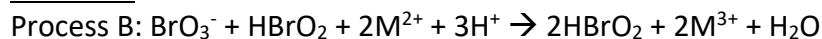
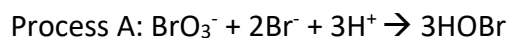
interacts with only its nearest neighboring oscillators whereas in global coupling, all oscillators are connected through the average signal of the group.³ Different topologies have also been studied in different homogeneous and heterogeneous oscillator networks.²³ Chimera and chimera-like behaviors in small networks of oscillators have been observed in theoretical studies of diffusively coupled chemical oscillator systems²⁴ and in experimental studies of coupled pendula²⁵ and optoelectronic oscillator systems.²⁶ A network of three identical oscillators with mutual all-to-all coupling exhibited three types of chimeras: in-phase, chaotic, and antiphase. In all these chimeras, two coherent oscillators coexist with an incoherent oscillator.²⁷

The smallest chemical network reported to support chimeric behavior is a system of two diffusively coupled identical Lengyel-Epstein (LE) oscillators, which models the chlorite-iodide-malonic acid reaction. One oscillator behaves nearly periodically while the other oscillator behaves chaotically.²⁴ Experimental observation of chimeras in small chemical networks remains an open research question.

Incorporating time-delay in simulations of coupled nonlinear oscillator systems more realistically models various dynamical biological, chemical, and physical systems.²⁸ In nature, time-delay is associated with finite reaction times of chemicals, latency times of neuronal excitations, and finite propagation velocities of information signals. Time-delay has been shown to serve as a powerful control mechanism that either stabilizes or destabilizes chimera patterns.²⁹

In this work, we utilize the Belousov-Zhabotinsky (BZ) chemical oscillator, which was first discovered by Boris Belousov when he was attempting to model Krebs Cycle and continued by Anatol Zhabotinsky.³⁰ The reaction involves a complex reaction mixture in which concentrations of chemical species exhibit periodic change and has been used with great success to model various biological phenomena, including spiral wave phenomenon in slime mold.³¹

Numerous models have been proposed to explain the experimental behavior of the BZ system. In 1972, Field, Körös, and Noyes proposed the FKN Mechanism to understand the BZ reaction chemistry. The mechanism includes 21 intermediate species and 80 elementary steps. The elementary steps can be summed up by processes A through C, which occur in a cycle where the process with the dominating rate law constant occurs and where f is the stoichiometric coefficient and M is the metal catalyst.^{31,32}



In Process A, bromide reacts with bromate to produce bromous acid as the intermediate species. When the concentration of bromide falls below a critical level, process B is initiated in which bromous acid is autocatalytically produced. Bromous acid oxidizes the metal catalyst from a reduced +2 state to an oxidized +3 state in ferriin and ruthenium catalyzed reactions.

Once the catalyst is in its oxidized state, process C begins in which the organic species are oxidized to form bromide ion and other products. The metal catalyst is reduced, and this increases the concentration of bromide, resetting the clock.⁴ Bromous acid generally acts as an activator and bromide as an inhibitor. Increasing the concentration of an activator shortens the oscillation period whereas increasing concentration of inhibitory species lengthens the period.

We investigate chimera and other complex dynamics in small networks of Belousov-Zhabotinsky (BZ) oscillators to explore the necessary conditions for supporting these behaviors. A three-oscillator network is used to study the effects of time-delay and network structure experimentally. The effects of time-delay, initial conditions, and heterogeneity are studied theoretically using a two-oscillator network. A non-dimensional, two-variable ZBKE model of the BZ reaction is used to examine and compare the dynamics of delay-coupled homogeneous and heterogeneous oscillators.

2. Three Oscillator System

Prior to the COVID-19 pandemic in March 2020, I worked on observing chimera states experimentally in small networks of coupled BZ chemical oscillators. This project focused on the effect of network structure, specifically linear and triangular networks, and time-delay coupling on the emergence of complex behavior in a three BZ oscillator network. The two network topologies differed in the way the oscillators interacted with each other. In a linear network structure, the behavior of the central oscillator was influenced by the two outer oscillators whereas in the triangular network structure, all three oscillators interacted with each other. From these studies, we hoped to gain insights in the factors that support chimera state behavior in small chemical oscillator networks.

2.1 Experimental Approach

2.1.1 Preparing Oscillators and BZ Solution

BZ chemical oscillators were prepared by mixing 3.0 grams of Dowex 50WX2 cation exchange beads with 5.0 mL of 25 mM 1,10-phenanthroline solution. The mixture was stirred for 3 hours, filtered to collect the catalyst loaded beads, and dried for 48 hours. Ferroin catalyst was chosen given the two distinct colors for its oxidized and reduced forms, which were used in image processing, and bioavailability of Fe(II) in living systems.³³ The catalyst-loaded beads were used as independent oscillators. The catalyst-free BZ solution was prepared by mixing 0.82M NaBrO₃, 0.12M C₃H₄O₄, 0.84M H₂SO₄, and 0.06M NaBr.

2.1.2 Arrange Oscillators into Desired Network Structure in BZ Solution

Chemical oscillators were initially placed in the BZ solution such that they were touching each other. After allowing the oscillators to influence each other to a similar period, the three oscillators were arranged into either a linear or triangular network structure (**Figure 1**). Oscillators interacted with each other through the diffusion of chemical species, and the time taken by the chemical species to reach the other oscillator induced a time-delay response dependent on the distance between oscillators.

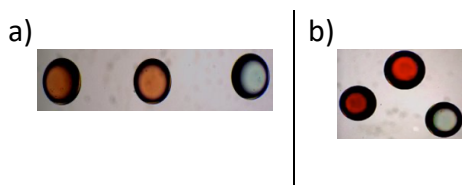


Figure 1: Oscillators arranged in a) linear network or b) triangular network.

2.1.3 Image Capture and Analysis

Images of the oscillations exhibited by the BZ chemical oscillators were captured every 3 seconds over a period of 50 minutes (**Figure 2**). The images were analyzed in MATLAB to extract period and phase information. The intensity in the color of the images was correlated to concentration. Period was defined as the distance from one oscillation peak to the next peak or time for a complete cycle of oscillations. Phase, which is a measure of how far along the oscillator is in a cycle of an oscillation from 0 to 2π , was determined by linear interpolation between the peaks.

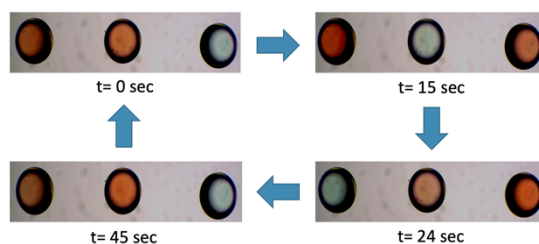


Figure 2: Cycle of oscillations in the ferroin-catalyzed BZ system.

2.2 Experimental Results

Chemical oscillators exhibited in-phase synchronization and period cycling behaviors. During in-phase synchronization, the oscillation peaks of each oscillator aligned, and the maximum amplitude of the normalized mean intensity signal was 1. The oscillators had about the same phase and period (**Figure 3**). The mean signal of the oscillators appeared the same as the signal of the individual oscillators because the oscillators were exhibiting the same behavior. Thus, their average signal was the same as that of the individual oscillator. In-phase synchronization was frequently observed in triangular networks with oscillators very close to each other.

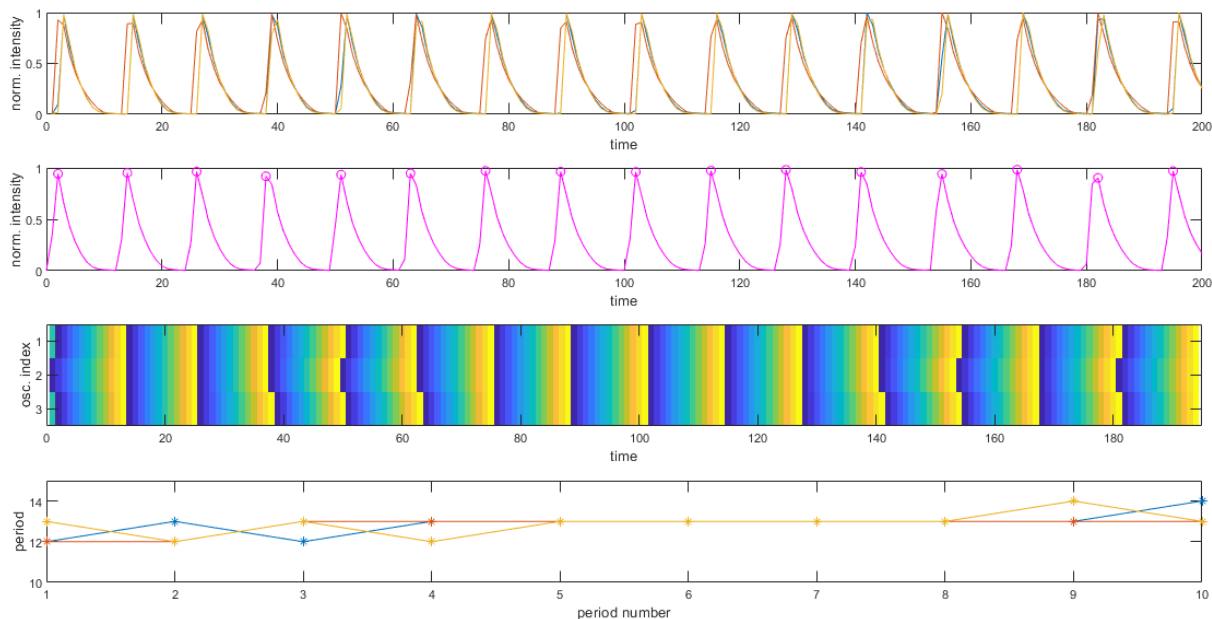


Figure 3: Normalized intensities of individual oscillators, mean intensity of oscillators, and phase and period evolution during in-phase synchronization.

In linear networks, period cycling behavior was frequently observed regardless of the distance between the oscillators. In period cycling behavior, the oscillation peaks of the oscillators were not aligned with each other. The oscillators perturbed each other's cycles differently each time, causing mixed effects of period lengthening and shortening. This resulted in a mean signal with varying amplitudes (**Figure 4**).

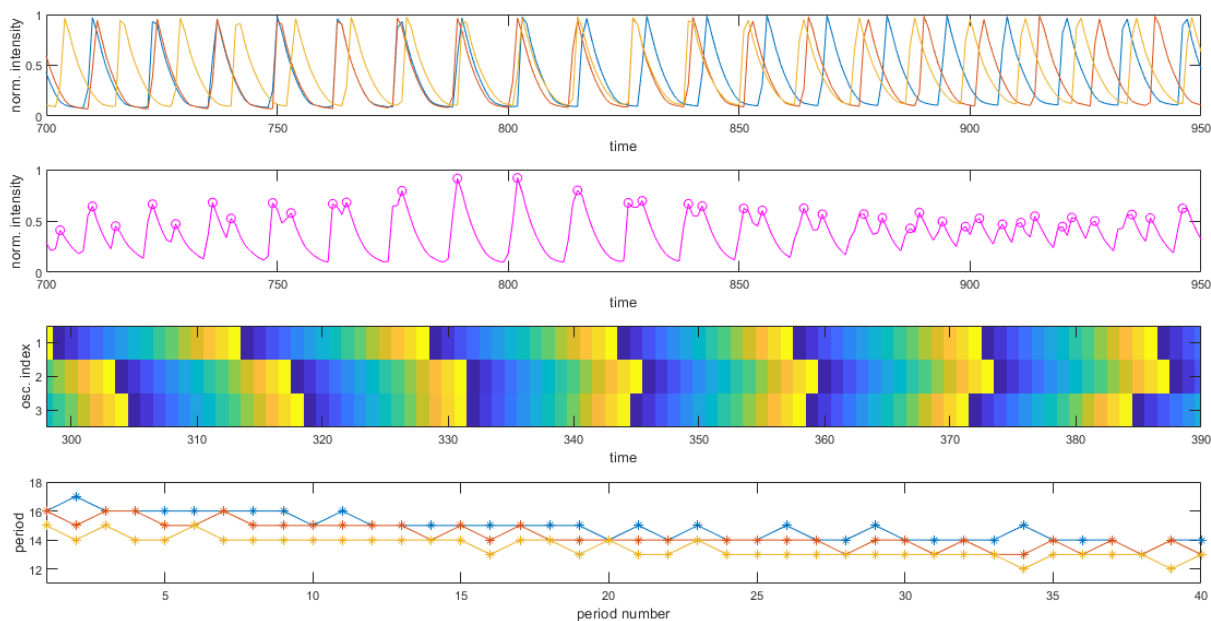


Figure 4: Normalized intensities of individual oscillators, mean intensity of oscillators, and phase and period evolution during period cycling behavior.

3. Two Oscillator System

As we did not observe chimera states experimentally in the three oscillator system, we continued the search for chimera states theoretically. The effects of time-delay, initial conditions, and heterogeneity using a two-oscillator network were investigated. By studying the dynamics of two oscillators, we eliminate the effect of network structure, reducing the number of factors to consider.

3.1 Model Setup

We considered oscillator systems of $N=2$ homogeneous and heterogeneous BZ oscillators. Numerical simulations were carried out using a modified Zhabotinsky-Buchholtz-Kiyatkin-Epstein (ZBKE) Model based on the photosensitive ruthenium-catalyzed BZ system³⁴:

$$\begin{aligned}\frac{dx}{d\tau} &= \frac{1}{\epsilon_1} \left(\varphi - x^2 - x + \epsilon_2 \gamma u_{ss}^2 + u_{ss}(1-z) + \frac{\mu-x}{\mu+x} \left(\frac{q\alpha z}{\epsilon_3+1-z} + \beta \right) \right) \\ \frac{dz}{d\tau} &= 2\varphi + u_{ss}(1-z) - \frac{\alpha z}{\epsilon_3+1-z}\end{aligned}$$

where q was the stoichiometric coefficient, and x and z were the dimensionless concentrations of HBrO_2 and $\text{Ru}(\text{bby})^{3+}$, respectively. The ZBKE model parameter values were $\epsilon_1=0.11$, $\epsilon_2=1.7 \times 10^{-5}$, $\epsilon_3=1.6 \times 10^{-3}$, $\alpha=0.1$, $\beta=1.7 \times 10^{-5}$, $\gamma=1.2$, $\mu=2.4 \times 10^{-4}$, and $q=0.02$. u_{ss} was the steady-state concentration of HBrO_2^+ , and φ was the coupling term.³⁵

The ruthenium-catalyzed BZ model was utilized in simulations to explore coupling through a light feedback mechanism. The mechanism has been previously used in experimental studies of coupled oscillators. Depending on the concentrations of the reactive species and the light intensity, illumination of the reaction led to inhibition or acceleration of the autocatalytic reaction step (process B).³⁶

Simulations ran for approximately 2000 periods using the Euler method with a time step of 0.001. We explored the dynamics by varying the initial phase difference (IPD), coupling strength (σ) and time-delay (τ). For each coupling strength and time-delay combination, 50 simulation trials were conducted. The oscillators were coupled via delay signals of each other as shown below:

$$\begin{aligned}\varphi_1(t) &= \sigma[z_2(t-\tau) - z_1(t)] \\ \varphi_2(t) &= \sigma[z_1(t-\tau) - z_2(t)]\end{aligned}$$

Oscillator 1 started from random initial conditions, whereas the initial conditions for oscillator 2 were determined by the chosen phase difference. The initial phase difference (IPD) was varied from 0 to 1.18π (**Figure 5**).

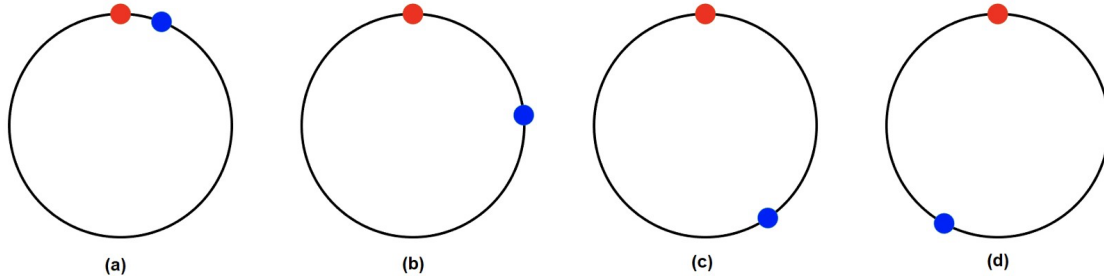


Figure 5: Initial phase difference (IPD) between two oscillators: (a) $IPD=0.12\pi$; (b) $IPD=0.47\pi$; (c) $IPD=0.81\pi$; (d) $IPD=1.18\pi$. Blue, oscillator 1; red, oscillator 2.

3.2 Simulation Results

3.2.1 Homogeneous Oscillators

Homogeneous oscillators had the same initial period. We analyzed the effect of coupling strength, time-delay, and initial phase difference by varying each of these parameters. Once the system had stabilized, the resulting states were characterized using plots of period, time series, and phase evolution. Simulations demonstrated that the final state— in-phase or out-of-phase— of the system depended on the initial phase difference (IPD), but the final period was insensitive to IPD.

In-phase and out-of-phase synchronization behaviors were observed at different values of time-delay τ . With in-phase synchronization, the oscillators were phase and frequency locked as shown in **Figure 6a**, whereas in the out-of-phase state, the two oscillators were π out of phase and had the same period. In the in-phase state, both oscillators had a period of 34.90, which was longer than the natural period of 34.40 (**Figure 6a**). For the out-of-phase state, the oscillators had the same period of 34.50, as illustrated by single dot in the next period plot (**Figure 6b**). Time-delay determined whether the period of the synchronized group was longer or shorter than the natural period. Once the system settled in each of these states, the behavior lasted for the duration of the simulations.

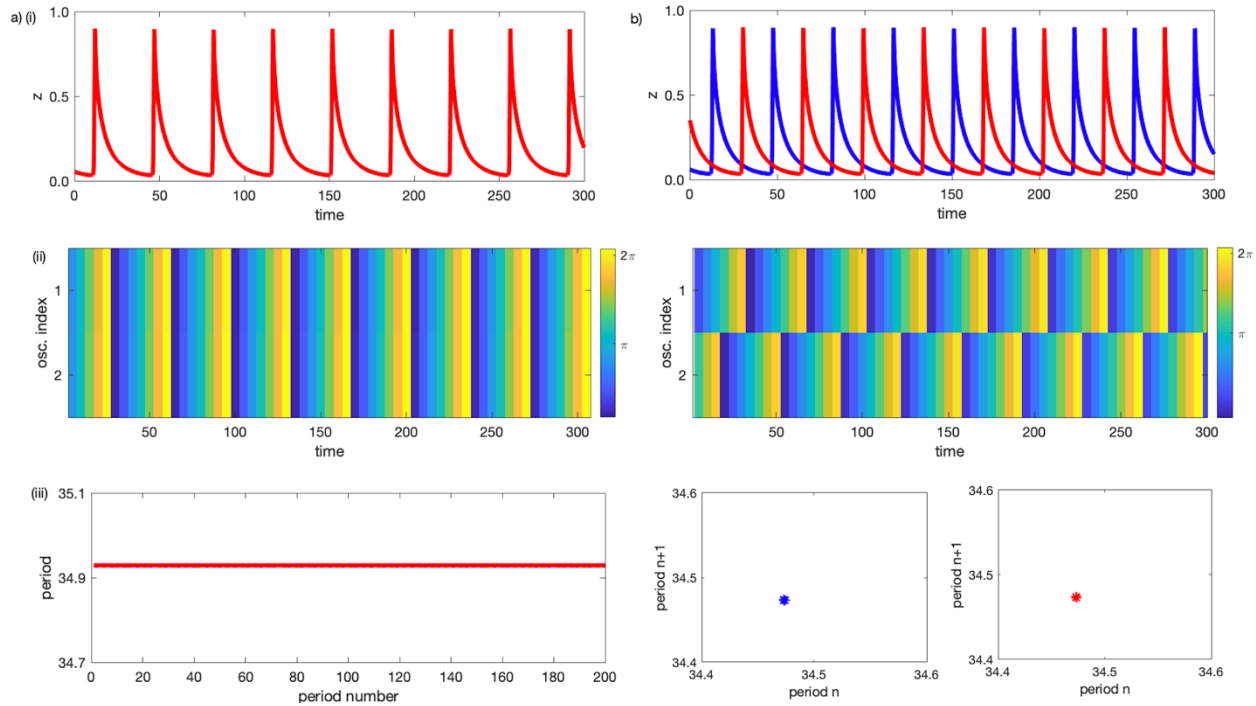


Figure 6: Time series (top panel), phase evolution (middle panel), and period evolution or next period graphs (bottom panel) for 2 homogeneous oscillators. (a) In-phase synchronization; (b) Out-of-phase synchronization. Blue, oscillator 1; red, oscillator 2.

Figure 7 summarizes the behaviors observed in simulations with homogeneous oscillators as σ and τ were varied. In-phase synchronization, represented by the blue region, was observed at $\tau = 3-13$ at low and high coupling and $\tau = 7-12$ for moderate coupling. Out-of-phase synchronization, shown by the red region, was observed at $\tau = 21-30$ with lower σ and $\tau = 22-25$ with stronger coupling. The narrowing of this region meant that increasing coupling strength increased the stability of the in-phase state. The light-green region between the in-phase and out-of-phase behaviors was the region of bistability and was the most prevalent behavior observed in the homogeneous oscillator system. In this region, simulations led to either the in-phase or out-of-phase synchronized state, depending on initial conditions. For $\tau = 1-5$ and $13-25$, the range of τ values for which bistability existed became narrower with increasing coupling strength. Thus, τ can be used to control the occurrence of in-phase and out-of-phase synchronization behaviors in the homogeneous system.

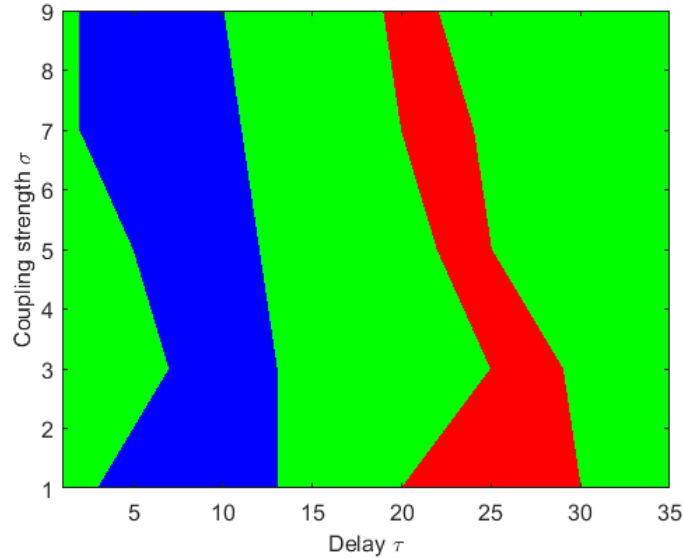


Figure 7: In-phase synchronization (blue), out-of-phase synchronization (red), and bistability region (light green) in the parameter plane (τ, σ) of the homogeneous oscillator system with initial phase differences of 0.11π and 0.93π .

3.2.2 Heterogeneous Oscillators

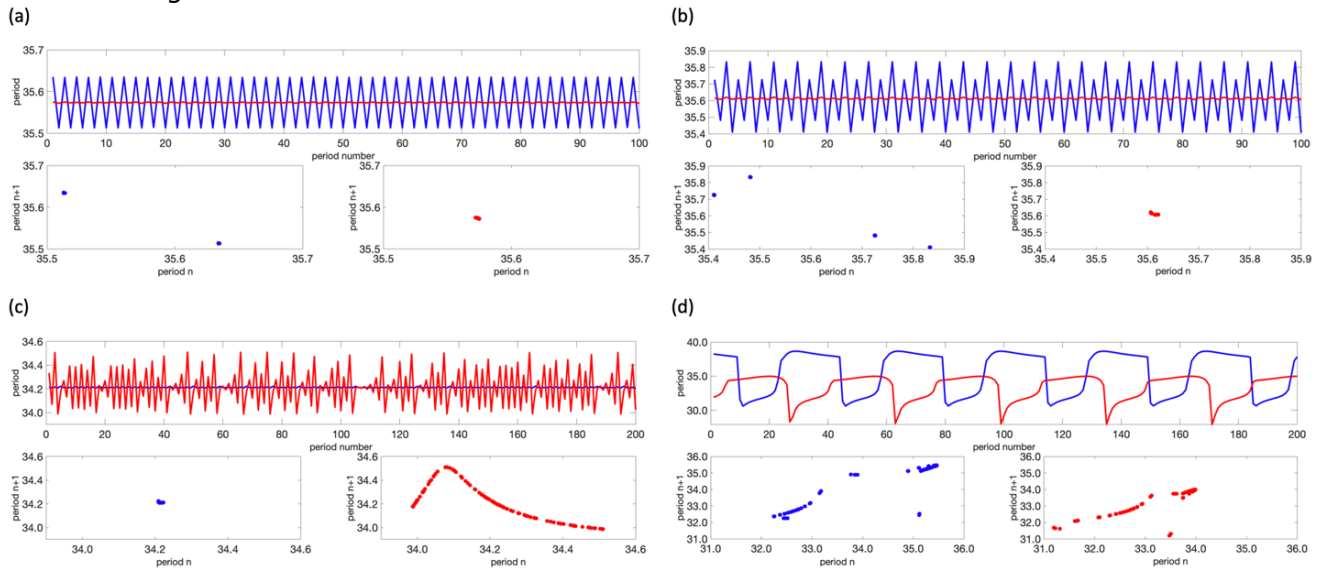


Figure 8: Period evolution (top panel) and next-period graphs (bottom panel) for 2 heterogeneous oscillators. Blue, oscillator 1; red, oscillator 2. (a) Mixed period state with period-2 oscillations; (b) Mixed period state with period-4 oscillations; (c) Chaotic chimera; (d) Period cycling.

In the heterogeneous system, oscillators had different natural periods. Periods were generated using random selections of values of parameter q in the ZBKE model from a Gaussian distribution with a standard deviation of 0.02. **Figure 8** shows the behaviors, in addition to the in-phase and out-of-phase synchronization, observed in the heterogeneous system. The behaviors that lasted for more than 1500 periods were characterized using period evolution and period return maps. We generalized the observed behaviors as mixed period states as the oscillators exhibited more than one period. The states were further characterized into mixed period, chaotic chimera, and period cycling.

Figure 8a shows a mixed period state in which oscillator 1 exhibited period-2 oscillations while oscillator 2 had period-1 oscillations. The period of oscillator 1 fluctuated between 35.51 and 35.63 while oscillator 2 oscillated with an almost constant period of 35.58. The phase difference between the oscillators when the period was 35.51 as 0.71π , which was less than 1.29π , occurring when the period was 35.63. This behavior was observed with parameter values of $\sigma=3$ and $\tau=13, 15, 23, 24,$ and 31 .

Another mixed period state had oscillators 1 and 2 exhibiting period-4 and period-1 oscillations, respectively (**Figure 8b**). This state occurred least frequently among the four behaviors characterized in **Figure 8**. Examples of this behavior were seen with $\sigma=3$ and 5 and $\tau=13, 19,$ and 23 .

Figure 8c shows an example of a chaotic chimera, which was characterized by the aperiodic behavior of one oscillator while the other oscillator maintained a regular period.^{22,25} The next-period plot of oscillator 1 showed a point, which denoted a constant period of 34.22. The plot of oscillator 2 showed a distribution of periods because of its aperiodic behavior. The chaotic chimera state was found at an intermediate coupling of $\sigma=3$ and $\tau=16-24$.

The last type of behavior observed was period cycling (**Figure 8d**). Period cycling was characterized by a broad distribution of points in the next-period graphs and a regular periodic pattern in the period plot. In this state, both oscillators cycled through a series of shorter and longer periods. The oscillators were mostly out-of-phase. The period cycling behavior was mostly observed at $\tau=11-14$ and $29-30$ regardless of coupling strength.

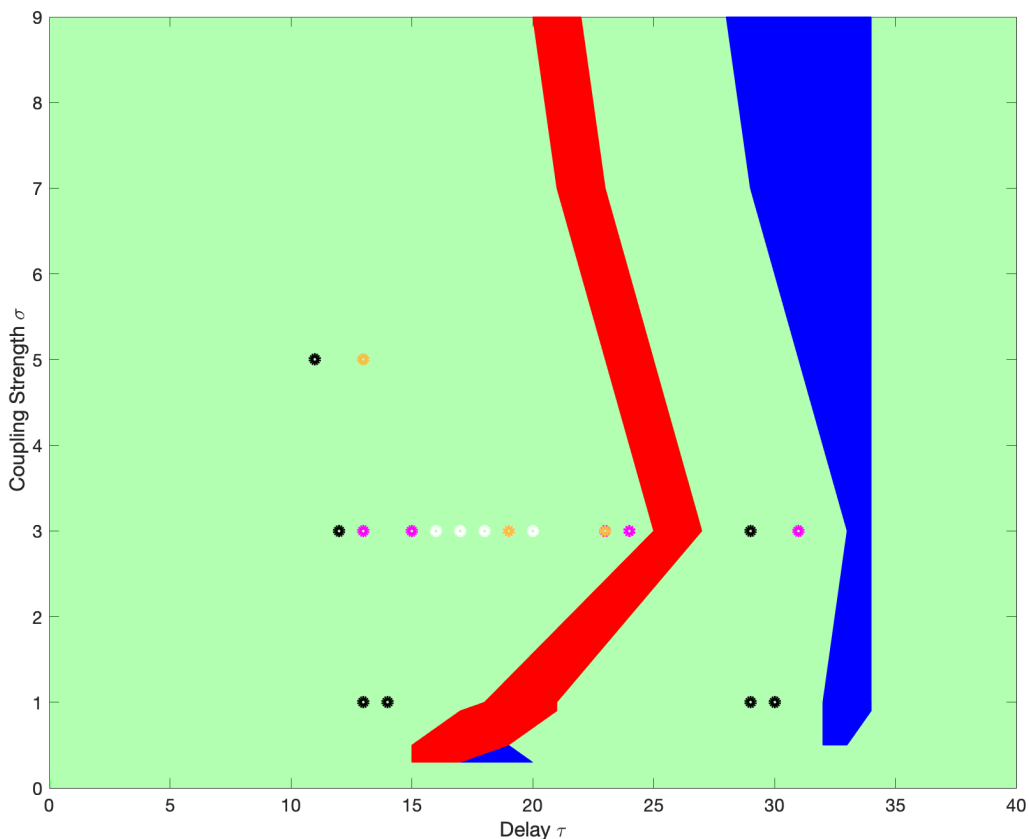


Figure 9: In the parameter plane (τ, σ) of the heterogeneous oscillator system for different values of heterogeneity: in-phase synchronization (blue), out-of-phase synchronization (red), and multi-states region (light green). Mixed period state with period-2 oscillations (magenta dot), mixed period state with period-4 oscillations (orange dot), chaotic chimera (white dot), and period cycling behavior (black dot).

Multi-states, represented by the light green region in **Figure 9**, was the most dominant feature of the heterogeneous oscillator system. Within the multi-states region, occurrence of in-phase and out-of-phase synchronization depended on time-delay, coupling strength, and heterogeneity. Out-of-phase synchronization was found at $\tau= 15-25$ at $\sigma= 0.3-3.0$ and $\tau= 20-25$ at $\sigma= 3.0-9.0$. Increasing coupling strength broadened the range of time-delays at which in-phase synchronization was observed as shown in the blue region of **Figure 9**. Time-delays in which oscillators were synchronized in-phase were $\tau= 28-34$.

The behaviors summarized in **Figure 8** (page 9) occurred in the region of multi-states at $\sigma = 0.3$ and $\tau= 19$ and $23-24$ and was represented by overlaying colored dots in **Figure 8**. Mixed period state with period-4 oscillations and chaotic chimera were observed at $\tau = 19$. At $\tau= 23$, chaotic chimera and both types of mixed period states were found. In addition to chimeric behavior, mixed periods behavior with period-2 oscillations occurred at $\tau= 24$ (**Figure 9**).

Our demonstration of the simplest BZ network that supported chimera and other complex behaviors using a realistic model of an experimental system provides a foundation for seeking experimental evidence in simple chemical networks. In summary, we conclude that the

appropriate choice of coupling strength and time-delay in the heterogenous oscillator system is important for observing the different types of behaviors.

4. Conclusion

Chimera states are found in many biological, physical, and chemical systems. Their applications to natural phenomena include the ability of some mammals to cease activity in one hemisphere of the brain while the other hemisphere remains active during sleep.³⁷ While most chimera state studies have focused on chimeras in large oscillator networks, this study examines the smallest BZ network. Using a simple network allows us to focus on the behavior of individual oscillators and understand the mechanism that is driving the occurrence of complex behavior.

In experiments, in-phase synchronization is observed in both the linear and triangular network structures (**Figure 3**, page 5). In linear networks, period cycling is found in which oscillators are in and out of synchronization and had different phase and period (**Figure 4**, page 5). Both experiments and simulations show that small BZ chemical oscillator systems could support in and out-of-phase synchronization and period cycling patterns. Complex periodic patterns are mostly found in linear network structures and systems with long time-delays.

In simulations, our analysis shows that the appropriate choice of time-delay and coupling strength leads to in-phase and out-of-phase synchronization in the homogeneous system. Final behavior of the oscillators was dependent on the initial phase difference. In the heterogeneous system, additional behaviors of mixed period, chaotic chimera, and period cycling behaviors, are observed (**Figure 8**, page 9). Complex patterns and chaotic chimera are seen with moderate coupling strength and moderate time-delays while period cycling is observed at all coupling strengths but only at moderate time-delays. Strong coupling leads to in-phase synchronization in both homogeneous and heterogeneous oscillator systems (**Figure 7**, page 9 and **Figure 9**, page 11), and heterogeneity contribute to the emergence of chimera states, which are not observed in homogeneous oscillators.

Based on our simulation studies, complex patterns frequently occur in regions where the stability of the system switches from one behavior to another. For example, as time-delay is varied, we explored the region where the behavior switches from in-phase to out-of-phase synchronization. This region may be very small, so large changes in time-delay or other parameters may result in complex patterns being inadvertently missed. The narrow region of occurrence for complex patterns could be the reason behind non-observance of chimera states in the three oscillator experiments. To observe complex dynamics, regions where the behavior changes should be identified and the parameters for this region should be adjusted in small increments within this region. This approach will improve the chances of finding these states in experiments.

5. References

1. Rosenblum, M.; Pikovsky, A. Synchronization: From pendulum clocks to chaotic lasers and chemical oscillators. *Contemp. Phys.* **2003**, *44*, 401-416.
2. Steur, E. Synchronous behavior in networks of coupled systems: with applications to neuronal dynamics. *Technische Universiteit Eindhoven.* **2011**, 1-102.
3. Pikovsky, A.; Rosenblum, M.; Kurths, J. *Synchronization A Universal Concept in Nonlinear Sciences*; Cambridge University Press: New York, NY; **2003**, pp 8-12, 328-329.
4. Taylor A. Mechanism and Phenomenology of an Oscillating Chemical Reaction. *Prog. React. Kinet.* **2002**, *27*, 247-325.
5. Uhlhaas, P.J.; Singer, W. Neuronal synchrony in brain disorders: relevance for cognitive dysfunctions and pathophysiology. *Neuron.* **2006**, *52*, 155-168.
6. Ke, H.; Tinsley, M.R.; Steele, A.; Wang, F.; Showalter, K. Link weight evolution in a network of coupled chemical oscillators. *Phys. Rev. E.* **2014**, *89*, 1-4.
7. Crowley, M.F.; Epstein, I.R. Experimental and theoretical studies of a coupled chemical oscillator: phase death, multistability and in-phase and out-of-phase entrainment. *J. Phys. Chem.* **1989**, *93*, 2496-2502.
8. Dolnik, M.; Epstein, I.R. Coupled chaotic chemical oscillators. *Phys. Rev. E.* **1996**, *54*, 3361-3368.
9. Yengi, D.; Tinsley, M.R.; Showalter, K. Autonomous cycling between excitatory and inhibitory coupling in photosensitive chemical oscillators. *Chaos.* **2018**, *28*, 1-11.
10. Abrams, D.M.; Strogatz, S.H. Chimera states for coupled oscillators. *Phys. Rev. Lett.* **2004**, *93*, 1-4.
11. Kuramoto, Y.; Battogtokh, D. Coexistence of Coherence and Incoherence in Nonlocally Coupled Phase Oscillators. *ArXiv preprint cond-mat/0210694.* **2002**, 1-17.
12. Tinsley, M.R.; Nkomo, S.; Showalter, K. Chimera and phase-cluster states in populations of coupled chemical oscillators. *Nat. Phys.* **2012**, *8*, 662-665.
13. Hagerstrom, A.M.; Murphy, T.E.; Roy, R.; Hövel, P.; Omelchenko, I.; Schöll, E. Experimental observation of chimeras in coupled-map lattices. *Nat. Phys.* **2012**, *8*, 658-661.
14. Rosin, D.P.; Rontani, D.; Gauthier, D.J.; Schöll, E. Experiments on autonomous Boolean networks. *Chaos.* **2013**, *23*, 1-9.
15. Bastidas, V.; Omelchenko, I.; Zakharova, A.; Schöll, E.; Brandes, T. Quantum signatures of chimera states. *Phys. Rev. E.* **2015**, *92*, 1-8.
16. Omel'chenko, O.E.; Wolfrum, M.; Yanchuk, S.; Maistrenko, Y.L.; Sudakov, O. Stationary patterns of coherence and incoherence in two-dimensional arrays of non-locally-coupled phase oscillators. *Phys. Rev. E.* **2012**, *85*, 1-5.
17. Lesku, J.A.; Martinez-Gonzalez, D.; Rattenborg, N.C. *The Neuroscience of Sleep*; Elsevier, **2009**, pp. 61-69.
18. Bansal, K.; Garcia, J.O.; Tompson, S.H.; Verstynen, T.; Vettel, J.M.; Muldoon, S.F. Cognitive chimera states in human brain networks. *Cogn. Neurosci.* **2019**, *5*, 1-14.
19. Levy, R.; Hutchison, W.D.; Lozano, A.M.; Dostrovsky, J.O. High-frequency synchronization of neuronal activity in the subthalamic nucleus of parkinsonian patients with limb tremor. *J Neurosci.* **2000**, *20*, 7766-7775.
20. González-Avella, J.C.; Cosenza, M.G.; Miguel, M.S. Localized coherence in two interacting populations of social agents. *Physica.* **2014**, *24*, 1-6.
21. Bera, B.K.; Ghosh, D.; Parmananda, P.; Ospio, G.; Dana, S.K. Coexisting synchronous and asynchronous states in locally coupled array of oscillators by partial self-feedback control. *Chaos.* **2017**, *27*, 1-13.
22. Yeldesbay, A.; Pikovsky, A.; Rosenblum, M. Chimera-like states in an ensemble of globally coupled oscillators. *Phys. Rev. E.* **2014**, *112*, 1-5.
23. Hizanidis, J.; Lazarides, N.; Neofotistos, G.; Tsironis, G. Chimera states and synchronization in magnetically driven SQUID metamaterials. *Eur. Phys. J. Spec. Top.* **2016**, *225*, 1231-1243.
24. Awal, N.M.; Bullara, D.; Epstein, I.R. The smallest chimera: Periodicity and chaos in a pair of coupled chemical oscillators. *Chaos.* **2019**, *29*, 1-12.
25. Kapitaniak, T.; Kuzma, P.; Wojewoda, J.; Czolczynski, K.; Maistrenko, Y. Imperfect chimera states for coupled pendula. *Sci. Rep.* **2014**, *4*, 1-4.
26. Hart, J.D.; Bansal, K.; Murphy, T.E.; Roy, R. Experimental observation of chimera and cluster states in a minimal globally coupled network. *Chaos.* **2016**, *26*, 1-8.

27. Maistrenko, Y.; Brezetsky, S.; Jaros, P.; Levchenko, R.; Kapitaniak, T. Smallest chimera states. *Phys. Rev. E* **2017**, *95*, 1-5.
28. Schuster, H. G.; Wagner, P. *Prog. Theor. Phys.* **1989**, *81*, 939-945; Niebur, E.; Schuster, H. G.; Kammen, D. M. *Phys. Rev. Letter.* **1991**, *67*, 2753-2757; Kim, S.; Park, S. H.; Ryu, C. *Phys. Rev. Letter.* **1997**, *79*, 2911-2914; Ramanda Reddy, D. V.; Sen, A.; Johnston, G. L. *Phys. Rev. Letter.* **1998**, *80*, 5109-5112; Yeung, S.; Strogatz, S. H. *Phys. Rev. Letter.* **1999**, *82*, 648-651; Ramanda Reddy, D. V.; Sen, A.; Johnston, G. L. *Phys. Rev. Letter.* **2000**, *85*, 3381-3384; Atay, F. M. *Phys. Rev. Letter.* **2003**, *91*, 1-4; Dodla, R.; Sen, A.; Johnston, G. L. *Phys. Rev. Letter.* **2004**, *69*, 1-12.
29. Sawicki, J.; Omelchenko, I.; Zakharova, A.; Schöll. Chimera states in complex networks: interplay of fractal topology and delay. *Eur. Phys. J. Special Topics.* **2017**, *226*, 1883-1892.
30. Pellitero, M.; Lamsfus, C.; Borge, J. The Belousov-Zhabotinskii Reaction: Improving the Oregonator Model with the Arrhenius Equation. *J. Chem. Educ.* **2013**, *90*, 82-89.
31. Szabo, E. Oregonator generalization as a minimal model of quorum sensing in Belousov-Zhabotinsky reaction with catalyst confinement in large populations of particles. *RSC Advances.* **2015**, *120*, 99547-99554.
32. Noyes, R.M.; Field, R; Körös, E. Oscillations in chemical systems. I. Detailed Mechanism in a system showing temporal oscillations. *J. Am. Chem. Soc.* **1972**, *94*, 8649-8664.
33. Riyaz, S.; Peerzada, G.M.; Ganaie, N.B.; Gull, U. Kinetics of the acetaminophen-based oscillatory chemical reaction with and without ferrioxalate as catalyst: an inorganic prototype model for acetaminophen-ethanol syndrome. *Prog. React. Kinet.* **2017**, *42*, 163-181.
34. Zhabotinsky, A.M.; Buchholtz, F.; Kiyatkin, A.B.; Epstein, I.R. Oscillations and waves in metal-ion-catalyzed bromate oscillating reactions in highly oxidized states. *J. Phys. Chem.* **1993**, *97*, 7578-7584.
35. Kádár, T.; Amemiya, T.; Showalter, K. Reaction Mechanism for Light Sensitivity of the Ru(bpy)₃²⁺-Catalyzed Belousov-Zhabotinsky Reaction. *J. Phys. Chem. A.* **1997**, *101*, 8200-8206.
36. Roth, R.; Taylor, A.F. The Tris (2,2'-Bipyridyl)Ruthenium-Catalyzed Belousov-Zhabotinsky Reaction. *Prog. React. Kinet.* **2006**, *31*, 59-115.
37. Rattenborg, N.C.; Amlaner, C.J.; Lima, S.L. Behavioral, neurophysiological and evolutionary perspectives on unihemispheric sleep. *Neurosci. Biobehav. Rev.* **2000**, *24*, 817-842.

Chapter II: Structural Aspects of Binding Interactions with Tropomyosin Receptor Kinase B (TrkB)

1. Introduction

Neurotrophins are a class of closely-related proteins initially identified for their critical role in the development, regeneration, and maintenance of the central and peripheral nervous systems. Over 60 years ago, Rita Levi-Montalcini, Victor Hamburger, and Stanley Cohen discovered nerve growth factor (NGF), the first of four mammalian neurotrophins. This finding prompted the search for other neurotrophins that could regulate neuronal survival and differentiation in the central nervous system. In 1982, Yves-Alain Barde purified brain-derived neurotrophic factor (BDNF) from pig brain. BDNF has subsequently been shown to promote sensory neuron survival and together with NGF affects neuronal survival.¹

Eight years later, researchers discovered neurotrophin 3 (NT-3) and neurotrophin 4 (NT-4), the last two members of the mammalian neurotrophin family. All four neurotrophins are structurally and functionally related and are initially synthesized as proneurotrophins and cleaved to form mature neurotrophins. Mature neurotrophins bind to members of the tyrosine kinase receptor/tropomyosin receptor kinase family (Trk) and p75 neurotrophin receptor (p75^{NTR}) to activate cellular signaling to support the growth and differentiation of developing neurons and act on neurons implicated by neurodegenerative diseases and psychiatric pathologies.¹

The first reported neurotrophin receptor (75-kiloDalton pan-neurotrophin receptor or p75^{NTR}) was discovered as the receptor for the human nerve growth factor (NGF).² p75^{NTR} is expressed in the nervous system, which includes spinal motor neurons and brain stem motor nuclei, during development.² Tropomyosin receptor kinases (Trk) are cell-surface, transmembrane proteins crucial for cell survival and differentiation. The extracellular domain of each Trk receptor is targeted by specific neurotrophins, promoting Trk receptor dimerization and activating phosphorylation pathways within the intracellular domain.³

Tropomyosin receptor kinase A (TrkA) is expressed in sympathetic, trigeminal, and dorsal root ganglia and in cholinergic neurons of the basal forebrain and striatum.^{3,4} TrkB is located in the central and peripheral nervous system,^{4,5} whereas TrkC is expressed in mammalian neural tissues.⁶ The four mammalian neurotrophins— NGF, BDNF, NT-3, NT-4— bind with similar affinity to p75^{NTR} but bind selectively with each Trk receptor (Table 1).⁷

Table 1. Neurotrophin binding with receptors.⁷

receptors	mammalian neurotrophins, IC ₅₀			
	NGF	BDNF	NT-3	NT-4
p75 ^{NTR}	Low-affinity binding	Low-affinity binding	Low-affinity binding	Low-affinity binding
TrkA	IC ₅₀ = 62 pM	---	IC ₅₀ = 20 nM	---
TrkB	---	IC ₅₀ = 81 pM	IC ₅₀ = 18 nM	IC ₅₀ = 200 pM
TrkC	---	---	IC ₅₀ = 95 pM	---

Abbreviations: nerve growth factor (NGF); brain-derived neurotrophic factor (BDNF); neurotrophin 3 (NT-3); neurotrophin 4 (NT-4); p75^{NTR} (75 kiloDalton pan neurotrophin receptor); tropomyosin receptor kinase (Trk); tropomyosin receptor kinase A (TrkA); tropomyosin receptor kinase B (TrkB); tropomyosin receptor kinase C (TrkC).

The ability for neurotrophins to prevent or reverse the degeneration of neurons, promote neurite regeneration, and enhance synaptic plasticity highlights their potential as a primary or adjunctive therapy for various neurological disorders. Altered BDNF expression and TrkB signaling is correlated with numerous pathological conditions, including traumatic brain injury, Rett Syndrome, Huntington Disease, and Alzheimer's Disease. BDNF/TrkB dysregulation leads to degenerative and behavioral changes in the brain and changes in cellular proliferation.⁸ Upregulation of TrkB signaling is observed in the pathogenesis of cancer and metabolic diseases, while the downregulation of TrkB signaling has implications in neurodegenerative diseases and some psychiatric disorders.⁹

However, neurotrophins have limited therapeutic potential due to their short *in vivo* half-life. As TrkB and TrkC are distributed throughout motor neurons, a vast expanse of tissue needs to be crossed, limiting pharmacological selectivity. Additionally, as NT-3 binds TrkC and p75^{NTR}, neurotrophin therapies may inadvertently target p75^{NTR}.¹⁰ Thus, non-peptide, small TrkB ligands may activate TrkB signaling with high potency and specificity and optimized blood-brain barrier penetration and pharmacological properties.

This review will begin by describing similarities and differences between neurotrophin and Trk receptor binding, and then describe how this information pertains specifically to small molecule activators of TrkB, which act on binding sites in the extracellular domain of the receptor. Tyrosine kinase inhibitors, specifically of Trk receptors, involve interactions of small molecule drugs with the intracellular domain, and have been recently reviewed.¹¹

2. Neurotrophin and Trk Receptor Structures

Neurotrophins are small globular proteins, with significant conservation of amino acids in the primary sequences, that favor dimeric structures.^{12,13} They share a secondary structure of 8 β -strands, with a cystine knot drawing together 2 cysteine residues between 2 other cysteine bridges (**Figure 1**).¹³ Neurotrophins are overall positively charged, with more cationic lysine and arginine residues than anionic aspartate and glutamate groups.¹²

	NGF, 120 aa 26 kD	BDNF, 119 aa 27.8 kD	NT-3, 119 aa 22.4 kD	NT-4, 130 aa 27.2 kD
conserved cystine links	C15-C80 C58-C108 C68-C110	C13-C80 C58-C109 C68-C111	C14-C79 C57-C108 C67-C110	C17-C90 C61-C119 C78-C121
charge at pH 8.4	+5	+10	+7	+3

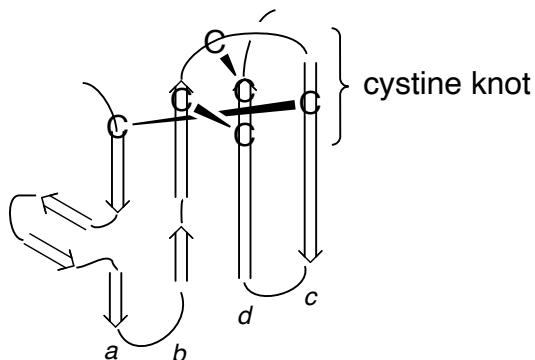


Figure 1: Conserved structure of neurotrophins.

Selective binding of each neurotrophin with its Trk receptor is remarkable considering the sequence homologies for neurotrophins and the Trk receptor family. Overall homology of TrkA, TrkB, and Trk C is 67 - 69%, with 87 - 88% homology in their respective tyrosine kinase domains.^{7a} Mature NT-4 shares 60%, 58%, and 51% amino acid identity with mature BDNF, NT-3, and NGF, respectively. NT-3 is more closely related to NGF, and NT-4 is more similar to BDNF. Highly conserved regions for all 4 proteins were G68 to Y76 and T85 to T91. Most differences in amino acid sequence between NT-4 and the other 3 neurotrophins were found within 3 variable regions: R59 to S67 and D93 to A98.¹⁴

Trk receptors have a conserved domain organization, which include from *N*-terminus to *C*-terminus: five extracellular domains, transmembrane region (TMD), and intracellular kinase domain.^{4,6,15} Trk receptor extracellular domain has consensus sequences for *N*-glycosylation.¹⁶ Glycosylation sites prevent ligand-independent activation of Trk and localize Trk to the cell surface to trigger Ras/Raf/MAPK cascade. TrkA has 4 potential highly conserved *N*-glycosylation sites and 9 additional less well-conserved sites.¹⁷ Extracellular domains of TrkB and TrkC have

11 and 13 *N*-linked glycosylation sites, respectively.^{7a} Among the Trk family, only four *N*-glycosylation sites are conserved: N26, N90, N174, and N223.¹⁶

The extracellular domain, where neurotrophins bind to the respective Trk receptor, includes a leucine-rich motif domain/domain 2 (LRM/D2) sandwiched between 2 cysteine cluster domains (C1/domain 1 (D1), C2/domain 3 (D3)), and 2 immunoglobulin domains (Ig1/domain 4, Ig2/domain 5) closer to the cell membrane.¹⁸ Notably, the cysteine linkages within each domain are highly conserved among all 3 Trk receptors, as are the 3 leucine-rich 11-amino acid substructures within domain 2.¹⁸ Likewise, both immunoglobulin domains of the three Trk receptors share common tertiary structures.¹²

Domains 1-3 (D1D2D3) are integrated together as a structural domain with super-helical topology. Domain 2 consists of 3 leucine-rich motif (LRM) units, which form the central part of D1D2D3.¹⁹ LRMs are found in many protein families and are thought to be involved in protein-protein interactions, several cell adhesion proteins, and extracellular matrix components.^{17,18,19} Each repeat is a circle of the superhelix consisting of 19-29 amino acids, a well-conserved N-terminal stretch of 9-12 amino acids that form a β -strand, and a C-terminal stretch of 10-19 amino acids that are variable in length, sequence, and structure.^{18,19} The tandem leucine repeats form a horseshoe-shaped solenoidal structure in which stacked β -sheets form the concave surface and variable stretches make up the convex surface.¹⁸

LRMs link TrkA Ig1 through a conserved disulfide C215-265 bond. At the interface of the LRM and Ig1 is a short linker peptide 187-192 connecting the two domains with a C154-C191 bond. Van der Waals interactions are formed by a hydrophobic cluster between residues 255-261 in Ig1 and residues 306-310 and 337-341 in Ig-C2. LRM/Ig1 and Ig1/Ig2 boundaries are highly structurally constrained, so large conformational modifications are unlikely when a neurotrophin binds.¹⁹

Early work suggested that the second leucine-rich motif in the extracellular domains of the Trk receptors bound to neurotrophins.²⁰ However, stronger evidence indicates that Ig2 is responsible for the specificity of selective neurotrophin binding to each Trk receptor protein to activate the intracellular kinase domain.²¹ The crystal structure data shows the extracellular domain of TrkA binding to nerve growth factor (NGF).¹⁹

Chimeras and truncated versions of Trk receptors have also substantiated this claim. Removing small portions of TrkA-domain 5 abolished neurotrophin binding.²² TrkC chimeras, where domain 5 was exchanged for homologous sequences from TrkA and TrkB, had high affinity binding to NGF or BDNF, respectively. Deleting domain 5 in TrkC or TrkA abolished binding to NT-3 or NGF, respectively.¹² Domain 4, however, is required for efficient expression and folding of domain 5 *in vitro*.²²

Amino acids in positions 103-181, containing the third LRM and CC2, and amino acid residues 342-394, which were close to Ig2, were key ligand binding domains where TrkB binds BDNF.²³

Although NT-4 can bind TrkB, it had distinct effects than BDNF. NT-4 binding to TrkB produced long-lasting activation signals and enhanced activation of downstream signaling. NT-4 was less susceptible to the degradative pathway whereas BDNF signaling, due to subsequent and rapid ubiquitination and degradation of TrkB, had short-lived activation signals. However, both neurotrophins induced TrkB phosphorylation with similar intensities.²⁴

Unlike the other mammalian neurotrophins, NT-3 can interact with non-cognate Trk receptors. It binds to TrkA and TrkB at two positively charged variable residues: R31 and H33. When these residues are mutated, NT-3 binding to TrkC is not altered. Hence, compared to TrkC, NT-3 binding to TrkA and TrkB occurs at a common but separate site.²⁵ Conserved residues (R103, R56, Y51, E54, and E10) and variable residues at positions 39-48 of the variable region II are necessary for NT-3 binding to TrkC.^{21,26}

The ligand-receptor interface involves the conserved and specificity patches. Interactions in the specificity patch are unique for the neurotrophin-receptor complex and are responsible for the specificity profile of the neurotrophin.²² Among all neurotrophin-receptor complexes, most of the residues in the conserved patch are homologous.^{22,27} 14 out of 23 NGF residues are occupied by homologous amino acids in BDNF and NT-3, and 8 out of 15 TrkA residues are conserved in TrkB and TrkC.²⁷ W21, I31, F54, and F86 on NGF make up a large portion of the conserved patch with the side chains of these residues packing against the TrkA residues.²²

Not all the above residues are integral for binding. In NGF, substituting W21 for phenylalanine or leucine did not alter NGF biological activity while mutating F86 to alanine resulted in a fully active protein. However, mutating I31 to alanine reduced TrkA-NGF binding 4-fold. The greatest effect was changing F54 to A54, which lowered biological activity 40-fold.²²

Crystallographic studies of the immunoglobulin domains for each Trk receptor indicate that the specificity patch is near the cystine bridge.²⁸ Specificity patch makes up residues 2-13 in NGF and packs against the ABED sheet of TrkA-d5.²⁷ The side chain of central hydrophobic residue I6 penetrates the hydrophobic pocket of the ABED sheet. The bottom of this pocket is formed by a solvent-exposed disulfide bridge, and residues surrounding this pocket are variable. However, the disulfide bridge is conserved among Trks.²²

In TrkA, the pocket is lined by V294, M296, P304, and L333 to form a hydrophobic environment.²² There is a salt bridge between R347 of TrkA and E11 of NGF.²⁹ In TrkB, T296, D298, P304, and H335 make up the pocket, forming a hydrophilic environment.²² TrkB has a salt bridge between D298 of TrkB and R11 of NT-4 and a pi-interaction between H343 of TrkB and R10 of NT-4.²⁹ TrkC lacks a pocket as side chains of E394, R316, E322, and Y353 block access.²²

3. Neurotrophin-Receptor Activation Models

Despite decades of research, there is no consensus on the mechanism of Trk (tyrosine receptor kinase) activation by their ligands. There are 2 main RTK (receptor tyrosine kinase) activation models: a) "diffusion-based" or "canonical" model and b) "pre-formed dimer model." In the "diffusion-based" model, in the absence of ligand, RTKs are monomeric. At endogenous levels,

FRET and single-particle tracking studies found that TrkA was 80% monomeric and NGF binding to the receptor resulted in an increase and stabilization of the dimer. With overexpression levels, TrkA dimers were not formed without the ligand, supporting the “diffusion-based” model. NGF was required for higher and complete activation of the receptor.³¹

In the “pre-formed dimer model,” in the absence and presence of ligands, Trks form dimers, which are activated when a ligand binds. Dimerization occurs due to the stabilizing interactions between the transmembrane and intracellular domains. Crystal structure of NGF binding TrkA extracellular domain reveal stabilization resulting from ligand binding to the dimer is solely through NGF-TrkA contacts. When a ligand binds TrkA or TrkB, the C-termini of the transmembrane domain moves further apart but the distances between the C-termini of the intracellular kinase domains of the receptors do not differ. This suggests there are structural modifications in the intracellular kinase domains of TrkA and TrkB upon ligand binding. For TrkC, there is an increase in C-termini separation in the intracellular kinase domains of the receptors. The distance between the C-termini of the transmembrane domains is not significantly altered (**Figure 2**). Together, these structural changes drive signal propagation across the plasma membrane.³⁰

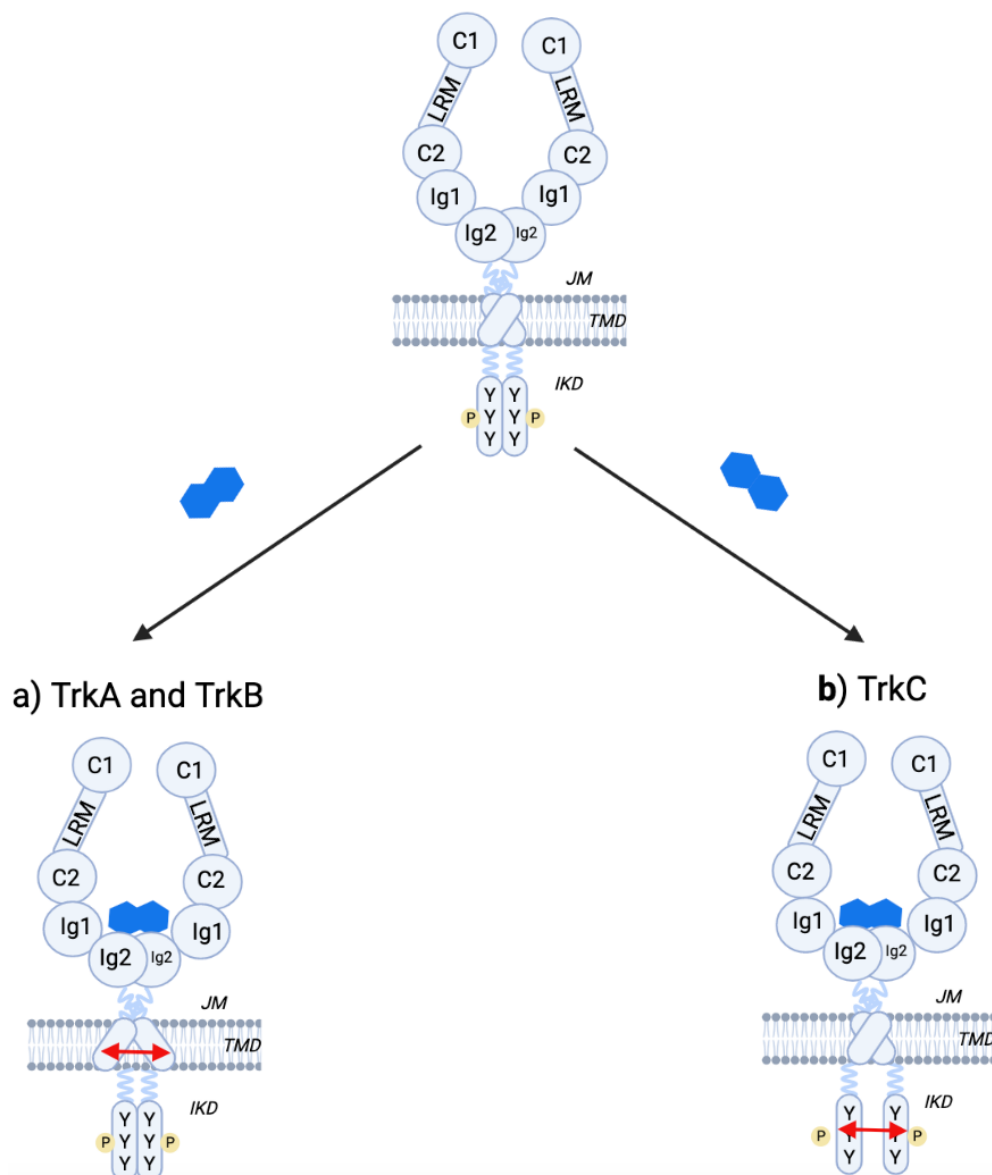


Figure 2: Upon ligand binding, Trk receptors encounter conformational changes. For TrkA and TrkB, there is an increase in transmembrane domain C-termini separation but no change in C-termini separation in the intracellular kinase domain. For TrkC, the trend is the opposite. Dimeric neurotrophin represented as two polygons as the size of each neurotrophin monomer is approximately the same size as each domain of the Trk receptor.

Abbreviations: C1 (cysteine cluster domain 1); LRM (leucine-rich motif); C2 (cysteine cluster domain 2); Ig1 (immunoglobulin domain 1); Ig2 (immunoglobulin domain 2); JM (extracellular juxtamembrane region); TMD (transmembrane domain); IKD (intracellular kinase domain).

A428 is a key residue in mediating the transition from inactive to active dimer, promoting NGF-induced TrkA activation. The mechanism of NGF-induced TrkA activation is postulated to include ligand-induced dimerization. Conformational change in the juxtamembrane occurs and through rotation of the transmembrane domain, the signal is transmitted to the intracellular kinase domain.³⁰ Specific tyrosine phosphorylation patterns trigger signaling cascades critical to

neuronal differentiation, survival and growth, and synaptic plasticity and neurotransmission (Figure 3).³

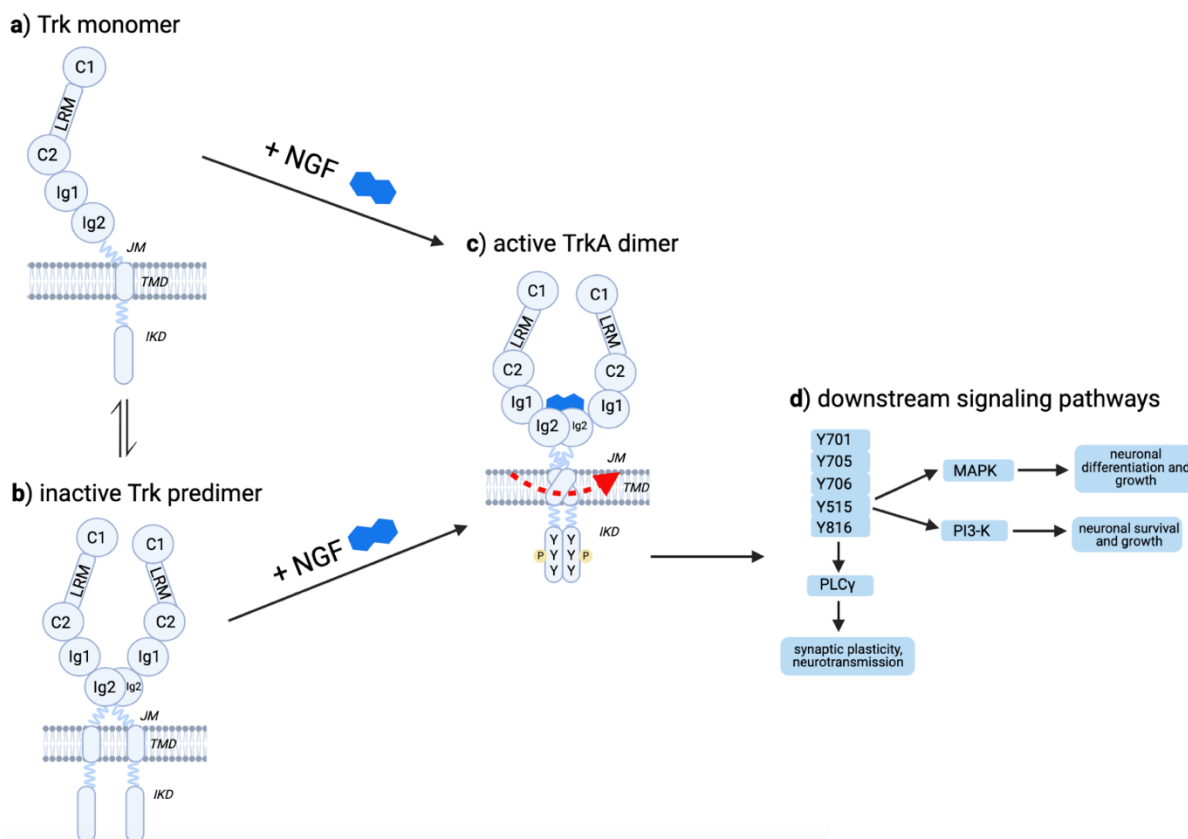


Figure 3: a) Trk monomer; b) inactive Trk predimer- stabilization due to Ig2 domain interactions; c) active TrkA dimer in the presence of NGF. Conformational changes in the extracellular juxtamembrane domains, induced by NGF binding to Ig2, results in formation of crossed transmembrane domain dimer. Transmembrane domain rotation transmits the change to the intracellular kinase domain, activating TrkA kinase autophosphorylation; d) Trk receptor catalyzes tyrosine phosphorylation to activate downstream signaling pathways.

4. TrkB Antagonists

TrkB antagonists, including ANA-12, are used to determine whether mitigation by the agonist is due to activation of TrkB receptors. Additionally, given that ANA-12 non-competitively prevents BDNF activation, it has been used to investigate the role of BDNF in the context of various disease states and for discovering new TrkA, TrkB, and TrkC agonists.³²

4.1 ANA-12 (*N*-[2-[(2-oxoazepan-3-yl)carbamoyl]phenyl]-1-benzothiophene-2-carboxamide)

TrkB inhibition may provide a therapeutic approach for treating human mood disorders by inducing strong antidepressive effects. Despite their potential clinical importance, small-molecule TrkB antagonists were unavailable prior to ANA-12. ANA-12, identified through *in silico* screening and high-capacity functional assays in recombinant and neuronal cells, is a non-peptide TrkB antagonist that demonstrated potent anxiolytic and antidepressant-like activities in mice and had high efficacy and potency in inhibiting TrkB at submicromolar concentrations.³²

In computational studies involving ANA-12 docking to TrkB-d5, the lactam moiety of ANA-12 interacted with the main chain atoms TrkB residues H299 and H300. Hydrogen bonds were present between the ANA-12 acyclic amide moiety and side chains of TrkB residues Q347 and D298 (**Figure 4**). ANA-12 fitted into the TrkB-d5 ADEB beta-sheet through hydrophobic interactions between the 7-membered ring and the C302-C347 disulfide bridge, and aromatic-aromatic interactions with H299, H300, and H335.³²

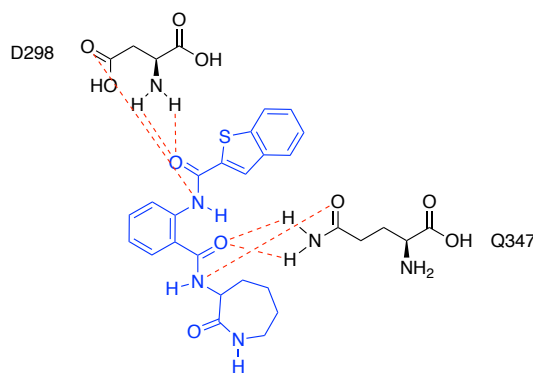
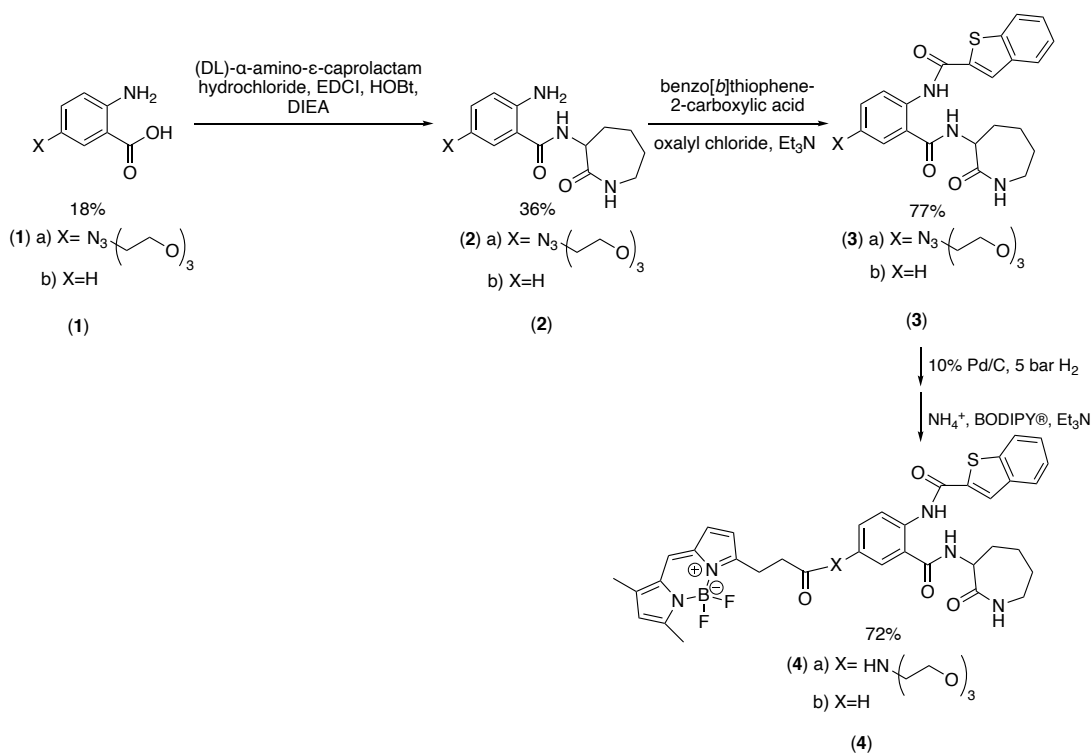


Figure 4: Hydrogen bonding interactions between ANA-12 (blue) and D298 and Q347.⁷¹

ANA-12 bound TrkB extracellular domain in a dose-dependent manner. When BDNF was added to an ANA-12/TrkB complex, binding between TrkB extracellular domain and ANA-12 dropped by 60%. This suggested that BDNF and ANA-12 did not compete for the same TrkB binding sites but operated through a two-site mode of action. ANA-12 bound the low-affinity site with $K_d = 12 \mu\text{M}$ and the high-affinity site with $K_d = 10 \text{ nM}$. Both binding sites coexisted on TrkB extracellular domain with the high-affinity site accounting for 20% of total binding.³²

Although the synthesis of ANA-12 is not available, we assume it follows the synthesis of Bodipy ANA-12 (**Scheme 1, (4)**).³²



Scheme 1. Synthesis of Bodipy-ANA-12.³²

4.1.1 ANA-12 and Neuronal Survival

ANA-12 did not degrade in mouse serum before reaching the brain. It crossed the blood-brain barrier with active concentrations of ANA-12 found in the brain 30 minutes to 6 hours post-administration. 0.5 mg/kg of ANA-12 partially inhibited total endogenous TrkB activity in the brain with 8% and 25% of activity inhibited at 2 hours and 4 hours, respectively.³²

Non-uniform inhibition by ANA-12 led to partial TrkB inhibition in the whole brain with some brain structures more inhibited than others. TrkB inhibition was more effective in the striatum compared to the hippocampus and cortex 2 hours after 0.5 mg/kg ANA-12 injection. However, inhibition was comparable among all the structures and low concentrations of ANA-12 was sufficient to induce TrkB inhibition homogenously in the brain after 4 hours.³²

Chronic ANA-12 administration did not induce toxicity to the brain or compromise neuronal survival.³² However, future efforts should investigate whether ANA-12 can provide long-lasting effects and the contexts for which it promotes maximal benefits.

4.1.2 ANA-12, HIOC, and Ocular Blast-Induced Vision Loss

Blast exposure affects retinal ganglion cells in the retina and results in the thinning of the inner plexiform layer. Mice underwent a blast exposure in the right eye and were treated with HIOC. HIOC treated mice had significant improvement in visual function and higher contrast sensitivity compared to vehicle-treated mice one week post-blast. HIOC was an effective therapy for blast injury as long as it was administered within 3 hours post-blast. Initial HIOC treatment occurring

1 day post-blast yielded no protective effects, and a treatment period of 1 week was sufficient to protect against blast induced vision loss for at least 4 months in mice.³³

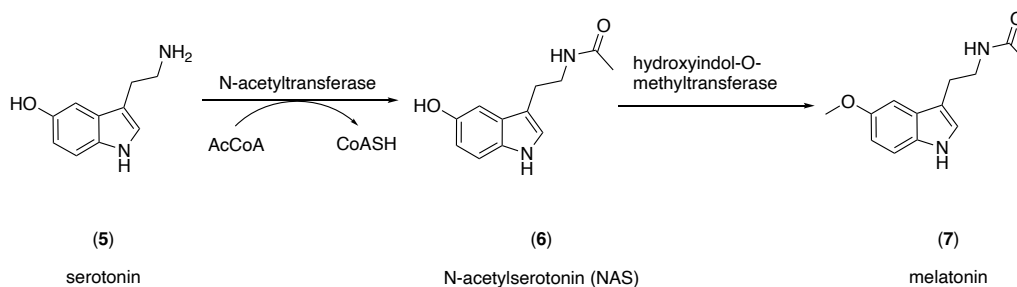
To determine if HIOC was responsible for mitigating blast-induced vision loss, ANA-12 was injected into mice 2.5 hours before blast injury to the right eye. ANA-12 had no effect on blast-induced loss in contrast sensitivity and completely blocked the effect of HIOC, supporting the hypothesis that HIOC acted through TrkB to ameliorate blast-induced vision loss.³³

5. TrkB Agonists

Specific targeting of Trk receptors with small-molecule ligands is a strategy for overcoming the limitations of therapeutic applications of neurotrophins. These ligands modulate various aspects of the TrkB signaling pathway and do not act in an identical matter to their native neurotrophin. In this next section, we explore the structural interactions of small-molecule agonists with TrkB and their ability to promote motor and functional recovery in the context of various disease states.

5.1 *N*-Acyl Serotonin Amides

5.1.1 *N*-Acetylserotonin (*N*-(2-(5-hydroxy-1*H*-indol-3-yl)ethyl)acetamide, NAS)



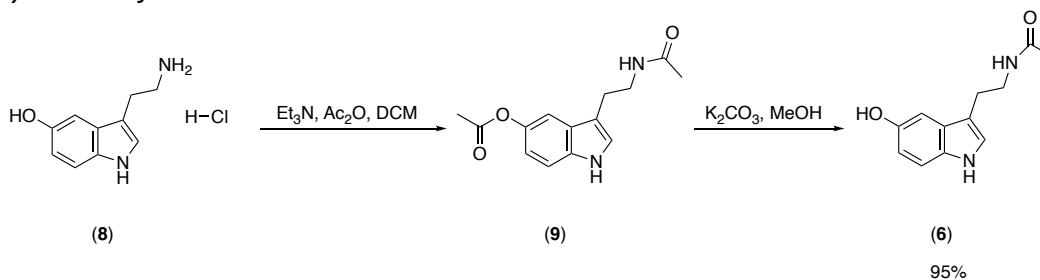
Scheme 2. Metabolic pathway converting serotonin to melatonin.³⁴

N-acetylserotonin (6) is an intermediate in the endogenous synthesis of melatonin (7) from serotonin (5) and exerts neuroprotective effects *in vivo* and *in vitro*. Serotonin *N*-acetyltransferase produces NAS from serotonin, which is converted to melatonin through hydroxyindole-*O*-methyltransferase in pineal gland and retina cells (**Scheme 2**).³⁴

5.1.1a Kinetic Characteristics of NAS

After *N*-acetylserotonin (NAS) was injected in rats, initial phase half-life was measured 10 minutes post-injection. NAS initial phase half-life was around 3 minutes while NAS terminal phase half-life was about 34 minutes.³⁵ Terminal phase half-life was the time needed such that the decrease in drug plasma concentration was attributed only to drug elimination.³⁶ Overall, NAS was labile *in vivo* and had a relatively short half-life.³⁵

5.1.1b Synthesis of NAS



Scheme 3. Synthesis of *N*-acetylserotonin.³⁷

In the presence of triethylamine, serotonin hydrochloride (**8**) reacts with 2 equivalents of acetic anhydride. Basic methanolysis selectively removes phenyl ester intermediate (**9**) to give *N*-acetylserotonin (**6**) as a white solid in 95% yield (**Scheme 3**).³⁷

Although NAS was once considered solely as the precursor of melatonin, later studies revealed NAS was an endogenous activator for the TrkB receptor, exerting anti-depressant effects in a TrkB-dependent manner. NAS induced activation of TrkB and its signaling cascades, triggering downstream pathways and ameliorating biochemical and biophysical disruptions arising from traumatic brain injury (TBI).³⁸

5.1.1c NAS and Traumatic Brain Injury (TBI)

External mechanical force to the brain results in Traumatic Brain Injury (TBI).^{39,40} In addition to disability, TBI increases the risk of other health complications. In a study of patients 1-3 years post-TBI, compared to the general population, they were 11 times as likely to develop epilepsy; 7.5 times as likely to die as new health problems may arise in conjunction with aging; and 1.8 times more likely to binge drink.^{40,41,42}

Injury-induced oxidative stress and apoptotic events affect the survival and proliferation of neuronal cells, leading to neurological function deficits through direct mechanical tissue damage (primary injury) and subsequent biochemical changes (secondary injury).³⁸ In secondary injury, free radical overload and oxidative stress, alterations in neurotransmitter release, mitochondria dysfunction, rupture of the blood-brain barrier, increase in brain water content, and release of inflammatory factors occur. Researchers have been targeting secondary biochemical pathways to limit additional brain damage in hopes of developing a therapy for TBI.^{38,43}

In mice, NAS (10 mg/kg) was found to activate TrkB receptor and its signaling cascades, triggering downstream pathways to ameliorate TBI-induced brain edema, blood-brain barrier disruption. NAS also increased brain water content and decreased claudin-5 expression.³⁸ Claudin-5 determines the sealing properties of blood-brain barrier tight junctions and is susceptible to impairment in neuroinflammatory and neurodegenerative disorders.⁴⁴ These outcomes were attributed to TrkB/Akt pathway activation, which inhibited autophagic dysfunction and apoptosis activation. NAS also inhibited TBI-induced downregulation of phosphorylated TrkB expression, restored levels of anti-apoptotic factor Bcl-2, and decreased

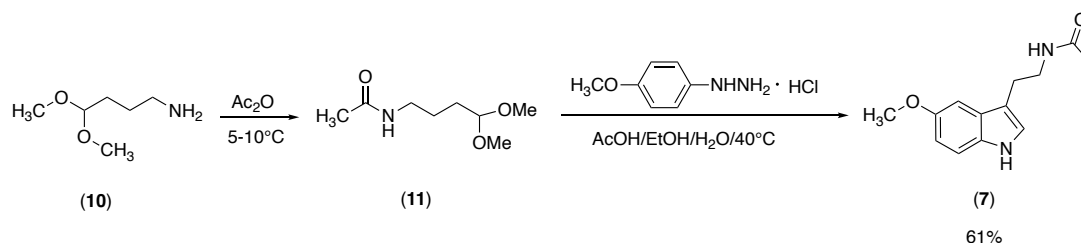
expression of pro-apoptotic factors cleaved caspase-3 and Bax.³⁸ Overall, these results demonstrated the effect of NAS in recovering hippocampus-dependent cognitive and behavioral functions post-TBI.⁴³

5.1.2 HIOC (*N*-[2-(5-hydroxy-1*H*-indol-3-yl)ethyl]-2-oxopiperidine-3-carboxamide)

HIOC is an NAS derivative and full TrkB agonist that is more clinically relevant due to its ability to effectively cross the blood-brain barrier and protect against blast-induced retinal degeneration and vision loss when administered shortly after blast exposure.⁴⁵ Compared to NAS, HIOC has a longer *in vivo* half-life and activates tropomyosin-related kinase receptor type B (TrkB) for up to 16 hours following intraperitoneal injection. Half-life of HIOC in retinas and brain tissues were 45 minutes and 4 hours, respectively. TrkB was activated within 1 hour with levels increasing around 8 to 16 hours. In contrast, NAS-induced TrkB phosphorylation peaked at 2 hours.⁴⁶

HIOC first appeared in patent literature in 2007 by Russian researchers in the Ivashchenko group⁴⁷ and Ruiqiong Ran from China in 2012.⁴⁸ These patents, however, did not describe the source of HIOC, but it may have originated as a byproduct of the Fischer Indole reaction synthesizing melatonin.^{49,50}

Melatonin (**7**), a biologically active indole derivative, is prepared by a simple one pot synthesis with 4-aminobutyraldehyde dimethylacetal (**10**) and 4-methoxy phenylhydrazine hydrochloride in acetic acid/ethanol/water. Free 4-methoxyphenylhydrazine cannot not be substituted for 4-methoxyphenylhydrazine HCl salt, and reaction temperature must be kept at 40-45°C to avoid side reactions (**Scheme 4**).⁵⁰



Scheme 4: Synthesis of melatonin.⁵⁰

5.1.2a Synthesis of HIOC

2-oxopiperidine-3-carboxylic acid (**12**), the intermediate in the preparation of 3-dioxopiperidine 3-phenylhydrazone from ethyl 2-oxopiperidine-3-carboxylate, composes the aminoethyl and 2 carbons of the pyrrole sector of the indole used in the synthesis of HIOC.⁵¹

5.1.2d HIOC and Subarachnoid Hemorrhage (SAH)

Managing early brain injury after subarachnoid hemorrhage (SAH) is a continuing challenge for physicians due to the prevalence of high death rates and complications. Injured neurons may be associated with delayed neurological deterioration and poor long-term outcomes. Previous work has shown BDNF/TrkB was involved in apoptosis after SAH, and phosphorylating TrkB ameliorated brain injury in ischemic stroke models.⁵⁴

HIOC and BDNF were equally potent in TrkB phosphorylation 6 hours post-SAH. However, HIOC was more potent 24 hours post-SAH as the HIOC treated group more potently activated TrkB, had higher phosphorylated Trk and ERK levels, and displayed greater improvement in neurobehavioral outcomes compared to BDNF group. BDNF induced TrkB degradation and polyubiquitination but suffered from poor blood-brain barrier penetrability and short serum half-life.

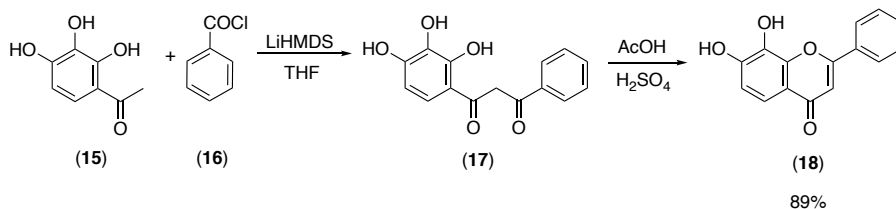
In summary, HIOC is a stable, potent NAS derivative and full TrkB agonist. HIOC delivers significant doses to the central nervous system to activate and phosphorylate TrkB with great potency and efficiency. Given that HIOC is more efficient and has prolonged effects in activating TrkB and its downstream effectors, HIOC is more clinically relevant than NAS.^{46,54} The specific region of TrkB receptor that HIOC binds remains unclear.

5.2 7,8-DHF (7,8-Dihydroxyflavone)

Another TrkB agonist is 7,8-DHF, which was identified by screening natural product libraries for compounds protecting against staurosporine-induced apoptosis in murine brain-derived cell line overexpressing TrkB. The agonist is a naturally occurring flavone found in primula tree leaves.⁵⁵

Binding assay determined 7,8-DHF bound directly to TrkB extracellular domain. Ligand to receptor ratio was 1:1 with binding constant $K_d = 320$ nM. The agonist did not bind TrkA or p75^{NTR}. Truncation assay revealed that 7,8-DHF strongly associated with amino acid residues 103-181.⁵⁶ 7,8-DHF induced TrkB dimerization and activation of downstream signaling molecules, including Akt and Erk1/2, in a dose-dependent, BDNF-independent manner. It promoted BDNF-dependent activities *in vivo*, crossed the blood-brain barrier, and increased survival of cortical, hippocampal, retinal ganglion, and spiral ganglion neurons. Overall, its stimulatory effect was mediated by TrkB autophosphorylation.^{56,57}

The classical synthesis approach to 7,8-DHF (**18**) is short, avoids *O*-acylated intermediates, and provides 7,8-DHF in high yield without side products (**Scheme 6**).⁵⁸ Other syntheses include a rhodium catalyzed cycloaddition with phenylacetylene and trihydroxybenzaldehyde.⁵⁹



Scheme 6. Synthesis of 7,8-DHF.⁵⁸

5.2.1a 7,8-DHF and Obesity

Obesity is a disease in which the adipose tissue does not function normally and is associated with comorbidities including diabetes and cardiovascular disease.⁶⁰ In humans and mice, BDNF/TrkB mutations causes hyperphagia and obesity phenotype. Hence, manipulating BDNF/TrkB signaling may be a useful strategy for combating and preventing obesity. However, the benefits of chronic TrkB activation in preventing long-term diseases, like obesity, has not been fully investigated due to the short half-life of BDNF and nonbioavailable nature of BDNF.⁶¹

Orally bioavailable BDNF mimetic 7,8-DHF was found to sufficiently protect against the development of diet-induced obesity in female mice by activating muscular TrkB. 0.17 mg/ml 7,8-DHF was administered and did not induce significant toxicity or undesirable side effects. However, when administered to male mice on a high-fat diet, body weight gain was not prevented. When muscular TrkB was knocked out in female mice, 7,8-DHF did not mitigate against diet-induced obesity.⁶¹

Uncoupling protein 1 (UCP1) is a mitochondrial protein that regulates non-shivering thermogenesis in brown adipose tissue. 7,8-DHF increased expression of UCP1 in skeletal muscle, which increased systemic energy expenditure and lipid utilization and reduced body weight gain in female mice fed a high-fat diet. Additionally, phosphorylation of AMPK in muscle and ERK phosphorylation in liver and muscle increased. ERK upregulation was most likely a protective response to increased oxidative stress. These results suggested that lipid oxidation pathways were activated in skeletal muscle of mice after continuous 7,8-DHF treatment.⁶

5.2.1b 7,8-DHF and Huntington's Disease

3-nitropropionic acid (3-NP) is a toxin in the mitochondria that interferes with the electron transport chain, leading to mitochondria mediated apoptosis and cell death. When administered to mice, it generates symptoms and pathological changes similar to that of Huntington's Disease (HD) patients.⁶²

7,8-DHF improved motor and behavior parameters and neurological deficits in HD mice in a dose-dependent manner. The mechanism underlying neurotrophic action of the agonist was activation of TrkB and upregulation of CREB/BDNF signaling. 400 nM 7,8-DHF increased phosphorylated TrkB expression 1.20 fold and phosphorylated CREB levels 1.45 fold. In the presence of TrkB inhibitor ANA-12, there was a 1.86 fold and 1.53 fold decrease in phosphorylated TrkB and phosphorylated CREB expression, respectively. Additionally, 3-NP exposure led to a 3.42 fold decrease in BDNF levels, but 7,8-DHF increased BDNF levels 2.46

fold. Mitochondrial integrity was restored, and apoptosis was inhibited by activating the PI3K/Akt pathway.⁶²

5.2.1c Chemical Modifications to 7,8-DHF

While 7,8-DHF was able to protect against the development of diet-induced obesity in female mice on a high-fat diet and ameliorated neurological and behavior deficits in Huntington's Disease mice, the catechol moiety in 7,8-DHF made it labile for fast metabolism in the liver. The agonist also suffered from suboptimal brain exposure and oral bioavailability and short half-life.^{63,64}

To address these drawbacks, structural analogs, such as R13 ((4-oxo-2-phenyl-4*H*-chromene-7,8-diyl bis(methylcarbamate)), **20**) and R7 (4-oxo-2-phenyl-4*H*-chromene-7,8-diyl bis(dimethylcarbamate), **21**) have been synthesized. These prodrugs have modifications in the catechol group to gain intestine microsomal, liver microsomal, and plasma stability (**Figure 5**).⁶³

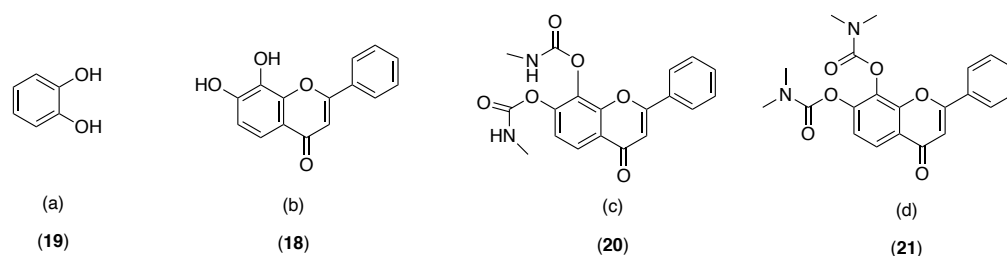
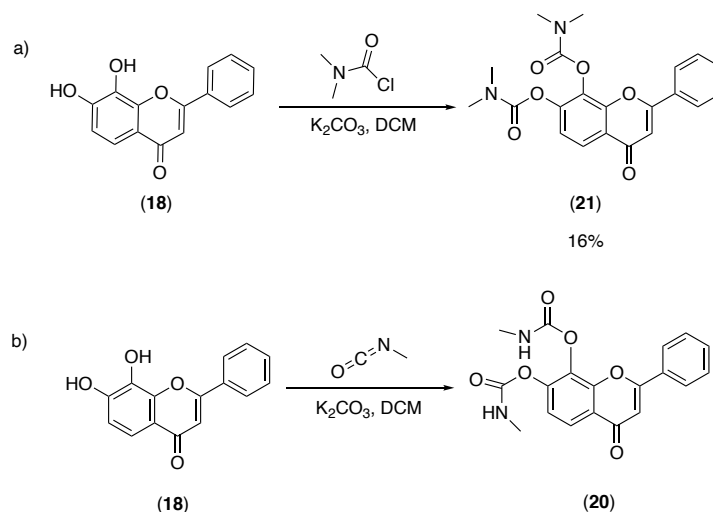


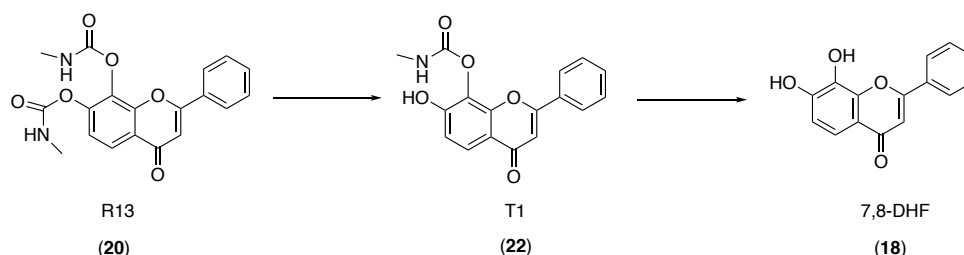
Figure 5. Structures of (a) catechol moiety (**19**); (b) 7,8-dihydroxyflavone (7,8-DHF, **18**), (c) prodrug R13 (**20**); (d) prodrug R7 (**21**).

R7 (**21**) arises from *O*-acylation with *N*-methylcarbamoyl chlorides, promoted by potassium carbonate (**Scheme 7a**). Unlike R7, R13 (**20**) is readily hydrolyzed in human liver microsomes into 7,8-DHF.⁶³ R13 synthesis involves 7,8-DHF (**18**) addition to K_2CO_3 and methyl isocyanate in dichloromethane (**Scheme 7b**).⁶⁵



Scheme 7. a) Synthesis of prodrug R7⁵¹ (**21**); b) synthesis of prodrug R13 (**20**).⁶⁵

Prodrug R13 (**20**) had good absorption and was readily hydrolyzed into intermediate T1 (**22**) before decaying into 7,8-DHF (**18**) in liver microsomes (**Scheme 8**). Compared to its parent compound, R13 oral bioavailability improved from 4.6% to 10.5%. Half-life of 7,8-DHF released from R13 (36 mg/kg) was 219.6 minutes whereas 7,8-DHF half-life was 134 minutes. *In vivo* BBB studies found 7,8-DHF plasma concentrations from R13 were higher than those of 7,8-DHF (50 mg/kg) upon oral administration.⁶³ This suggested R13 can sustainably release 7,8-DHF into the circulation system.



Scheme 8. Hydrolysis route of prodrug R13 (**16**) in human liver microsomes.⁶³

Chen et al., 2021 reported CF₃CN, a newly optimized 7,8-DHF derivative. CF₃CN had a higher affinity to TrkB than 7,8-DHF. K_d was 80.2 nM and 184.5 nM for CF₃CN and 7,8-DHF, respectively. Biacore binding assay found CF₃CN and 7,8-DHF bound most strongly with LRM followed by CC2 (**Figure 6**). Both compounds did not associate with Ig1 or Ig2. These results were consistent with findings that 7,8-DHF interacted with the LRM of the TrkB extracellular domain. Binding between 7,8-DHF and TrkB LRM/CC2 recombinant proteins was reduced when CF₃CN concentration increased, indicating 7,8-DHF and CF₃CN may occupy the same TrkB binding site.⁶⁴

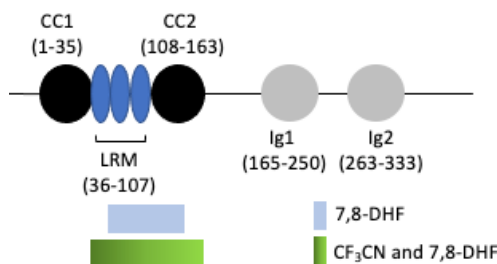


Figure 6: 7,8-DHF and CF₃CN binding with extracellular domain of TrkB receptor. The darker region of the green gradient depicts stronger binding interactions.⁶⁴

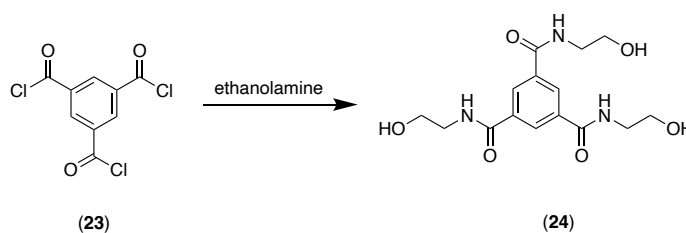
CF₃CN activated TrkB and its downstream targets and promoted cell survival in a dose-dependent manner. Chronic CF₃CN administration in an Alzheimer's disease mice model had no toxicity, blocked delta-secretase activation, demonstrated improved oral bioavailability and *in-vivo* half-life, and alleviated cognitive dysfunction. Thus, CF₃CN, a structural derivative of 7,8-DHF, is promising for the treatment of neurodegenerative diseases.⁶³

5.3 LM22A-4 ((N,N',N'-tris [2-hydroxyethyl])-1,3,5-benzene tricarboxamide)

LM22A-4 was identified by *in silico* screening method based on structural analysis of BDNF loop II and is 98% smaller than BDNF.^{66,67} It binds TrkB directly, displaces BDNF from TrkB relatively

potently, and has binding selectivity for TrkB. LM22A-4 has no effect on cells expressing TrkA, TrkC, or p75^{NTR}.⁶⁷

Loop II was responsible for BDNF activity and was key to mediating TrkB binding and activation.^{66,67} When added to hippocampal neuronal cultures, there was a 15% reduction in the neurotrophic response of BDNF. Additionally, absence of binding to p75^{NTR} made LM22A-4 a TrkB partial agonist.^{67,68} LM22A-4 (**24**) had maximal activities 80-89% of that of BDNF and arose from *N*-acylation of 1,3,5-benzenetricarbonyl trichloride (**23**) with ethanolamine (**Scheme 9**).^{67,69}



Scheme 9. Synthesis of LM22A-4 (**24**).⁶⁹

Signaling induced by LM22A-4 required TrkB.^{67,68} In demyelinated lesions, phosphorylated Erk1/2 levels peaked 5 minutes after administration and significantly declined from 15-240 minutes when compared to BDNF. This suggested that Erk 1/2 phosphorylation was upstream of TrkB phosphorylation, and LM22A-4 did not mimic the BDNF-TrkB signaling cascade.⁶⁶

LM22A-4 bound to TrkB directly, displaced BDNF from TrkB, and acted selectively through TrkB.⁶⁶ Boltaev et al., 2017 reported LM22A-4 did not activate TrkB after observing LM22A-4 failed to induce dose-dependent Akt or Erk activation in a cortical neuron culture.⁶⁹ In contrast, Nguyen et al., 2019 reported that LM22A-4 did not promote remyelination or increase oligodendroglial density in oligodendrocyte TrkB knockout mice. This highlighted the importance of TrkB for the action of LM22A-4 and was the first *in vivo* evidence that the agonist required TrkB for its activity.⁶⁶ The difference in findings may be attributed to methodology differences as *in vitro* assays are not readily applicable *in vivo* as they may not accurately represent *in vivo* receptor complexes.⁶⁹

5.3.1 LM22A-4 and Spinal Cord Injury

In 2016, roughly 17,000 US citizens suffered from spinal cord injury (SCI). SCI has historically been prevalent in younger adult men, but over the last few decades, SCI incidence among the elderly has steadily increased. In addition to spinal cord trauma, patients suffer from many complications including significant reductions in life expectancy, associated traumatic brain injury, and cerebrovascular damage.⁷⁰

10 mg/kg and 15 mg/kg doses of LM22A-4 upregulated phosphorylated TrkB, phosphorylated Akt, and phosphorylated ERK levels. LM22A-4 also significantly inhibited apoptosis-related

protein cleaved-caspase-3 expression and promoted anti-apoptotic protein Bcl-2 expression. Increased neurons and decreased apoptotic neurons were also observed with treatment.⁷¹

5.3.2 LM22A-4 and Hypoxic-Ischemic Stroke

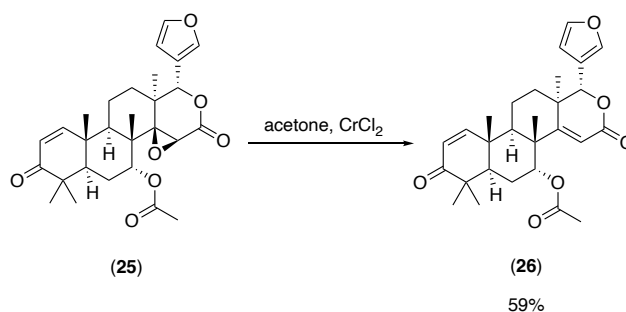
Stroke is the leading cause of long-term disability in the US. Currently, there are no drugs to improve recovery.⁷² Stroke rates are projected to increase due to demographic changes with the World Health Organization labeling stroke “an epidemic of the 21st century.”⁷³

0.22 mg/kg LM22A-4 doubled neurogenesis in areas adjacent to the stroke:dorsolateral striatum and penumbral cortex. When administered 3 days post-hypoxic-ischemic stroke, LM22A significantly improved gait in mice as evident by improvement in limb swing speed and acceleration in the return of normal gait accuracy. These effects were achieved by LM22A-4 entering the brain and increasing TrkB phosphorylation 1.2 fold after the stroke incident. The agonist did not affect stroke size, suggesting that motor function differences were due to the enhancement of neurological recovery rather than through primary neuroprotective effects induced by the agonist.⁷²

5.4 Deoxygedunin and Deprenyl

Deoxygedunin was identified during screening for compounds that protect against staurosporine-induced apoptosis in murine brain-derived cell line overexpressing TrkB in natural product libraries.⁷⁴ The agonist functioned as a selective, full TrkB agonist and prevented neuronal apoptosis in a TrkB dependent manner.^{74,75} Filter assay found deoxygedunin bound TrkB extracellular domain to stimulate its dimerization and autophosphorylation. Scatchard plot analysis revealed ligand to receptor ratio was 1:1 with $K_d=1.4 \mu\text{M}$.⁷⁴ Deoxygedunin provoked TrkB dimerization with a stronger effect than BDNF and did not bind TrkA.^{74,75}

Gedunin, a tetranortriterpenoid isolated from Indian neem tree *Azadirachta indica*, has been isolated for use in deoxygedunin synthesis. Studies on gedunin have been hindered by the lack of information that a total synthesis might provide, but syntheses of two separate gedunin substructures have been reported.^{69,76,77} Deoxygedunin (**26**) arises from chemoselective deoxygenation of the epoxide (**25**), using excess chromium(II) chloride in degassed acetone (**Scheme 10**).⁶⁹



Scheme 10. Synthesis of deoxygedunin from gedunin.⁶⁹

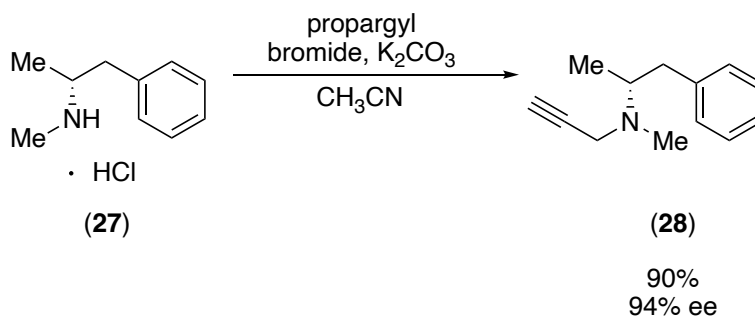
5.4.1a Deoxygedunin and Parkinson's Disease

Parkinson's disease is one of the most common neurodegenerative diseases, affecting 1.5% of the population over 65 years old. Pathogenesis of Parkinson's involves dopaminergic neurons loss in the substantia nigra (SN) and dopamine loss in the striatum.⁷⁸

Activation of the TrkB signaling pathway likely contributed to the neuroprotective effects of deoxygedunin. Rats pretreated with the agonist had higher phosphorylated TrkB levels compared to the control and post-treatment groups. The neuroprotective effects by deoxygedunin were independent of altering BDNF expressions.⁷⁸

TrkB receptor agonist deprenyl (selegiline) displays neuroprotection action, protecting cultured cells from apoptosis induced by oxidative stress-related agents and nitric oxide⁷⁹ and peroxynitrite.⁸⁰ TrkB phosphorylation by deprenyl is prolonged compared to BDNF activation of TrkB. However, deprenyl-induced TrkC activation is not very intense. Cytoprotective effects of deprenyl is reduced when Trk is inhibited.⁸¹

N-propargylation of methamphetamine hydrochloride (**27**) in acetonitrile with K₂CO₃ yields deprenyl (**28**) in 90% yield and preserves the chiral center (**Scheme 11**).⁸²



Scheme 11. Synthesis of R-deprenyl from methamphetamine hydrochloride.⁸²

5.4.1b Deprenyl and Parkinson's Disease

Deprenyl induced antioxidative proteins HO-1, Prx1, Trx1, TrxR1 in SH-SY5Y neuroblastoma cells. Antioxidative proteins reached maximal levels 12-16 hours post-deprenyl administration. Deprenyl also induced nuclear accumulation of NF-E2-related factor-2 (Nrf2) in a dose-dependent manner. Nrf2 acts as a transcription factor as it translocates into the nucleus where it forms heterodimers and binds to the antioxidant response element (ARE). ARE is a *cis*-acting enhancer sequence that regulates cytoprotective gene expression. A 3.3-fold increase of Nrf2 nuclear accumulation was obtained 6 hours post-deprenyl treatment.⁸⁰

TrkB phosphorylation by deprenyl was prolonged compared to BDNF activation of TrkB. Activation of TrkC by deprenyl was not as intense as it was for TrkB. Nrf-2 mediated the induction of antioxidative proteins following deprenyl treatment and involved PI3K-Akt intracellular signaling pathway. PI3K-Akt was significantly activated by deprenyl, and phosphorylation of PI3K-Akt was observed 1-2 hours after treatment. Maximal PI3K-Akt

activation occurred 90 minutes after deprenyl was given. Akt and ERK1/2 were not phosphorylated by deprenyl.⁸⁰

Given its neuroprotective effects and ability to induce expression of oxidative stress-related molecules, deprenyl is being considered a therapeutic approach for treating Parkinson's disease.⁸¹ Future research should investigate whether deprenyl induces TrkB phosphorylation directly or indirectly.

6. Non-TrkB Specific Agonists

In section 5, we reported several small, non-peptide ligands that selectively bind and activate TrkB. However, through various screening methods, LM22B-10, amitriptyline, and DMAQ-B1 were discovered to bind multiple Trk receptors to promote neuronal survival and address functional deficits in neurodegenerative diseases.

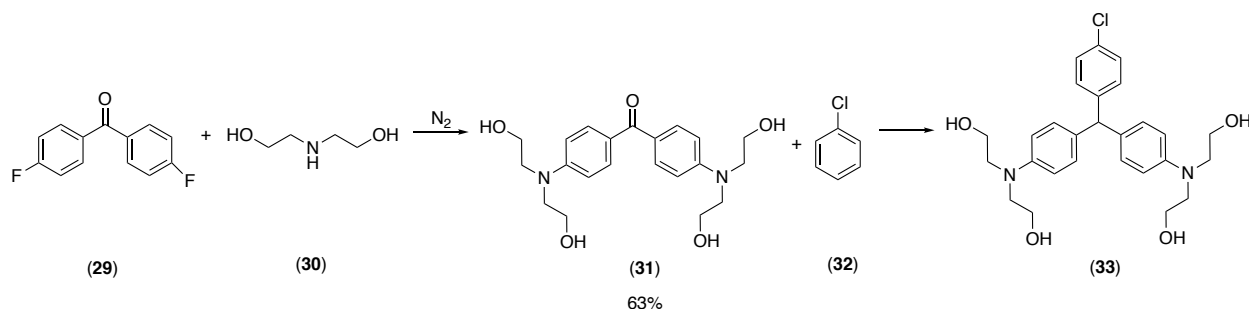
6.1 LM22B-10 (2-[[4-[[4-[Bis-(2-hydroxy-ethyl)-amino]-phenyl-(4-chloro-phenyl)-methyl]-phenyl]-(2-hydroxy-ethyl)-amino]-ethanol]): TrkB, TrkC agonist

In silico screening with a pharmacophore based on BDNF loop II domain identified LM22B-10, a TrkB and TrkC agonist. It had no effect on NGF or BDNF-binding to TrkA-expressing cells. Its biological and signaling effects were distinct from that of BDNF and NT-3.⁸³

LM22B-10 bound to the extracellular domains of TrkB and TrkC, displacing BDNF from TrkB and NT-3 from TrkC. In cognate NT competition studies, LM22B-10 selectively inhibited BDNF binding to TrkB-expressing cells and NT-3 binding to TrkC-expressing cells. No effect was reported for NGF or BDNF binding to TrkA-expressing cells. Although LM22B-10 binding to TrkB was slightly less than its binding with TrkC, 1 μ M of the agonist displaced 1 nM BDNF completely but only reduced NT-3 binding by 40%. Additionally, Western blot findings revealed IgG-C2 domain or a nearby region may be involved in LM22B-10-induced receptor activation.⁸³

The agonist demonstrated effects on cell survival, neurite outgrowth, and dendritic spine density. Additionally, it had maximum neurotrophic survival activity levels higher than what was maximally achieved with BDNF and NT-3: 53 \pm 7.2% above BDNF at 0.7 nM and 91 \pm 8.6% above NT-3 at 0.7 nM. In neurons, LM22B-10 induced acute TrkB, TrkC, Erk1/2, and Akt signaling. However, it was significantly lower than that produced by either BDNF or NT-3.⁸³

While a total synthesis for LM22B-10 has not been reported, we believe that 4,4-difluorobenzophenone (**29**) reacts with excess diethanolamine (**30**) under nitrogen for 3 days at 180°C to form bis(4-(bis(2-hydroxyethyl)amino)phenyl)methanone (**31**).⁸⁴ Compound (**31**) reacts with chlorobenzene (**32**) to obtain LM22B-10 (**Scheme 12, (33)**).



Scheme 12. Proposed total synthesis of LM22B-10.⁸⁴

In closing, LM22B-10 is a TrkB and TrkC agonist that mimics BDNF loop II domain and binds to the extracellular domains of TrkB and TrkC. It promotes cell survival, neuronal outgrowth, and dendritic spine density increases in a dose-dependent manner, activating Erk1/2 and Akt signaling.

6.1.1 LM22B-10 and Neuronal Survival and Process Outgrowth

1000 nM LM22B-10 yielded maximum neurotrophic effects. In hippocampal neuron cultures of mouse fetuses, cell death was reduced by $68 \pm 2.3\%$ with BDNF treatment; $64 \pm 4.3\%$ with NT-3; and $85 \pm 1.4\%$ with LM22B-10. At 2 days *in vitro*, maximal survival effects were obtained using 0.04-1.85 nM of BDNF and NT-3 in which hippocampal neurons had average lengths of 20-30 μm while 1000 nM LM22B-10 induced neurites with average lengths up to 40 μm . Contributions of TrkB and TrkC activation, differential interactions with p75^{NTR}, and involvement of Trk extracellular domain were identified as factors responsible for these outcomes.⁸³

6.2 Amitriptyline: TrkA, TrkB agonist

Amitriptyline (Elavil) is a tricyclic antidepressant used to treat migraine attacks and certain types of neuropathic or inflammatory pain. The agonist played a neuroprotective role by binding to TrkA and TrkB extracellular domains.^{85,86,87} None of the immunoglobulin-like domains were needed for amitriptyline activity, but the first leucine-rich motif (aa 72-97) was needed for full amitriptyline binding to TrkA. Deleting the extracellular domain significantly decreased amitriptyline binding.⁸⁷

Amitriptyline induced TrkA and TrkB homo- and heterodimerization in mouse brain. TrkA-TrkB receptor heterodimerization was not needed for Trk activation. Amitriptyline-induced TrkA phosphorylation on Y751 and Y794 but not Y490 whereas NGF activated all three tyrosine residues on TrkA. MAPK and Akt pathways in mice hippocampal neurons were activated in a manner similar to NGF. However, it could not compete with NGF or BDNF for the extracellular domains, indicating its low affinity to TrkA and TrkB.⁸⁷

6.2.1 Amitriptyline and Huntington's Disease

Mutant huntingtin protein (mHTT) suppresses BDNF expression. BDNF protects striatal cells from excitotoxic insults in Huntington's disease. When mHTT accumulates, lower BDNF levels are observed in the postmortem brain of Huntington disease patients and in Huntington's

disease mouse models. Decreased TrkB expression and impaired BDNF-mediated neurotrophic signaling pathways may contribute to the emergence of Huntington's disease.⁸⁸

No effective treatment is available for Huntington's disease. Drug development is expensive, risky, and time-consuming, so reusing a previously FDA approved, well tolerated therapeutic, like amitriptyline (Elavil) may provide a promising drug discovery route for Huntington disease.⁸⁸

Amitriptyline treatment did not induce body weight gain or alter or extend lifespan in male and female Huntington's disease mice. mHTT protein expression in the cortex and striatum was significantly reduced by amitriptyline. Increases in striatal mature BDNF and improvements in motor coordination and fine motor control were observed, but striatal phosphorylated ERK1/2 and Akt levels were not altered.⁸⁸

6.2.2 Amitriptyline and Neurotrophic Activity

Pretreatment of primary hippocampal neurons with amitriptyline followed by glutamate treatment significantly prevented apoptosis of hippocampal neurons. Amitriptyline stimulated TrkA tyrosine phosphorylation on Y751 and Y794 and activated Akt and ERK1/2. TrkA and TrkB activation was provoked by amitriptyline, independent of its native neurotrophins, in a dose-dependent manner.⁸⁷

Neurite outgrowth was triggered by 100 nM amitriptyline and required activation of PI3K-Akt and MAPK signaling pathways. This suggested that the agonist had significant neurotrophic activity, and neurite outgrowth effect was dependent on the Trk receptor. TrkA was not required for amitriptyline-induced phosphorylation of TrkB, but TrkA played a greater role than TrkB in mediating neuronal survival by amitriptyline.⁸⁷

In conclusion, amitriptyline may be considered in treating neurodegenerative diseases and promoting neuro-regeneration due to its neuroprotective activity, arising by binding to the extracellular domain of TrkA and/or TrkB.

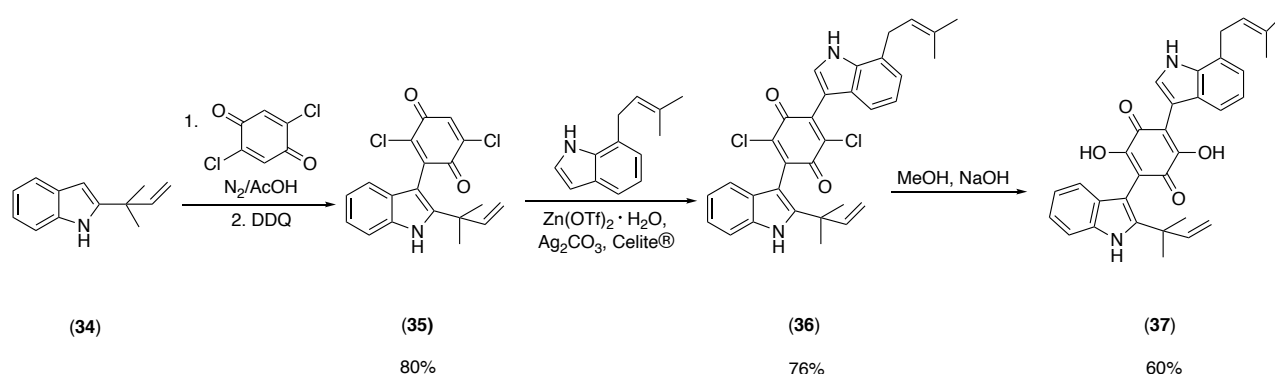
6.3 DAQ-B1/DMAQ-B1 (Demethylasterriquinone B1): TrkA, TrkB, TrkC agonist

Demethylasterriquinone B1 (DMAQ-B1) is an orally active, small molecule-mimetic of insulin and was discovered during a screening of over 50,000 natural product extracts for insulin receptor activation in cells.⁸⁹ DMAQ-B1 is extracted from tropical fungus *Pseudomassaria sp.* and is a TrkA, TrkB, and TrkC agonist.^{90,91} When bound to the receptor, DMAQ-B1 did not compete with insulin but altered the proteolysis pattern at K1030 near the ATP binding site in the tyrosine kinase domain.⁸⁹

From methyl scanning, the most structurally important parts of DMAQ-B1 were the quinone and 7-substituted indole ring.⁸⁹ DMAQ-B1 did not elicit any inhibitory or potentiation effects on Trk activation by neurotrophins, suggesting it acted independently of neurotrophins. Its mode of action was likely through TrkA intracellular domain. It activated the full-length TrkA receptor and the chimera containing TrkA extracellular domain and transmembrane and intracellular

domains of the platelet-derived growth factor receptor (PDGF). It failed to activate the chimera with the transmembrane and intracellular portions of TrkA and extracellular portion of PDGF.⁹¹

Fully regiocontrolled total synthesis of DMAQ-B1 involved two indole building blocks without prior derivation to a quinone core. DDQ (2,3-dichloro-5,6-dicyano-1,4-benzoquinone) addition following starting material consumption aided in oxidizing the conjugate addition product to the quinone. The oxidant was not excluded in the addition step as a second addition was unlikely. DMAQ-B1 (**37**) was prepared by basic hydrolysis of 2,5-dichloro-3-(7-(3-methylbut-2-en-1-yl)-1*H*-indol-3-yl)-6-(2-(2-methylbut-3-en-2-yl)-1*H*-indol-3-yl)cyclohexa-2,5-diene-1,4-dione (**36**) (Scheme 13).⁸⁹



Scheme 13. Total synthesis of DMAQ-B1.⁸⁹

6.3.1 DMAQ-B1 and Trk Neurotrophin Receptors

DMAQ-B1 was evaluated for its effects on the Trk receptor family in cell lines that overexpress Trk receptor subtypes and in primary cultures of cortical neurons and dorsal root ganglion (DRG).⁹¹ DRGs in the spinal cord relay neural signaling from peripheral sensory systems to the brain and are important in neural development, neurodegeneration in diseases, and neuropathic pain.⁹²

TrkA was phosphorylated upon administration of 20 μ M of DMAQ-B1. Phosphorylation was $41 \pm 6\%$ of the maximal NGF response at the 10-minute mark. Higher concentrations of DMAQ-B1 did not increase Trk phosphorylation. When insulin was tested on Trk phosphorylation using cells that naturally have a small proportion of insulin receptors, insulin did not affect Trk phosphorylation, indicating DMAQ-B1 did not act indirectly through the insulin receptor to stimulate Trk phosphorylation. 20 μ M of DMAQ-B1 stimulated TrkB phosphorylation to $37 \pm 1\%$ of maximal BDNF response and TrkC phosphorylation to $14 \pm 4\%$ of the maximal NT-3 response. In the case of TrkA phosphorylation by DMAQ-B1, after 3 minutes, stimulation was $59 \pm 8\%$ of maximal NGF response, $11 \pm 3\%$ of maximal NGF response after 45 minutes, and undetectable after 2 hours.⁹¹

In summary, DMAQ-B1 is an orally active, small molecule-mimetic of insulin and a TrkA, TrkB, and TrkC agonist. However, it has three limitations. First, DMAQ-B1-stimulated Trk activation gradually decreased in a time-dependent manner as it was undetectable 2 hours post-

administration in TrkA receptors. Second, DMAQ-B1 stimulated a response less than half of the maximal neurotrophin response. Lastly, when examining cytotoxicity of DMAQ-B1 in rat dorsal root ganglion (DRG) cultures and primary cultures of rat cortical neurons, widespread cell death occurred when the agonist concentration was greater than 10 μ M. Cytotoxicity mechanism remained unclear but may be attributed to interactions with additional kinase domains or by redox effects in cellular metabolism.⁹¹

7. Conclusion

BDNF administration has therapeutic potential for many disease states, including neurological disorders. However, its short *in vivo* half-life and poor pharmacological properties limits its therapeutic efficacy. This has led to the discovery of small TrkB agonists and antagonists that mimic the physiological functions of BDNF.

We examine the ability for TrkB agonists *N*-acetylserotonin (NAS), HIOC, 7,8-DHF, deoxygedunin, and deprenyl to activate and phosphorylate TrkB with high potency and efficiency; improve motor, neurological, and motor deficits in the context of various diseases; and bind specific regions of the TrkB extracellular domain. Non-TrkB specific agonists LM22B-10, amitriptyline, and DMAQ-B1 bind to a combination of TrkA, TrkB, and TrkC receptors to induce receptor activation. Their biological and signaling effects are distinct from neurotrophins and help promote cell survival and neuronal outgrowth.

Current therapeutics target symptoms instead of underlying disease mechanisms. A key factor in disease states, such as neurodegenerative diseases, is the upregulation or downregulation of TrkB signaling. Using small molecule agonists that selectively target the Trk receptors offer novel mechanism-based therapeutics for a diverse range of diseases. In cases where it is unknown, future research should explore the specific regions of the Trk receptor the agonist binds. In addition, cytotoxicity mechanisms and chemical modifications to existing agonists should also be investigated.

8. References

1. a) Abu El-Asrar, A.M.; Mohammad, G.; De Hertogh, G.D.; Nawaz, M.I.; Van Den Eynde, K.; Siddiquei, M.M.; Struyf, S.; Opdenakker, G.; Geobes, K. Neurotrophins and Neurotrophin Receptors in Proliferative Diabetic Retinopathy. *PLOS ONE*. **2013**, *8*, 1-12. b) Gibon, J.; Barker, P.A. Neurotrophins and Proneurotrophins: Focus on Synaptic Activity and Plasticity in the Brain. *Neuroscientist*. **2017**, *23*, 587-604.
2. a) Johnson, D.; Lanahan, A.; Buck, C.R.; Sehgal, A.; Morgan, C.; Mercer, E.; Bothwell, M.; Chao, M. *Cell*. **1986**, *47*, 545-554. b) Radeke, M.J.; Misko, T.P.; Hsu, C.; Herzenberg, L.A.; Shooter, E.M. *Nature*. **1987**, *325*, 593-597. c) Brahim, F.; Maira, M.; Barcelona, P.F.; Galan, A.; Aboukassim, T.; Teske, K.; Rogers, M-L.; Bertram, L.; Wang, J.; Yousefi, M.; Rush, R.; Fabian, M.; Cashman, N.; Saragovi, H.U. The Paradoxical Signals of Two TrkC Receptor Isoforms Supports a Rationale for Novel Therapeutic Strategies in ALS. *PLOS ONE*. **2016**, *11*, 1-25.
3. a) Reichardt, L.F. Neurotrophin-regulated signalling pathways. *Phil. Trans. R. Soc. B*. **2006**, *361*, 1545-1564. b) Huang, E.J.; Reichardt, L.F. Trk receptors: roles in neuronal signal transduction. *Annu. Rev. Biochem.* **2003**, *72*, 609-642.
4. a) Martin-Zanca, D.; Hughes, S.H.; Barbacid, M. A human oncogene formed by the fusion of truncated tropomyosin and protein tyrosine kinase sequences. *Nature*. **1986**, *319*, 743-748. b) Martin-Zanca, D.; Oskam, R.;

Mitra, G.; Copeland, T.; Barbacid, M. Molecular and biochemical characterization of the human trk proto-oncogene. *Mol. Cell. Biol.* **1989**, *9*, 24-33.

5. a) Kaplan, D.R.; Hempstead, B.L.; Martin-Zanca, D.; Chao, M.V.; Parada, L.F. The trk proto-oncogene product: a signal transducing receptor for nerve growth factor. *Science*. **1991**, *252*, 554-558. b) Kaplan, D.R.; Martin-Zanca, D.; Parada, L.F. Tyrosine phosphorylation and tyrosine kinase activity of the trk proto-oncogene product induced by NGF. *Nature*. **1991**, *350*, 158-160. c) Hempstead, B.L.; Martin-Zanca, D.; Kaplan, D.R.; Parada, L.F.; Chao, M.V. High-affinity NGF binding requires coexpression of the trk proto-oncogene and the low-affinity NGF receptor. *Nature*. **1991**, *350*, 678-683.

6. a) Klein, R.; Lamballe, F.; Bryant, S.; Barbacid, M. The trkB tyrosine protein kinase is a receptor for neurotrophin-4. *Neuron*. **1992**, *8*, 946-956. b) Lamballe, F.; Klein, R.; Barbacid, M. trkC, a new member of the trk family of tyrosine protein kinases, is a receptor for neurotrophin-3. *Cell*. **1991**, *66*, 967-979. c) Cordon-Cardo, C.; Tapley, P.; Jing, S.Q.; Nanduri, V.; O'Rourke, E.; Lamballe, F.; Kovary, K.; Klein, R.; Jones, K.R.; Reichardt, L.F.; Barbacid, M. The trk tyrosine protein kinase mediates the mitogenic properties of nerve growth factor and neurotrophin-3. *Cell*. **1991**, *66*, 173-183.

7. a) Shelton, D.L.; Sutherland, J.; Gripp, J.; Camerato, T.; Armanini, M.P.; Phillips, H.S.; Carroll, K.; Spencer, S.D.; Levinson, A.D. Human trks: Molecular Cloning, Tissue Distribution, and Expression of Extracellular Domain Immuno adhesins. *J. Neurosci.* **1995**, *15*, 477-491. b) Dechant, G.; Tsoulfas, P.; Parada, L.F.; Barde, Y-A. The Neurotrophin Receptor p75 Binds Neurotrophin-3 on Sympathetic Neurons with High Affinity and Specificity. *J. Neurosci.* **1997**, *17*, 5281-5287. c) Allington, C.; Shamovsky, I.L.; Ross, G.M.; Riopelle, R.J. Zinc inhibits p75^{NTR}-mediated apoptosis in chick neural retina. *Cell Death Differ.* **2001**, *8*, 451-456.

8. a) Boulle, F.; Kenis, G.; Cazorla, M.; Hamon, M.; Steinbusch, H.W.M.; Lanfumey, L.; van den Hove, D.L.A. TrkB inhibition as a therapeutic target for CNS-related disorders. *Prog. Neurobiol.* **2012**, *98*, 197-206. b) Gupta, V.K.; You, Y.; Gupta, V.B.; Klistorner, A.; Graham, S.L. TrkB receptor signalling: implications in neurodegenerative psychiatric and proliferative disorders. *Int. J. Mole. Sci.* **2013**, *14*, 10122-10142.

9. Longo, F.M.; Massa, S.M. Small-molecule modulation of neurotrophin receptors: a strategy for the treatment of neurological disease. *Nat. Rev. Drug. Discov.* **2013**, *12*, 507-525.

10. Brahim, F.; Maira, M.; Barcelona, P.F.; Galan, A.; Aboukassim, T.; Teske, K.; Rogers, M-L.; Bertram, L.; Wang, J.; Yousefi, M.; Rush, R.; Fabian, M.; Cashman, N.; Saragovi, H.U. The Paradoxical Signals of Two TrkC Receptor Isoforms Supports a Rationale for Novel Therapeutic Strategies in ALS. *PLOS ONE*. **2016**, *11*, 1-25.

11. a) Yan, W.; Lakkanna, R.; Carlomagno, F.; Santoro, M.; McDonald, N.Q.; Lv, F.; Gunaganti, N.; Frett, B.; Li, H-Y. Insights into Current Tropomyosin Receptor Kinase (TRK) Inhibitors: Development and Clinical Application. *J. Med. Chem.* **2019**, *62*, 1731-1760. b) Bailey, J.J.; Schirmacher, R.; Farrell, K.; Bernard-Gauthier, V. Tropomyosin receptor kinase inhibitors: an updated patent review for 2010-2016- Part I. *Expert Opin. Ther. Pat.* **2017**, *27*, 733-751. c) Bailey, J.J.; Schirmacher, R.; Farrell, K.; Bernard-Gauthier, V. Tropomyosin receptor kinase inhibitors: an updated patent review for 2010-2016- Part II. *Expert Opin. Ther. Pat.* **2017**, *27*, 831-849.

12. Philo, J.; Talvenheimo, J.; Wen, J.; Rosenfeld, R.; Welcher, A.; Arakawa, T. Interactions of Neurotrophin-3 (NT-3), Brain-derived Neurotrophic Factor (BDNF), and the NT-3•BDNF Heterodimer with the Extracellular Domains of the TrkB and TrkC Receptors. *J. Biol. Chem.* **1994**, *269*, 27840-27846.

13. (a) McDonald, N.Q.; Lapato, R.; Rust, J.M.; Gunning, J.; Wlodawer, A.; Blundell, T.L. New protein fold revealed by a 2.3-Å resolution crystal structure of nerve growth factor. *Nature*. **1991**, *354*, 411-414. (b) McDonald, N.Q.; Hendrickson, W.A. A structural superfamily of growth factors containing a cystine knot motif. *Cell*. **1993**, *73*, 421-424.

14. Hallböök, F.; Ibáñez, C.F.; Persson, H. Evolutionary studies of the nerve growth factor family reveal a novel member abundantly expressed in *Xenopus* ovary. *Neuron*. **1991**, *6*, 845-858.
15. Klein, R.; Parada, L.F.; Coulier, F.; Barbacid, M. trkB, a novel tyrosine protein kinase receptor expressed during mouse neural development. *EMBO J.* **1989**, *8*, 3701-3709.
16. Haniu, M.; Talvenheimo, J.; Le, J.; Katta, V.; Welcher, A.; Rodhe, M.F. Extracellular Domain of Neurotrophin Receptor trkB: Disulfide Structure, *N*-Glycosylation Sites, and Ligand Binding. *Arch. Biochem. Biophys.* **1995**, *322*, 256-264.
17. Watson, F.L.; Porcionatto, M.A.; Bhattacharyya, A.; Stiles, C.D.; Segal, R.A. TrkA Glycosylation Regulates Receptor Localization and Activity. *J. Neurobiol.* **1999**, *39*, 323-336.
18. Dolan, J.; Walshe, K.; Alsbury, S.; Hokamp, K.; O'Keefe, S.; Okafuji, T.; Miller, S.F.C.; Tear, G.; Mitchell, K.J. The extracellular leucine-rich repeat superfamily; a comparative survey and analysis of evolutionary relationships and expression patterns. *BMC Genom.* **2007**, *8*, 1-24.
19. Wehrman, T.; He, X.; Raab, B.; Dukipatti, A.; Blau, H.; Garcia, K.C. Structural and Mechanistic Insights into Nerve Growth Factor Interactions with the TrkA and p75 Receptors. *Neuron*. **2007**, *53*, 25-38.
20. Windisch, J.M.; Marksteiner, R.; Lang, M.E.; Auer, B.; Schneider, R. Brain-Derived Neurotrophic Factor, Neurotrophin-3, and Neurotrophin-4 Bind to a Single Leucine-Rich Motif of TrkB. *Biochem.* **1995**, *34*, 11256-11263.
21. Urfer, R.; Tsoulfas, P.; O'Connell, L.; Shelton, D.L.; Parada, L.F.; Presta, L.G. An immunoglobulin-like domain determines the specificity of neurotrophin receptors. *EMBO J.* **1995**, *14*, 2795-2805.
22. Wiesmann, C.; de Vos, A.M. Nerve growth factor: structure and function. *Cell. Mol. Life. Sci.* **2001**, *58*, 748-759.
23. Haniu, M.; Montestrucque, S.; Bures, E.J.; Talvenheimo, J.; Toso, R.; Lewis-Sandy, S.; Welcher, A.A.; Rohhe, M.F. Interactions between Brain-derived Neurotrophic Factor and the TrkB Receptor. *J. Biol. Chem.* **1997**, *272*, 25296-25303.
24. Proenca, C.C.; Song, M.; Lee, F.S. Differential effects of BDNF and neurotrophin 4 (NT4) on endocytic sorting of TrkB receptors. *J. Neurochem.* **2016**, *138*, 397-406.
25. Ilag, L.L.; Lönnerberg, P.; Persson, H.; and Ibáñez, C.F. Role of variable beta-hairpin loop in determining biological specificities in neurotrophin family. *J. Biol. Chem.* **1994**, *269*, 19941-19946.
26. Rydén, M.; Ibáñez, C.F. Binding of Neurotrophin-3 to p75^{LNGFR}, TrkA, and TrkB Mediated by a Single Functional Epitope Distinct from That Recognized by TrkC. *J. Biol. Chem.* **1996**, *271*, 5623-5628.
27. Wiesmann, C.; Ultsch, M.H.; Bass, S.H.; de Vos, A.M. Crystal structure of nerve growth factor in complex with the ligand-binding domain of the TrkA receptor. *Nature*. **1999**, *401*, 184-188.
28. Ultsch, M.H.; Wiesmann, C.; Simmons, L.C.; Henrich, J.; Yang, M. Crystal structures of the neurotrophin-binding domain of TrkA, TrkB and TrkC. *J. Mol. Biol.* **1999**, *290*, 149-159.
29. Banfield, M.J.; Naylor, R.L.; Robertson, A.G.S.; Allen, S.J.; Dawbarn, D.; Brady, R.L. Specificity in Trk Receptor: Neurotrophin Interactions: The Crystal Structure of TrkB-d5 in Complex with Neurotrophin-4/5. *Structure* **2001**, *9*, 1191-1199.

30. Ahmed, F.; Hristova, K. Dimerization of the Trk receptors in the plasma membrane: effects of their cognate ligands. *Biochem. J.* **2018**, *475*, 3669-3685.
31. Franco, M.L.; Nadezhdin, K.D.; Goncharuk, S.A.; Mineev, K.S.; Arseniev, A.S.; Vilar, M. Structural basis of the transmembrane domain dimerization and rotation in the activation mechanism of the TrkA receptor by nerve growth factor. *J. Biol. Chem.* **2020**, *295*, 275-286.
32. Cazorla, M.; Prémont, J.; Mann, A.; Girard, N.; Kellendonk, C.; Rognan, D. Identification of a low-molecular weight TrkB antagonist with anxiolytic and antidepressant activity in mice. *J. Clin. Investig.* **2011**, *121*, 1846-1857.
33. Dhakal, S.; He, L.; Lyuboslavsky, P.; Sidhu, C.; Chrenek, M.A.; Sellers, J.T.; Boatright, J.H.; Geisert, E.E.; Setterholm, N.A.; McDonald, F.E.; Iuvone, P.M. A Tropomyosin-Related Kinase B Receptor Activator for the Management of Ocular Blast-Induced Vision Loss. *J. Neurotrauma.* **2021**, *38*, 2896-2906.
34. Yoo, J.M.; Lee, B.D.; Sok, D.E.; Ma, J.K.; Kim, M.R. Neuroprotective action of *N*-acetyl serotonin in oxidative stress-induced apoptosis through the activation of both TrkB/CREB/BDNF pathway and Akt/Nrf2/Antioxidant enzyme in neuronal cells. *Redox Biol.* **2016**, *11*, 592-599.
35. Chan, M.Y.; Pang, S.F.; Tang, P.L.; Brown, G.M. Studies on the kinetics of melatonin and *N*-acetyl serotonin in the rat at mid-light and mid-dark. *J. Pineal Res.* **1984**, *1*, 227-236.
36. Toutain, P.L.; Bousquet-Mélou. Plasma terminal half-life. *J. Vet. Pharmacol. Ther.* **2004**, *27*, 427-429.
37. Buendia, I.; Navarro, E.; Michalska, P.; Gameiro, I.; Egea, J.; Abril, S.; López, A.; González-Lafuente, López, M.G.; León, R. New melatonin-cinnamate hybrids as multi-target drugs for neurodegenerative diseases: Nrf2-induction, antioxidant effect and neuroprotection. *Future Med. Chem.* **2015**, *7*, 1961-1969.
38. Rui, T.; Wang, Z.; Li, Q.; Wang, H.; Wang, T.; Zhang, M.; Tao, L.; Luo, C. A TrkB receptor agonist *N*-acetyl serotonin provides cerebral protection after traumatic brain injury by mitigating apoptotic activation and autophagic dysfunction. *Neurochem. Int.* **2020**, *132*, 1-9.
39. Gardner, R.C.; Dams-O'Connor, K.; Morrissey, M.R.; Manley, G.T. Geriatric traumatic brain-injury: epidemiology, outcomes, knowledge gaps, and future directions. *J. Neurotrauma.* **2018**, *35*, 889-906.
40. Horner, M.D.; Ferguson, P.L.; Selassie, A.W.; Labbate, L.A.; Kniele, K.; Corrigan, J.D. Patterns of alcohol use 1 year after traumatic brain injury: a population-based, epidemiological study. *J. Int. Neuropsychol. Soc.* **2005**, *11*, 322-330.
41. Holsinger, T.; Steffens, D.C.; Phillips, C.; Helms, M.J.; Havlik, R.J.; Breitner, J.C.S.; Guralnik, J.M.; Plassman, B.L. Head injury in early adulthood and the lifetime risk of depression. *Arch. Gen. Psychiatry.* **2002**, *59*, 17-22.
42. Mackelprang, J.L.; Bombardier, C.H.; Fann, J.R.; Temkin, N.R.; Barber, J.K.; Dikmen, S.S. Rates and predictors of suicidal ideation during the first year after Traumatic Brain Injury. *Am. J. Public Health.* **2014**, *104*, e100-e107.
43. Li, Q.; Wang, P.; Huang, C.; Chen, B.; Liu, J.; Zhao, M.; Zhao, J. *N*-acetyl serotonin protects neural progenitor cells against oxidative stress-induced apoptosis and improves neurogenesis in adult mouse hippocampus following traumatic brain injury. *J. Mol. Neurosci.* **2019**, *67*, 574-588.
44. Brunner, N.; Stein, L.; Cornelius, V.; Knittel, R.; Fallier-Becker, P.; Amasheh, S. Blood-brain barrier protein claudin-5 expressed in paired *Xenopus laevis* oocytes mediates cell-cell interaction. *Front. Physiol.* **2020**, *11*, 1-9.
45. Dutca, L.M., Stasheff, S.F., Hedberg-Buenz, A., Rudd, D.S., Batra, N., Blodi, F.R., Yorek, M.S., Yin, T., Shankar, M., Herlein, J.A., Naidoo, J., Morlock, L., Williams, N., Kardon, R.H., Anderson, M.G., Pieper, A.A. & Harper, M.M. Early

- detection of subclinical visual damage after blast-mediated TBI enables prevention of chronic visual deficit by treatment with P7C3-S243. *Investig. Ophthalmol. Vis. Sci.* **2014**, *55*, 8330-8341.
46. Shen, J.; Ghai, K.; Sompol, P.; Liu, X.; Cao, X.; Iuvone, P.M.; Ye, K. *N*-acetyl serotonin derivatives as potent neuroprotectants for retinas. *PNAS.* **2012**, *109*, 3540-3545.
47. Tkachenko, S.E.; Okun, I.M.; Rivkis, S.A.; Kravchenko, D.V.; Khvat, A.V.; Ivashchenko, A.V. Heterocyclic compounds for inhibiting the melanocortin receptor MC2R. RU 2303597, May 12, 2006.
48. Ran, R. Preparation of aspartic acid-modified melatonin derivatives and application thereof. CN 102816103, August 20, 2012.
49. Bartolucci, S.; Mari, M.; Bedini, A.; Piersanti, G.; Spadoni, G. Iridium-catalyzed direct synthesis of tryptamine derivatives from indoles: exploiting *N*-protected β -amino alcohols as alkylating agents. *J. Org. Chem.* **2015**, *80*, 3217-3222.
50. Hwang, K-J.; Lee, T-S. A practical synthesis of *N*-acetyl-5-methoxytryptamine (melatonin). *Synth. Commun.* **1999**, *29*, 2099-2104.
51. Setterholm, N.A.; McDonald, F.E.; Boatright, J.H.; Iuvone, P.M. Gram-scale, chemoselective synthesis of *N*-[2-(5-hydroxy-1H-indol-3-yl)ethyl]-2-oxopiperidine-3-carboxamide (HIOC). *Tetrahedron Lett.* **2015**, *56*, 3413-3415.
52. Shen, J.; Maruyama, I.N. Brain-derived neurotrophic factor receptor TrkB exists as a preformed dimer in living cells. *J. Mol. Signal.* **2012**, *7*, 1-7.
53. Perlman, I. Relationships between the amplitudes of the b wave and the a wave as a useful index for evaluating the electroretinogram. *Br. J. Ophthalmol.* **1983**, *67*, 443-448.
54. Tang, J.; Hu, X.; Chen, Y.; Liu, F.; Zheng, Y.; Tang, J.; Zhang, J.; Zhang, J. Neuroprotective role of an *N*-acetyl serotonin derivative via activation of tropomyosin-related kinase receptor B after subarachnoid hemorrhage in a rat model. *Neurobiol. Dis.* **2015**, *78*, 126-133.
55. Colombo, P.S.; Flamini, G.; Christodoulou, M.S.; Rodondi, G.; Vitalini, S.; Passarella, D.; Fico, G. Farinose alpine *Primula* species: phytochemical and morphological investigations. *Phytochemistry.* **2014**, *98*, 151-159.
56. Jang, S-W.; Liu, X.; Yepes, M.; Shepherd, K.R.; Miller, G.W.; Liu, Y.; Wilson, W.D.; Xiao, G.; Bianchi, B.; Sun, Y.E.; Ye, K. A selective TrkB
57. Chan, C.B.; Tse, M.C.L.; Liu, X.; Zhang, S.; Schmidt, R.; Otten, R.; Liu, L.; Ye, K. Activation of muscular TrkB by its small molecular agonist 7,8-dihydroxyflavone sex-dependently regulates energy metabolism in diet-induced obese mice. *Chem. Biol.* **2015**, *22*, 355-368.
58. Cushman, M.; Nagarathnam, D. A method for the facile synthesis of ring-A hydroxylated flavones. *Tetrahedron Lett.* **1990**, *31*, 6497-6500.
59. Zhao, X.; Jia, H.; Wang, Q.; Song, H.; Tang, Y.; Ma, L.; Shi, Y.; Yang, G.; Wang, Y.; Zang, Y.; Xu, S. The oxidative coupling between benzaldehyde derivatives and phenylacetylene catalyzed by rhodium complexes via C-H bond activation. *Heterocycl. Comm.* **2020**, *26*, 20-25.
60. Fastenau, J.; Kolotkin, R.L.; Fuijoka, K.; Alba, M.; Canovatchel, W.; Traina, S. A call to action to inform patient-centered approaches to obesity management: development of a disease-illness model. *Clin. Obes.* **2019**, *9*, 1-10.

61. Chan, C.B.; Tse, M.C.L.; Liu, X.; Zhang, S.; Schmidt, R.; Otten, R.; Liu, L.; Ye, K. Activation of muscular TrkB by its small molecular agonist 7,8-dihydroxyflavone sex-dependently regulates energy metabolism in diet-induced obese mice. *Chem. Biol.* **2015**, *22*, 355-368.
62. Ahmed, S.; Kwatra, M.; Gawali, B.; Panda, S.R.; Naidu, V.G.M. Potential role of TrkB agonist in neuronal survival by promoting CREB/BDNF and PI3K/Akt signaling in vitro and in vivo model of 3-nitropropionic acid (3-NP)-induced neuronal death. *Apoptosis.* **2021**, *26*, 53-70.
63. Chen, C.; Wang, Z.; Zhang, Z.; Liu, X.; Kang, S.S.; Zhang, Y.; Ye, K. The prodrug of 7,8-dihydroxyflavone development and therapeutic efficacy for treating Alzheimer's disease. *PNAS.* **2018**, *115*, 578-583.
64. Chen, C.; Ahn, E.H.; Liu, X.; Wang, Z-H.; Luo, S.; Liao, J.; Ye, K. Optimized TrkB Agonist Ameliorates Alzheimer's Disease Pathologies and Improves Cognitive Functions via Inhibiting Delta-Secretase. *ACS Chem. Neurosci.* **2021**, *12*, 2448-2461.
65. Ye, K. Substituted dihydroxyflavone derivatives, compositions, and methods related thereto. WO 2020033960, February 13, 2020.
66. Nguyen, H.T.H.; Wood, R.J.; Prawdiuk, A.R.; Furness, S.G.B.; Xiao, J.; Murray, S.S.; Fletcher, J.L. TrkB agonist LM22A-4 increases oligodendroglial populations during myelin repair in the corpus callosum. *Front. Mol. Neurosci.* **2019**, *12*, 1-12.
67. Massa, S.M.; Yang, T.; Xie, Y.; Shi, J.; Bilgen, M.; Joyce, J.N.; Nehama, D.; Rajadas, J.; Longo, F.M. Small molecule BDNF mimetics activate TrkB signaling and prevent neuronal degeneration in rodents. *J. Clin. Investig.* **2010**, *120*, 1774-1785.
68. Han, J.; Pollak, J.; Yang, T.; Siddiqui, M.R.; Doyle, K.P.; Taravosh-Lahn, K.; Cekanaviciute, E.; Han, A.; Goodman, J.Z.; Jones, B.; Jing, D.; Massa, S.M.; Longo, F.M.; Buckwalter, M.S. Delayed administration of a small molecule tropomyosin-related kinase B ligand promotes recovery after hypoxic-ischemic stroke. *Stroke.* **2012**, *43*, 1918-1924.
69. Boltaev, U.; Meyer, Y.; Tolibzoda, F.; Jacques, T.; Gassaway, M.; Xu, Q.; Wagner, F.; Zhang, Y.L.; Palmer, M.; Holson, E.; Sames, D. Multiplex quantitative assays indicate a need for re-evaluating reported small molecule TrkB agonists. *Sci. Signal.* **2017**, *10*, 1-10.
70. Eckert, M.J.; Martin, M.J. Trauma: spinal cord injury. *Surg. Clin. North. Am.* **2017**, *97*, 1031-1045.
71. Yu, G.; Wang, W. Protective effects of LM22A-4 on injured spinal cord nerves. *Int. J. Clin.* **2015**, *8*, 6526-6532.
72. Han, J.; Pollak, J.; Yang, T.; Siddiqui, M.R.; Doyle, K.P.; Taravosh-Lahn, K.; Cekanaviciute, E.; Han, A.; Goodman, J.Z.; Jones, B.; Jing, D.; Massa, S.M.; Longo, F.M.; Buckwalter, M.S. Delayed administration of a small molecule tropomyosin-related kinase B ligand promotes recovery after hypoxic-ischemic stroke. *Stroke.* **2012**, *43*, 1918-1924.
73. Sarikaya, H.; Ferro, J.; Arnold, M. Stroke Prevention- Medical and Lifestyle Measures. *Eur. Neurol.* **2015**, *73*, 150-157.
74. Jang, S.W.; Liu, X.; Chan, C.B.; France, S.A.; Sayeed, I.; Tang, W.; Lin, X.; Xiao, G.; Andero, R.; Chang, Q.; Ressler, K.J.; Ye, K. Deoxygedunin, a natural product with potent neurotrophic activity in mice. *PLoS ONE.* **2010**, *5*, 1-15.
75. Kipnis, P.A.; Sullivan, B.J.; Carter, B.M.; Kadam, S.D. TrkB agonists prevent postischemic emergence of refractory neonatal seizures in mice. *JCI Insight.* **2020**, *5*, 1-19.

76. Pinkerton, D.M.; Bernhardt, P.V.; Savage, G.P.; Williams, C.M. Towards the total synthesis of gedunin: construction of the fully elaborated ABC ring system. *Asian J. Org. Chem.* **2017**, *6*, 583-597.
77. Fernández-Mateos, A.; Teijón, P.H.; Coca, G.P.; González, R.R.; Simmonds, M.S.J. Synthesis of limonoid CDE fragments related to limonin and nimbinin. *Tetrahedron.* **2010**, *66*, 7257-7261.
78. Tsai, H.J.; Chou, S-Y. A novel hydroxyfuroic acid compound as an insulin receptor activator structure and activity relationship of a prenylindole moiety to insulin receptor activation. *J. Biomed. Sci.* **2009**, *16*, 1-12.
79. Mytilineou, C.; Leonardi, E.K.; Radcliffe, P.; Heinonen, E.H.; Han, S.K.; Werner, P.; Cohen, G.; Olanow, C.W. Deprenyl and desmethylselegiline protect mesencephalic neurons from toxicity induced by glutathione depletion. *J. Pharmacol. Exp. Ther.* **1998**, *284*, 700-706.
80. Maruyama, W.; Takahashi, T.; Naoi, M. (-)-Deprenyl protects human dopaminergic neuroblastoma SH-SY5Y cells from apoptosis induced by peroxynitrite and nitric oxide. *J. Neurochem.* **1998**, *70*, 2510-2515.
81. Nakaso, N.; Nakamura, C.; Sato, H.; Imamura, K.; Takeshima, T.; Nakashima, K. Novel cytoprotective mechanism of anti-parkinsonian drug deprenyl: PI3K and Nrf2-derived induction of antioxidative proteins. *Biochem. Biophys. Res. Commun.* **2006**, *339*, 915-922.
82. Ye, C-X.; Melcamu, Y.Y.; Li, H-H.; Cheng, J-T.; Zhang, T-T.; Ruan, Y-P.; Zheng, X.; Lu, X.; Huang, P-Q. Dual catalysis for enantioselective convergent synthesis of enantiopure vicinal amino alcohols. *Nat. Commun.* **2018**, *9*, 1-9.
83. Yang, T.; Massa, S.M.; Tran, K.C.; Simmons, D.A.; Rajadas, J.; Zeng, A.Y.; Jang, T.; Carsanaro, S.; Longo, F.M. A small molecule TrkB/TrkC neurotrophin receptor co-activator with distinctive effects on neuronal survival and process outgrowth. *Neuropharmacology.* **2016**, *110*, 343-361.
84. Lee, C.G.; Park, J.Y.; Park, Y.I.; Jung, S-H.; Lee, G.S.; Park, J.M.; Hwang, D-H.; Kong, H. Synthesis and characterization of novel triarylmethane-based dyes for thermally stable blue color filters. *J. Nanosci. Nanotechnol.* **2019**, *19*, 4782-4786.
85. Zhang, H.; Chen, X.; Zheng, T.; Lin, M.; Chen, P.; Liao, Y.; Gong, C.; Gao, F.; Zheng, X. Amitriptyline protects against lidocaine-induced neurotoxicity in SH-SY5Y cells via inhibition of BDNF-mediated autophagy. *Neurotox. Res.* **2021**, *39*, 133-145.
86. Zheng, X.; Chen, F.; Zheng, T.; Huang, F.; Chen, J.; Tu, W. Amitriptyline activates TrkA to aid in neuronal growth and attenuate anesthesia-induced neurodegeneration in rat dorsal root ganglion neurons. *Medicine.* **2016**, *95*, 1-6.
87. Jang, S-W.; Liu, X.; Chan, C-B.; Weinschenker, D.; Hall, R.A.; Xiao, G.; Ye, K. Amitriptyline is a TrkA and TrkB receptor agonist that promotes TrkA/TrkB heterodimerization and has potent neurotrophic activity. *Chem. Biol.* **2009**, *16*, 644-656.
88. Cong, W-N.; Chadwick, W.; Wang, R.; Daimon, C.M.; Cai, H.; Amma, J.; Wood III, W.H.; Becker, K.G.; Martin, B.; Maudsley, S. Amitriptyline improves motor function via enhanced neurotrophin signaling and mitochondrial functions in the murine N171-82Q Huntington Disease model. *J. Biol. Chem.* **2015**, *290*, 2728-2743.
89. Pirrung, M.C.; Liu, Y.; Deng, L.; Halstead, D.K.; Li, Z.; May, J.F.; Wedel, M.; Austin, D.A.; Webster, N.J.G. Methyl scanning: total synthesis of demethylasterriquinone B1 and derivatives for identification of sites of interaction with and isolation of its receptor(s). *J. Am. Chem. Soc.* **2005**, *127*, 4609-4624.

90. Tsai, H.J.; Chou, S-Y. A novel hydroxyfuroic acid compound as an insulin receptor activator structure and activity relationship of a prenylindole moiety to insulin receptor activation. *J. Biomed. Sci.* **2009**, *16*, 1-12.

91. Wilkie, N.; Wingrove, P.B.; Bilisland, J.G.; Young, L.; Harper, S.J.; Hefti, F.; Ellis, S.; Pollack, S.J. The non-peptidyl fungal metabolite L-783,281 activates TRK neurotrophin receptors. *J. Neurochem.* **2001**, *78*, 1135-1145.

92. Ahimsadasan, N.; Reddy, V.; Kumar, A. Neuroanatomy, Dorsal Root Ganglion. Treasure Island (FL): StatPearls Publishing, 2021. PMID: 30335324.

Chapter III: Assessing Lactam Ring Size in N-Acyl Serotonin Derivatives for Treating Trauma-Induced Vision Loss

1. Introduction

Each year, according to the Centers of Disease Control and Prevention, 1.7 million people are diagnosed with a traumatic brain injury (TBI) in the United States. Causes of TBI include falls (51%) and motor vehicle accidents (9%). For adults 65 and older, the rate of hospitalization for nonfatal TBI doubles to 155.9 per 100,000 population. In 2003, the cost of treating TBI in this population exceeded \$2.2 billion. Given the projected population growth in the United States by 2030, the cost of treating TBI and death toll will be staggering. Blast-related injuries are another cause of TBI, frequent on the battlefield. They are caused by blasts from mines, improvised explosive devices and were the leading cause of injury in recent wars in Iraq and Afghanistan.¹

Retinal damage is caused by sports injury, traumatic blast-related injury, or other blunt force trauma to the eye. Vision loss resulting from retinal damage is attributed to ocular damage and insult to optic nerve or central visual pathways.^{2,3} TBI patients suffer from prolonged visual consequences, including impaired visual acuity, light sensitivity, visual disturbances, and reading difficulties.¹ Current treatments for injuries and diseases to ocular structures and visual systems, including TBI, remain inadequate, so we aim to address the urgent need for a therapy that can be quickly administered following injury to the eye in a public emergency environment.

N-[2-(5-hydroxy-1H-indol-3-yl)ethyl]-2-oxopiperidine-3-carboxamide (HIOC, **(1)**, $n=1$) is a *N*-acetylserotonin (NAS) derivative that protects against blast-induced retinal degeneration and vision loss when administered shortly after blast exposure (**Figure 1**).⁴ While NAS and HIOC both activate tropomyosin-related kinase receptor type B (TrkB) and offer neuroprotective properties, HIOC is more clinically relevant due to its longer *in vivo* half-life and its ability to activate TrkB for up to 16 hours following injection.^{5,6} HIOC has also been studied in the context of retinal damage and Subarachnoid Hemorrhage (**Section 5.1.2c** and **Section 5.1.2d** of Chapter II).

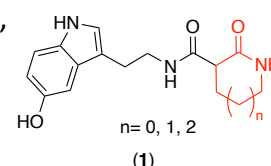
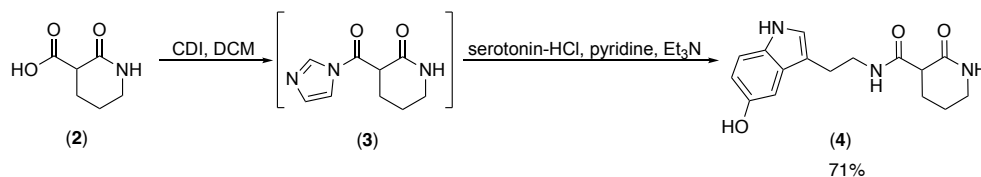


Figure 1: Chemical structure of HIOC with lactam in red.

Members of the McDonald and Iuvone labs are developing HIOC derivatives with superior blood brain/retina barrier penetrance and potency than HIOC. The origin of the 6-membered lactam ring of HIOC may have originated as a byproduct of the Fischer Indole reaction synthesizing melatonin.^{7,8} The first synthetic protocol for HIOC (**(4)**), published in 2015, involves carbonyldiimidazole (CDI) activating the carboxylic acid (**(2)**) to a soluble *N*-acyl imidazole derivative followed by addition of serotonin-hydrochloride to the intermediate (**(3)**) (**Scheme 1**).⁹



Scheme 1: Synthesis of HIOC.⁹

Ring size has not been previously considered or studied. I hypothesize that modifying lactam ring size will alter the direction of the carbonyl and N-H bonds of the lactam, the preferred rotamer of the ring carbon attached to the carbonyl linking the serotonin core, and *in vivo* half-life and pharmacokinetics. In this chapter, I report the synthesis of the 7-membered lactam HIOC derivative and progress towards the 5-membered lactam HIOC analog. This work is part of the overall goal to create more potent analogs with selectivity for TrkB activation and other efficacious properties.

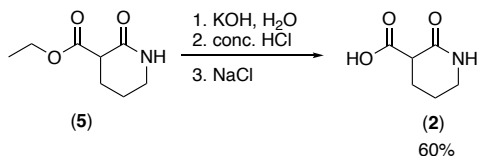
2. Experimental Approach

2.1 General Experimental Procedures

All reagents were purchased from Sigma-Aldrich, TCI, Alfa Aesar, and Oakwood Chemicals, ACS reagent grade or better, and used as received. ¹H, ¹³C, and COSY NMR were recorded in CDCl₃ or DMSO on INOVA 400 at 400 MHz. Tetramethylsilane was used as the internal standard.

2.2 Synthesis of *N*-(2-(5-hydroxy-1H-indol-3-yl)ethyl)-2-oxopiperidine-3-carboxamide (HIOC)

2.2.1 Synthesis of 2-oxopiperidine-3-carboxylic acid⁹ (2)

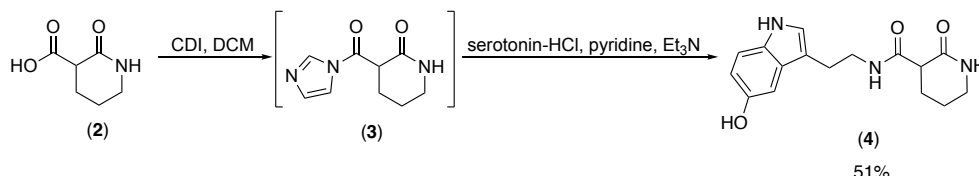


Scheme 2: Synthesis of 2-oxopiperidine-3-carboxylic acid.

Water (15 mL), 3-ethoxycarbonyl-2-piperidone (**5**) (1.00 g, 5.84 mmol, 1.0 equiv), and potassium hydroxide pellets (1.4477 g, 25.803 mmol, 4.4 equiv) were added to a 50 mL round bottom flask with a stir bar. Mixture stirred at room temperature under argon for 1 hour. The reaction was quenched by dropwise addition of concentrated HCl and monitored by pH paper until a pH of 3 was achieved. 10 g of NaCl was added, and the mixture was agitated. Aqueous layer was transferred to a separatory funnel by decanting. 50 mL of 85:15 chloroform:isopropanol was added to the aqueous layer and shaken vigorously with venting.

Organic layer was removed and collected, and extraction on the aqueous layer was repeated 5 times. Brine was added to the organic layers, which were combined and transferred back into the separatory funnel. Anhydrous magnesium sulfate was added to the organic layer and filtered using a fritted funnel. The filtrate was concentrated by rotary evaporation to yield product (**2**) as a white solid (0.4909 g, 60%). ¹H NMR (400 MHz, DMSO): δ 12.61 (s, 1H), 7.78 (s, 1H), 3.86 – 3.71 (m, 0H), 3.33 (s, 2H), 3.24 – 3.03 (m, 3H), 2.07 – 1.54 (m, 3H), 1.04 (d, *J* = 6.1 Hz, 0H). ¹³C NMR: δ 172.7, 167.9, 48.4, 41.7, 24.9, 20.7.

2.2.2 Synthesis of *N*-(2-(5-hydroxy-1H-indol-3-yl)ethyl)-2-oxopiperidine-3-carboxamide (HIOC)⁹ (4)



Scheme 3: Synthesis of *N*-(2-(5-hydroxy-1H-indol-3-yl)ethyl)-2-oxopiperidine-3-carboxamide (HIOC).

Under an argon atmosphere, compound **(2)** (0.2024 g, 1.414 mmol, 2.43 equiv) and 1,1'-carbonyldiimidazole (0.2396 g, 1.478 mmol, 2.53 equiv) were added to an oven-dried 25 mL round bottom flask. Anhydrous dichloromethane (4.6 mL) was added, and the mixture stirred for 1 hour. Serotonin hydrochloride (0.1240 g, 0.5831 mmol, 1.0 equiv) was slowly added to the mixture followed by anhydrous pyridine (4.6 mL). Small portions of serotonin-HCl were added every 30 seconds. Lower yields of HIOC were obtained when serotonin-HCl was added more rapidly. Before and after serotonin addition, the mixture appeared clear red/brown. After 10 minutes, the majority of serotonin hydrochloride had dissolved. Triethylamine (0.40 mL, 2.9 mmol, 4.9 equiv) was added, and the clear red/brown colored mixture stirred for 4 hours at room temperature. After 4 hours, the reaction was analyzed by thin layer chromatography or TLC (9:1 ethyl acetate:methanol, stained with *p*-anisaldehyde). Serotonin and HIOC had purple spots on the baseline with HIOC appearing as an elongated purple spot. The reaction mixture was stirred for an additional 2 hours and concentrated by rotary evaporation to produce a brown sticky oil (3.3968 g).

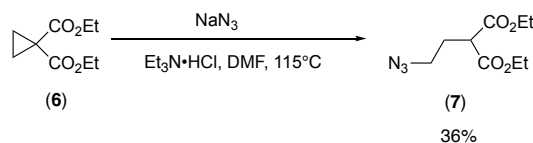
Crude product was dissolved in minimal ethyl acetate and silica gel. Rotary evaporation was performed to remove ethyl acetate. Crude product adsorbed on silica gel was dry-loaded onto a chromatography column, eluted via ethyl acetate:methanol gradient, and monitored by TLC. 98:2 ethyl acetate:methanol (150 mL) eluted the least polar material; 95:5 ethyl acetate:methanol (500 mL) eluted HIOC, and 93:7 ethyl acetate:methanol (500 mL) eluted remaining HIOC. HIOC began to appear after 400 mL of 95:5 ethyl acetate:methanol was ran through the column and appeared as a dark purple spot in TLC (9:1 ethyl acetate:methanol, stained with *p*-anisaldehyde). Combined fractions were concentrated by rotary evaporation to yield a white solid (0.2532 g).

Warm ether (90 mL) was added, boiled in a 41°C water bath, and decanted. This process was repeated twice. The solid remaining after decanting was concentrated under rotary evaporation to produce a light pale solid and loaded onto a fritted funnel. Acetone (10 mL) was added, and the suspension was agitated with a spatula prior to vacuum to remove traces of imidazole impurities that co-eluted with HIOC in silica gel column chromatography. HIOC (**4**) appeared as a pale solid (0.0907 g, 51%). ¹H NMR (400 MHz, DMSO) δ 10.64 – 10.36 (m, 1H), 8.58 (s, 1H), 8.06 (t, *J* = 5.6 Hz, 1H), 7.66 (s, 1H), 7.12 (dd, *J* = 8.6, 0.6 Hz, 1H), 7.06 (d, *J* = 2.4 Hz, 1H), 6.83 (d, *J* = 2.4 Hz, 1H), 6.58 (dd, *J* = 8.6, 2.3 Hz, 1H), 4.10 (q, *J* = 5.3 Hz, 1H), 4.04 (q, *J* = 7.1 Hz, 0H), 3.33 (s, 21H), 3.30 – 3.21 (m, 1H), 3.20 – 3.11 (m, 4H), 3.07 (dd, *J* = 7.9, 6.2 Hz, 1H), 2.72

(t, $J = 7.5$ Hz, 2H), 2.10 – 1.71 (m, 2H), 1.65 – 1.51 (m, 1H), 1.24 – 1.13 (m, 0H). ^{13}C NMR: δ 170.4, 168.8, 150.7, 131.4, 128.4, 123.7, 112.1, 111.7, 111.2, 102.3, 48.5, 41.8, 25.7, 25.0, 21.0.

2.3 Approach 1: Synthesis of 5-membered lactam through diethyl 2-azidoethylmalonate (**7**) and ethyl 2-oxo-3-pyrrolidinecarboxylate (**8**)

2.3.1 Synthesis of diethyl 2-azidoethylmalonate¹⁰ (**7**)

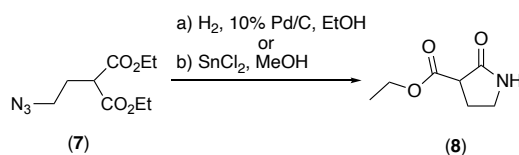


Scheme 4: Synthesis of diethyl 2-azidoethylmalonate.

Sodium azide (2.0778 g, 31.961 mmol, 1.0 equiv), triethylamine hydrochloride (44.4219 g, 32.149 mmol, 1.01 equiv), and diethyl 1,1-cyclopropane dicarboxylate (**6**) (10 mL) were added to a 25 mL round bottom flask and heated in N,N-dimethylformamide (2.85 mL) for 21 hours in a 92°C sand bath. After 21 hours, reaction mixture appeared orange with some white insoluble solid on the bottom of the flask. The product spot in TLC (8:2 EtOAc:methanol, *p*-anisaldehyde) appeared as a yellow spot.

Mixture was cooled to room temperature, diluted with ether, and washed with water (300 mL). Organic layer was dried with anhydrous MgSO_4 , and solvent was removed by rotary evaporation to obtain an orange oil (2.3949 g). Vacuum distillation (92°C) removed impurities present in crude to obtain purified product (**7**) as a clear oil (1.318 g, 36%). ^1H NMR (400 MHz, CDCl_3): δ 4.20 (qd, $J = 7.1, 1.8$ Hz, 4H), 3.47 (t, $J = 7.3$ Hz, 1H), 3.38 (t, $J = 6.6$ Hz, 2H), 2.15 (dt, $J = 7.4, 6.6$ Hz, 2H), 1.26 (t, $J = 7.2$ Hz, 6H).

2.3.2 Synthesis of ethyl 2-oxo-3-pyrrolidinecarboxylate^{10,11} (**8**)



Scheme 5: Synthesis of ethyl 2-oxo-3-pyrrolidinecarboxylate.

Approach 1: Hydrogenation¹⁰

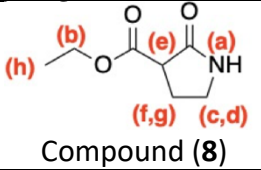
In a 15 mL round bottom flask and under argon atmosphere, distilled compound (**7**) (0.2486 g, 1.085 mmol, 4.95 equiv) in ethanol (4.34 mL) was hydrogenated over 10% Pd/C (0.0233 g, 0.219 mmol, 1.0 equiv) for 2.5 hours at room temperature and 1 atm using a hydrogen balloon. The mixture appeared black. Mixture was filtered through Celite on a 60 mL fritted funnel, and solvent was removed by rotary evaporation to obtain compound (**8**) as a white crystalline solid. Recrystallization from ethyl acetate-hexane was attempted but was unsuccessful in removing impurities. ^1H NMR (400 MHz, CDCl_3): δ 5.64 (s, 1H), 4.27 (q, $J = 7.1$ Hz, 2H), 4.15 (q, $J = 7.1$ Hz, 2H), 3.60 – 3.47 (m, 1H), 3.47 – 3.32 (m, 2H), 2.57 (dddd, $J = 13.0, 8.5, 7.0, 6.0$ Hz, 1H), 2.49 –

2.32 (m, 1H), 2.29 – 2.10 (m, 0H), 2.07 (s, 3H), 1.97 – 1.83 (m, 10H), 1.83 – 1.71 (m, 16H), 1.44 – 1.20 (m, 262H), 1.20 – 1.03 (m, 31H), 1.03 – 0.78 (m, 274H), 0.78 – 0.67 (m, 1H).

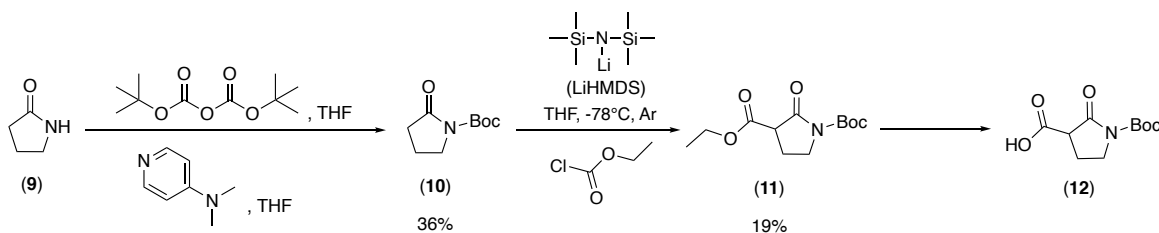
Approach 2: Reduction of azide to amide by SnCl₂ in MeOH¹¹

A stirred suspension of impure compound (**7**) (0.3306 g, 1.442 mmol, 1.0 equiv) in methanol (3.30 mL) was added dropwise to SnCl₂ (0.4947 g, 2.609 mmol, 1.81 equiv). Mixture stirred at room temperature for 2 hours. Methanol was removed by rotary evaporation, and residue was diluted with water and neutralized to pH 7 with NaOH. Ether was added, and the layers separated. Aqueous layer was saturated with NaCl and re-extracted with ether. Combined layers were dried over sodium sulfate and concentrated by rotary evaporation to obtain impure (**8**) as a clear, solid paste. ¹H NMR (400 MHz, CDCl₃): δ 6.54 (s, 1H), 5.43 – 5.19 (m, 0H), 4.57 – 4.31 (m, 1H), 4.28 – 4.16 (m, 10H), 4.10 – 3.88 (m, 0H), 3.85 – 3.58 (m, 2H), 3.58 – 3.46 (m, 2H), 3.46 – 3.34 (m, 4H), 3.20 – 2.83 (m, 0H), 2.79 – 2.60 (m, 0H), 2.59 – 2.45 (m, 1H), 2.43 – 2.30 (m, 1H), 2.17 (dt, *J* = 7.4, 6.1 Hz, 3H), 1.96 (d, *J* = 7.3 Hz, 0H), 1.51 – 1.37 (m, 1H), 1.37 – 1.21 (m, 15H), 1.01 – 0.67 (m, 0H).

Table 1. Comparison of NMR spectra of ethyl 2-oxo-3-pyrrolidinecarboxylate (**8**) obtained from hydrogenation (approach 1) and reduction of azide to amide by SnCl₂ in methanol (approach 2).

 Compound (8)	Approach 1: Hydrogenation	Approach 2: Reduction of azide to amide by SnCl ₂ in MeOH
Present	Peaks a, b, c, d, e, f, g, h	Peaks a, b, c, d, e, f, g, h
Impurities	Diethyl 2-azidoethylmalonate (7) and impurities at 1.89 ppm, 1.75 ppm, 1.11 ppm, and 0.74 ppm	Most of the impurities were from the use of impure diethyl 2-azidoethylmalonate (7). Impurity also present at 2.66 ppm.

2.4 Approach 2: Synthesis of 5-membered lactam through tert-butyl 2-oxopyrrolidine-1-carboxylate¹² (10**), 1-(tert-butyl)-3-ethyl 2-oxopyrrolidine-1,3 dicarboxylate (**11**), and 1-(tert-butoxycarbonyl)-2-oxopyrrolidine-3-carboxylic acid (**12**)**



Scheme 6: Synthesis of tert-butyl 2-oxopyrrolidine-1-carboxylate, 1-(tert-butyl)-3-ethyl 2-oxopyrrolidine-1,3 dicarboxylate, and 1-(tert-butoxycarbonyl)-2-oxopyrrolidine-3-carboxylic acid.

2.4.1 Synthesis of tert-butyl 2-oxopyrrolidine-1-carboxylate (10**)**

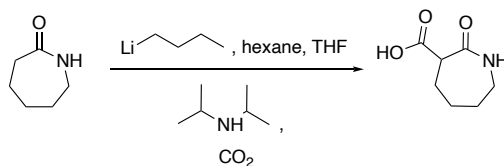
In a 100 mL round bottom flask, di-tert-butyl dicarbonate (6.8324 g, 31.305 mmol, 1.07 equiv) in dry THF (16 mL) was added to 2-pyrrolidone (**9**) (3.0252 g, 35.545 mmol, 1.22 equiv) and N,N-

4-dimethylaminopyridine (3.5733 g, 29.249 mmol, 1.0 equiv) in dry THF (32 mL) at room temperature for 3 hours.¹² Reaction appeared clear yellow. Solvent was evaporated by rotary evaporation, and ethyl acetate was added. Reaction mixture was washed with 0.5M HCl, brine, and sodium bicarbonate. Organic layer was dried with magnesium sulfate, and solvent was evaporated by rotary evaporation to obtain purified product (**10**) as a clear yellow oil (2.3659 g, 36% yield). ¹H NMR (400 MHz, CDCl₃): δ 3.87 – 3.60 (m, 2H), 2.51 (tt, *J* = 8.4, 0.9 Hz, 2H), 2.12 – 1.89 (m, 2H), 1.64 – 1.40 (m, 9H). ¹³C NMR: δ 174.4, 150.3, 82.8, 46.5, 33.0, 28.1, 17.4.

2.4.2 Synthesis of 1-(tert-butyl)-3-ethyl 2-oxopyrrolidine-1,3 dicarboxylate (**11**)

Compound (**10**) (0.92 mL, 5.4 mmol, 1.0 equiv) in dry THF (10 mL) was added to 1 M LiHMDS in dry THF (4.20 mL, 21.6 mmol, 4.0 equiv), slowly under an argon environment at -78°C in a 25 mL round bottom flask. Mixture stirred for an hour at -78°C, and ethyl chloroformate (0.62 mL, 6.5 mmol, 1.20 equiv) was added dropwise under argon environment at -78°C. Reaction was warmed slowly to room temperature, stirred for an hour, quenched with ice, and extracted with ethyl acetate.¹³ Organic layer was washed with saturated sodium bicarbonate and brine, dried over sodium sulfate, and concentrated by rotary evaporation to obtain a brown oil (0.2623 g, 19%). Crude (**11**) was used without further purification. ¹H NMR (400 MHz, CDCl₃): δ 4.29 (dq, *J* = 22.2, 7.1, 0.9 Hz, 2H), 3.91 (ddd, *J* = 10.8, 8.5, 5.3 Hz, 1H), 3.79 – 3.67 (m, 1H), 3.55 (dd, *J* = 9.1, 7.5 Hz, 1H), 2.49 – 2.33 (m, 1H), 2.33 – 2.15 (m, 1H), 1.55 (s, 14H), 1.33 (td, *J* = 7.1, 1.1 Hz, 5H). ¹³C NMR: δ 174.4, 168.8, 150.0, 83.5, 62.0, 50.3, 44.9, 33.00, 28.2-28.0, 21.5, 14.1.

2.5 Approach 1: Synthesis of 7-membered lactam through a one-step approach^{14,15}



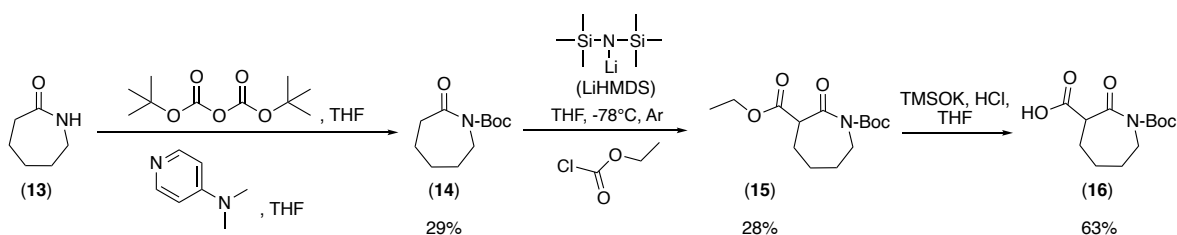
Scheme 7: Synthesis of 2-oxoazepane-3-carboxylic acid.

In a 100 mL round bottom flask, 1.82M solution of *n*-butyllithium (0.13 mL, 1.5 mmol, 1.1 equiv) in hexane and dry THF (3.80 mL) was added to 0.10M diisopropylamine (0.19 mL, 1.4 mmol, 1.0 equiv) at -50°C under an argon atmosphere. After stirring for 23 minutes at -5 to -7°C, caprolactam (0.4360 g, 3.853 mmol, 2.84 equiv) in THF (1.08 mL) was added to the mixture at -20 to -15°C for 10 minutes and then cooled to -70°C.

Mortar and pestle were used to mill dry ice into fine particles. Under an argon atmosphere, 22 mL of anhydrous THF was added to a 500 mL Erlenmeyer flask, which was cooled to -78°C. Freshly milled dry ice was slowly added via powder funnel. To avoid pressure buildup, flask was left open to atmosphere following dry ice addition. Flask was vigorously swirled to ensure dry ice was submerged in solvent. Resulting slurry was filtered by fritted funnel under an argon atmosphere, and milled dry ice was transferred to the reaction flask through powder funnel quickly.

Following dry ice addition, reaction was warmed to 0°C. During a two-hour period, the mixture was diluted with aqueous sodium hydrogen carbonate (8 mL) and ethyl acetate (8 mL). Aqueous layer was acidified with HCl to pH 2, saturated with saline, and extracted with methyl ethyl ketone. Extract was washed with saturated saline, dried over magnesium sulfate, and concentrated to obtain a clear oil. Product was not successfully synthesized.

2.6 Approach 2: Synthesis of 7-membered lactam through tert-butyl 2-oxoazepane-1-carboxylate (14), 1-(tert-butyl)-3-ethyl 2-oxoazepane-1,3-dicarboxylate (15), and 1-(tert-butoxycarbonyl)-2-oxoazepane-3-carboxylic acid (16)



Scheme 8: Synthesis of tert-butyl 2-oxoazepane-1-carboxylate, 1-(tert-butyl)-3-ethyl 2-oxoazepane-1,3-dicarboxylate, and 1-(tert-butoxycarbonyl)-2-oxoazepane-3-carboxylic acid.

2.6.1 Synthesis of tert-butyl 2-oxoazepane-1-carboxylate¹² (14)

Di-tert-butyl dicarbonate (6.97 mL, 30.3 mmol, 1.14 equiv) in dry THF (16 mL) was added to caprolactam (13) (3.0215 g, 26.701 mmol, 1.0 equiv) and N,N-dimethylaminopyridine (3.5670 g, 29.197 mmol, 1.09 equiv) in dry THF (32 mL) at room temperature for 3 hours in a 100 mL round bottom flask. Reaction appeared clear yellow. Solvent was evaporated by rotary evaporation, and ethyl acetate was added. Reaction mixture was washed with 0.5M HCl, brine, and sodium bicarbonate. Organic layer was dried with magnesium sulfate, and solvent was evaporated by rotary evaporation to obtain a clear yellow oil (14) (1.6210 g, 29% yield). ¹H NMR (400 MHz, CDCl₃): δ 3.80 – 3.71 (m, 2H), 2.69 – 2.60 (m, 2H), 1.83 – 1.71 (m, 5H), 1.50 (d, J = 20.3 Hz, 10H). ¹³C NMR: δ 175.8, 152.9, 82.7, 46.1, 39.5, 29.2, 28.7, 27.9, 23.5.

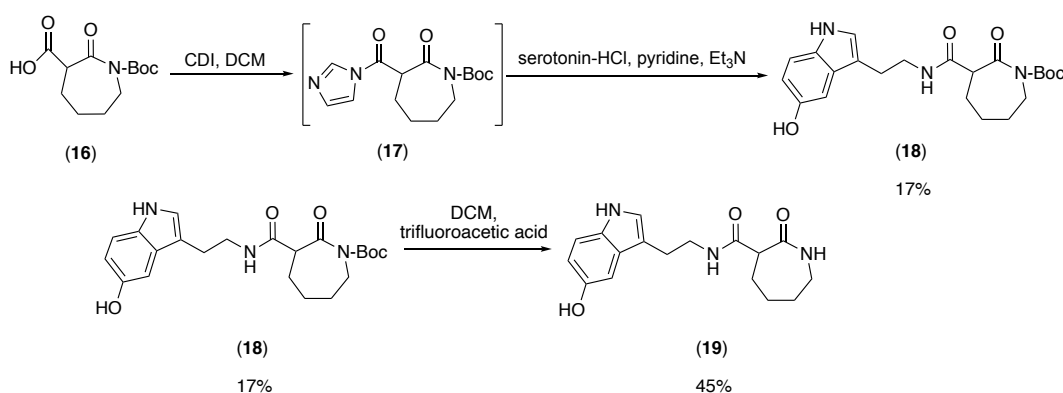
2.6.2 Preparation of 1-(tert-butyl)-3-ethyl 2-oxoazepane-1,3 dicarboxylate (15)

In a 25 mL round bottom flask, compound (14) (0.84 mL, 4.1 mmol, 1.0 equiv) in dry THF (8.72 mL) was added to 1 M LiHMDS in dry THF (3.18 mL, 16.4 mmol, 4.0 equiv), slowly under an argon environment at -78°C. Mixture stirred for an hour at -78°C, and ethyl chloroformate (0.47 mL, 4.91 mmol, 1.2 equiv) was added dropwise under argon environment at -78°C.¹³ Reaction was warmed slowly to room temperature, stirred for an hour, quenched with ice, and extracted with ethyl acetate. Organic layer was washed with saturated sodium bicarbonate and brine, dried over sodium sulfate, and concentrated by rotary evaporation to obtain a slightly dark yellow oil (0.3297 g, 28%). Crude (15) was used without further purification. ¹H NMR (400 MHz, CDCl₃): δ 4.24 (q, J = 7.2 Hz, 2H), 3.85 – 3.69 (m, 1H), 3.59 (s, 2H), 2.22 – 2.04 (m, 2H), 1.84 – 1.70 (m, 5H), 1.48 (d, J = 5.1 Hz, 10H), 1.34 (t, J = 7.1 Hz, 3H). ¹³C NMR: δ 175.8, 153.2, 81.0, 64.5, 46.2, 38.2, 31.3, 29.7, 28.2, 24.0, 14.2.

2.6.3 Synthesis of 1-(tert-butoxycarbonyl)-2-oxoazepane-3-carboxylic acid (**16**)

Compound (**15**) (0.2720 g, 1.057 mmol, 1.0 equiv) and TMSOK (0.3275 g, 2.553 mmol, 2.41 equiv) in THF (2.0 mL) stirred overnight for 19 hours.¹⁶ pH of the reaction was 14, and 2M HCl (4.0 mL) in ether (36 mL) was added to the mixture until pH 4.0 was achieved. Mixture was stirred for 22 minutes. Solid white precipitate formed and was filtered off before mixture was concentrated by rotary evaporation to obtain (**16**) as a brown paste (0.1540 g, 63%). ¹H NMR (400 MHz, DMSO): δ 3.91 (d, J = 7.1 Hz, 1H), 3.65 – 3.53 (m, 1H), 2.96 – 2.74 (m, 2H), 1.91 – 1.62 (m, 3H), 1.38 (d, J = 7.2 Hz, 13H), 1.25 – 1.01 (m, 4H). ¹³C NMR: δ 176.1, 156.0, 77.7, 67.5, 30.1, 28.8, 27.3, 26.8, 25.6, 2.5, 2.3. Mass spectrometry (APCI Positive): 257.24742

2.7 Synthesis of *N*-(2-(5-hydroxy-1*H*-indol-3-yl)ethyl)-2-oxoazepane-3-carboxamide (**19**)



Scheme 9: Synthesis of *tert*-butyl 3-((2-(5-hydroxy-1*H*-indol-3-yl)ethyl)carbamoyl)-2-oxoazepane-1-carboxylate and *N*-(2-(5-hydroxy-1*H*-indol-3-yl)ethyl)-2-oxoazepane-3-carboxamide.

2.7.1 Synthesis of *tert*-butyl 3-((2-(5-hydroxy-1*H*-indol-3-yl)ethyl)carbamoyl)-2-oxoazepane-1-carboxylate (**18**)

Under an argon balloon, compound (**16**) (0.1604 g, 0.6238 mmol, 2.4 equiv) and 1,1'-carbonyldiimidazole (0.1103 g, 0.6802 mmol, 2.62 equiv) were added to a 25 mL round bottom flask. Anhydrous dichloromethane (3.66 mL) was added, and the mixture stirred for 1 hour. Serotonin hydrochloride (0.0552 g, 0.260 mmol, 1.0 equiv) was slowly added to the mixture followed by anhydrous pyridine (3.66 mL). Before and after serotonin addition, the mixture appeared clear yellow. After 2-4 minutes, the majority of serotonin was dissolved. Triethylamine (0.18 mL, 1.3 mmol, 5.0 equiv) was added, and the clear red/brown colored mixture stirred for 6 hours at room temperature. Reaction mixture was concentrated by rotary evaporation to produce a brown paste (0.2307 g).⁹

Crude product was dissolved in minimal ethyl acetate and silica gel. Rotary evaporation was performed to remove ethyl acetate. Crude product adsorbed on silica gel was dry-loaded onto a chromatography column, eluted via ethyl acetate:methanol gradient, and monitored by TLC. 98:2 ethyl acetate:methanol (170 mL) eluted the least polar material, and 95:5 ethyl acetate:methanol (500 mL) eluted the remaining of the least polar material and some of the HIOC derivative. 93:7 ethyl acetate:methanol (50 mL) eluted the remaining HIOC derivative. HIOC derivative began to appear after 250 mL of 95:5 ethyl acetate:methanol was ran through

the column.⁹ The least polar material and HIOC derivative appeared as dark purple spots in TLC (9:1 ethyl acetate:methanol, stained with *p*-anisaldehyde) with HIOC derivative having a lower R_f . Combined fractions were concentrated by rotary evaporation to yield the HIOC derivative as a pale solid (0.0393 g).

Warm ether (45 mL) was added, boiled in a 41°C water bath, and decanted. This process was repeated twice. The solid remaining after decanting was concentrated under rotary evaporation to product a light pale solid and was loaded onto a fritted funnel. Acetone (10 mL) was added to remove traces of imidazole impurities that co-eluted with HIOC derivative in silica gel column chromatography.⁹ Product (**18**) fully dissolved in acetone and was concentrated by rotary evaporation to obtain a clear solid, which upon scraping had a pale color (0.0405 g, 17%). ¹H NMR (400 MHz, DMSO): δ 10.60 – 10.35 (m, 1H), 8.65 (t, J = 5.5 Hz, 1H), 8.23 (dt, J = 5.1, 1.1 Hz, 1H), 7.70 – 7.60 (m, 1H), 7.16 – 7.05 (m, 2H), 7.03 (ddd, J = 4.0, 2.1, 1.3 Hz, 2H), 6.87 (d, J = 2.3 Hz, 1H), 6.59 (ddd, J = 8.5, 6.2, 2.4 Hz, 1H), 3.54 – 3.09 (m, 8H), 3.01 – 2.85 (m, 4H), 2.85 – 2.63 (m, 1H), 1.54 – 1.41 (m, 1H), 1.38 (d, J = 2.4 Hz, 11H), 1.28 – 1.01 (m, 2H).

2.7.2 Synthesis of *N*-(2-(5-hydroxy-1*H*-indol-3-yl)ethyl)-2-oxoazepane-3-carboxamide (19**)**
Compound (**18**) (0.0405 g, 0.0395 mmol, 1.0 equiv) in DCM (2.02 mL) was added dropwise to trifluoroacetic acid (0.13 mL, 0.65 mmol, 17. mmol) under the cooling of ice.¹⁷ Reaction stirred for 3 hours, and the reaction mixture was clear yellow-brown with black solid spots in the mixture. Mixture was concentrated by rotary evaporation, and a methanol wash was performed to obtain crude (**19**) (0.0141 g, 45%). Impurities in the 1.2-1.9 ppm NMR region appeared after the acetone wash. ¹H NMR (400 MHz, DMSO): δ 10.51 (d, J = 20.4 Hz, 1H), 8.61 (d, J = 12.3 Hz, 1H), 8.24 (s, 0H), 7.66 (d, J = 7.4 Hz, 1H), 7.52 (s, 3H), 7.15 – 7.07 (m, 1H), 7.02 (s, 2H), 6.93 – 6.72 (m, 0H), 6.65 – 6.49 (m, 1H), 3.72 – 3.57 (m, 4H), 3.17 (d, J = 4.8 Hz, 163H), 3.00 (d, J = 3.9 Hz, 1H), 2.68 (dt, J = 3.7, 1.9 Hz, 2H), 1.56 (d, J = 35.9 Hz, 2H), 1.32 – 1.11 (m, 2H).

3. Results and Discussion

The synthesis of HIOC was challenging (**Scheme 3**- page 50). In initial attempts, purified yield of 7-9% was obtained. When serotonin hydrochloride instead of 2-oxopiperidine-3-carboxylic acid was the limiting reagent, 51% purified yield was reported. Additionally, the complete dissolving of serotonin hydrochloride was crucial, achieved by adding serotonin incrementally into the reaction mixture. These modifications from the original protocol reported by Setterholm et al., 2015 were adopted in subsequent HIOC synthesis runs and in the synthesis of (**18**) (**Scheme 9**- page 55).

For the 5-membered lactam synthesis, after diethyl 2-azidoethylmalonate (**7**) was synthesized (**Scheme 4**- page 51), crude product was purified by silica gel column chromatography with 90:10 ethyl acetate:methanol. However, column chromatography was unsuccessful in separating desired product from impurities. These impurities carried over into the subsequent step of the reaction in which ethyl 2-oxo-3-pyrrolidinecarboxylate (**8**) was synthesized. To remove impurities in (**7**), vacuum distillation was utilized.

We had safety concerns with azide (**7**), specifically the requirement for vacuum distillation to purify. Future experiments should take place behind a glass shield. We sought an alternative synthetic approach for the 5-membered lactam. During the literature search for synthetic routes that avoid generating azides, a one-step synthesis of the 7-membered lactam was discovered in a 1986 German patent by Hamashima and researchers (**Scheme 7**- page 53). This approach involved deprotonation of the lactam N-H, enolate formation to produce a dianion, and direct carboxylation of the enolate using dry ice. However, very little product conversion was observed in ^1H NMR.

Two different approaches (**Scheme 5**- page 51) were tested for the synthesis of ethyl 2-oxo-3-pyrrolidinecarboxylate (**8**): hydrogenation and reduction of azide by SnCl_2 in methanol. Silica gel column chromatography with 90:10 ethyl acetate:methanol was not successful in separating the compound obtained from both methods from impurities. ^1H NMR indicated product conversion, but (**7**) was present in the hydrogenation product. Recrystallization with ethyl acetate and hexanes was also unsuccessful in isolating purified product from impurities. Similarly, in the reduction of azide by SnCl_2 in MeOH, ^1H NMR revealed minor product conversion. Impure (**7**) was utilized, and most of product (**8**) was impurities from the synthesis of (**7**). Products from both approaches lacked clear methyl peaks, which may be masked by the impurities in this region.

The experimental approach for synthesizing the 5-membered lactam was similar to that of the 7-membered lactam (**Scheme 6**- page 52 and **Scheme 8**- page 54). To prevent carboxylation on the lactam N-H, *N*-Boc protecting group was added to synthesize (**10**) and (**14**). Compound (**15**) underwent basic hydrolysis to obtain carboxylic acid (**16**) without further purification as purification of (**15**) by silica gel column chromatography resulted in complete product loss.

Carboxylic acid (**16**) was activated by carbonyl diimidazole (CDI), and regioselective *N*-acylation of serotonin hydrochloride required *in situ* deprotonation and solubilization with pyridine. Triethylamine addition followed to drive the acylation reaction to completion to obtain the Boc-protected 7-membered lactam HIOC derivative (**18**). Boc was deprotected using DCM and trifluoroacetic acid to obtain the final 7-membered lactam HIOC derivative (**19**, **Scheme 9**- page 55). Synthesis of the 5-membered lactam HIOC derivative is underway with ethyl ester (**11**) undergoing basic ester hydrolysis to obtain carboxylic acid (**12**).

4. Conclusion

An improved synthesis of HIOC is reported in which serotonin hydrochloride was the limiting reagent. Incremental addition of serotonin was critical for higher yield. After mastery of HIOC synthesis, the 7-membered HIOC derivative was synthesized and characterized. Progress was made towards the synthesis of the 5-membered HIOC derivative. Biological testing is needed to determine the *in-vivo* properties and pharmacokinetics of the compounds.

5. References

1. a) Goodrich, G.L.; Flyg, H.M.; Kirby, J.E.; Chang, C-Y.; Martinsen, G.L. Mechanisms of TBI and Visual Consequences in Military and Veteran Populations. *Optom. Vis. Sci.* **2013**, *90*, 105-112. b) Armstrong, R.A. Visual problems associated with traumatic brain injury. *Clin. Exp. Optom.* **2018**, *101*, 716-726. c) Thompson, H.J.; McCormick, W.C.; Kagan, S.H. Traumatic Brain Injury in Older Adults: Epidemiology, Outcomes, and Future Implications. *J. Am. Geriatr. Soc.* **2006**, *54*, 1590-1595.
2. Chan, R.K.; Siller-Jackson, A.; Veerrett, A.J.; Wu, J.; Hale, R.G. Ten year of war: a characterization of craniomaxillofacial injuries incurred during operations Enduring Freedom and Iraqi Freedom. *J. Trauma Acute Care Surg.* **2012**, *73*, S453-458.
3. Cockherham, G.C.; Goodrich, G.L.; Weichel, E.D.; Orcutt, J.C.; Rizzo, J.F.; Bower, K.S. & Schuchard, R.A. (2009) Eye and visual function in traumatic brain injury. *J Rehabil. Res Dev*, **46**, 811-818.
4. Dutca, L.M.; Stasheff, S.F.; Hedberg-Buenz, A.; Rudd, D.S.; Batra, N.; Blodi, F.R.; Yorek, M.S.; Yin, T.; Shankar, M.; Herlein, J.A.; Naidoo, J.; Morlock, L.; Williams, N.; Kardon, R.H.; Anderson, M.G.; Pieper, A.A.; Harper, M.M. Early Detection of Subclinical Visual Damage After Blast-Mediated TBI Enables Prevention of Chronic Visual Deficit by Treatment with P7C3-S243. *Investig. Ophthalmol. Vis. Sci.* **2014**, *55*, 8330-8341.
5. Iuvone, C.R.; Boatright, J.H.; Tosini, G.; Ye, K. *N*-acetylserotonin: circadian activation of the BDNF receptor and neuroprotection in the retina and brain. *Adv. Exp. Med. Biol.* **2014**, *801*, 765-771.
6. Shen, J.; Ghai, K.; Somopol, P.; Liu, X.; Cao, X.; Iuvone, P.M.; Ye, K. *N*-acetyl serotonin derivatives as potent neuroprotectants for retinas. *PNAS* **2012**, *109*, 3540-3545.
7. Bartolucci, S.; Mari, M.; Bedini, A.; Piersanti, G.; Spadoni, G. Iridium-Catalyzed Direct Synthesis of Tryptamine Derivatives from Indoles: Exploiting *N*-Protected β -Amino Alcohols as Alkylating Agents. *J. Org. Chem.* **2015**, *80*, 3217-3222.
8. Hwang, K-J.; Lee, T-S. A Practical Synthesis of *N*-Acetyl-5-methoxy-tryptamine (Melatonin). *Synth. Commun.* **1999**, *29*, 2099-2104.
9. Setterholm, N.A.; McDonald, F.E.; Boatright, J.H.; Iuvone, P.M. Gram-scale, chemoselective synthesis of *N*-[2-(5-hydroxy-1H-indol-3-yl)ethyl]-2-oxopiperidine-3-carboxamide (HIOC). *Tetrahedron Lett.* **2015**, *56*, 3413-3415.
10. Lindstrom, K.J.; Crooks, S.L. An Improved Preparation of Ethyl 2-Oxo-3-Pyrrolidinecarboxylate. *Synth. Commun.* **1990**, *20*, 2335-2337.
11. Maiti, S.N.; Singh, M.P.; Micetich, R.G. Facile conversion of azides to amines. *Tetrahedron Lett.* **1986**, *27*, 1423-1424.
12. Aeyad, T.; Williams, J.D.; Meijer, A.J.H.M.; Coldham, I. Lithiation-Substitution of *N*-Boc-2-phenylazepane. *Synlett.* **2017**, *28*, 2765-2768.
13. Heinrich, T.; Seenisamy, J.; Blume, B.; Bomke, J.; Calderini, M.; Eckert, U.; Friese-Hamim, M.; Kohl, R.; Lehmann, M.; Leuthner, B.; Musil, D.; Rohdich, F.; Zenke, F.T. Discovery and Structure-Based Optimization of Next-Generation Reversible Methionine Aminopeptidase-2 (MetAP-2) Inhibitors. *J. Med Chem.* **2019**, *62*, 5025-5039.
14. Hamashima, Y.; Ishikura, K.; Kubota, T.; Minami, K. (Oxoheterocyclic carbonamido)cephem carboxylic acid derivatives. US4578378A, March 25, 1986.
15. O'Brien, C.J.; Nicewicz, D.A. Milled Dry Ice as a C1 Source for the Carboxylation of Aryl Halides. *Synlett.* **2021**, *32*, 814-816.
16. Gaudino, J.; Boyd, S.A.; Marlow, A.L.; Kaplan, T.; Fong, K.C.; Seo, J.; Tian, H.; Blake, J.; Koch, K. Preparation of quinoline derivatives as tyrosine kinases inhibitors. Dec 21, 2007. WO 2007146824. Page 156, [00589].
17. Hattori, K.; Niizuma, S.; Masubuchi, M.; Koyama, K.; Kondoh, O.; Tsukaguchi, T.; Okada, T. Preparation of 1-(2H)-isoquinolone derivatives as antitumor agents. Aug 31, 2006. WO 2006090743.